CANOPY REFLECTANCE MODELING OF FOREST STAND VOLUME

NEAL PILGER

B.A. Honours, Simon Fraser University, 2000

A Thesis
Submitted to the Council on Graduate Studies
of the University of Lethbridge
in Partial Fulfillment of the
Requirements for the Degree

MASTER OF SCIENCE

LETHBRIDGE, ALBERTA
January, 2004

ABSTRACT

Three-dimensional canopy reflectance models provide a physical-structural basis to satellite image analysis, representing a potentially more robust, objective and accurate approach for obtaining forest cover type and structural information with minimal ground truth data.

The Geometric Optical Mutual Shadowing (GOMS) canopy reflectance model was run in multiple-forward-mode (MFM) using digital multispectral IKONOS satellite imagery to estimate tree height and stand volume over $100m^2$ homogeneous forest plots in mountainous terrain, Kananaskis, Alberta.

Height was computed within 2.7m for trembling aspen and 1.8m for lodgepole pine, with basal area estimated within $0.05m^2$. Stand volume, estimated as the product of mean tree height and basal area, had an absolute mean difference from field measurements of 0.85 $m^3/100\ m^2$ and 0.61 $m^3/100\ m^2$ for aspen and pine, respectively.

ACKNOWLEDGEMENTS

I would like to acknowledge a number of people and organizations that have supported this research throughout its development to completion; without this individual and group assistance, this thesis research would not be possible.

First off, I would like to thank my thesis supervisor, Dr. Derek Peddle, who has provided funding, support and encouragement throughout this research project. I would also like to thank my thesis committee members, Dr. Ronald J. Hall and the Canadian Forest Service (CFS), Edmonton, for equipment, resources, and time in reviewing earlier drafts of this thesis, Dr. Stefan Kienzle, and Dr. Robert Rogerson for their evaluation and suggestions along the way, and the Department of Geography at the University of Lethbridge which provided office space, computing facilities and research materials for which I am grateful.

This research, including field and remote sensing data collection, was supported by NSERC research grants and other grants held by Dr. Derek R. Peddle, Department of Geography, University of Lethbridge. Additional financial support was made available through teaching assistantships provided by the School of Graduate Studies.

A special thank you to my field assistants, Jeff Jordan and Susie Saunders – summer 2001, and Jennifer Pegg – summer 2002, whose aid in performing manual measurements was invaluable. I would like to thank Grace Lebel and Judy Buchannan-Mappin of The University of Calgary Kananaskis Field Station who provided comfortable lodgings and laboratory access required for differential GPS correction, Ryan Johnson, now of Iunctus Geomatics Corp. was invaluable in teaching the intricacies of the MFM-GOMS model during a previous research project at the university, and Nicole Rabe of the University of Lethbridge, whose tireless communications with SpaceImaging provided the necessary inputs for radiometric correction of the IKONOS satellite imagery.

Finally I would like to thank the external thesis examiner, Dr Ed Cloutis of the University of Winnipeg, and Dr. Stewart Rood of the University of Lethbridge, chair of the thesis defense committee for comments and helpful final suggestions.

TABLE OF CONTENTS

LIST OF FIGURES

LIST OF TABLES

LIST OF EQUATIONS

LIST OF ABBREVIATIONS

AAC	Absolute Atmospheric Correction
a.m.s.l.	Above Mean Sea Level
ASD	Analytical Spectral Devices
AVI	Alberta Vegetation Inventory
BA	Basal Area
BRDF	Bi-Directional Reflectance Distribution Function
BRF	Bi-Directional Reflectance Factor
dbh	Diameter at Breast Height
DEM	Digital Elevation Model
DN	Digital Number
DOS	Dark Object Subtraction
DTM	Digital Terrain Model
EMR	Electromagnetic Radiation
GOMS	Geometric Optical Mutual Shadowing
GPS	Global Positioning System
LAI	Leaf Area Index
MFM	Multiple Forward Mode
NIR	Near Infrared
PIF	Pseudo Invariant Feature
ROI	Region Of Interest
SV	Stand Volume
SVI	Spectral Vegetation Indices
SZA	Solar Zenith Angle
TRAC	Tracing Radiant Architecture of Canopies instrument

CHAPTER 1

1.0 Introduction

1.1 Introduction

Forest resources are of paramount importance to the livelihood of the global economy. Accurate assessment of stand volume and biomass is required for the estimation of carbon sinks as well as a myriad of other ecological and environmental factors. To reliably manage forest resources on a renewable basis, current and accurate resource databases must be established on which to base decisions. The establishment and maintenance of such databases is vital for classification and/or change detection of forest biophysical parameters. It is both costly and time-consuming to use traditional aerial and ground survey methods, therefore, multi-spectral satellite-imaging sensors are becoming standardized sources of digital imagery for large area resource monitoring, providing repetitive global coverage on a timely basis. The data extracted from this imagery can be analysed to produce temporally accurate information on the health and vitality of forest biomass.

As the most widely distributed terrestrial ecosystem on Earth, forests produce 70 percent of the annual net global terrestrial carbon accumulation which results in the uptake of atmospheric carbon and the conversion of greenhouse CO_2 to O_2 (Wulder, 1998). Canada contains 10 percent of the global forest cover at over 417 million hectares, with over 50 percent, or 2.4 x 10^{10} m^3 being commercially viable (CFS, 1997; Wulder, 1998; Hall *et al.*, 2001). Traditionally, forested landscapes in Canada have been classified based upon distinct forested regions. Each forest region is representative of a fairly uniform vegetation cover in terms of dominant species and stand type over a geographic zone. This forest classification,

established by Rowe (1972) does not incorporate all biophysical environmental variables as it relies solely on the composition of the forest vegetation as stratified by latitudinal and longitudinal gradients, not on ecological classifiers (www.cfl.scf.rncan.gc.ca/ , 2003) such as height, stem diameter, and volume.

Vegetation classifications integrate knowledge about species assemblages but lack information on biophysical attributes. Commercial assessments of standing volume are insufficient by themselves to derive estimates of leaf area or canopy characteristics. In addition, both of these types of information are generally dependent on infrequent ground sampling over relatively small areas. Key field measurements, such as canopy dimensions and height, synthesized with satellite imagery within a model can allow for inferences of ecosystem biophysical parameters that would be nearly impossible to obtain over large areas through ground surveys alone (Waring and Running, 1998).

Forest stand volume has been included in forest inventories and in estimates of carbon stocks along with a variety of ecological and environmental parameters, where forest stand volume refers to the total above ground volume of trees that is typically expressed in cubic metres per hectare (m^3/ha). This differs somewhat from merchantable timber volume, which is the net volume that may be processed to produce certain wood products based on utilization limits that define the proportion of the tree that may be harvested for a given product (Alberta Environmental Protection 1994) although the volume expression is the same. Individual tree volume is derived as a function of tree height and basal area. Basal area is the cross-sectional area at breast height defined at 1.3 m above ground. Several previous remote sensing studies have estimated biomass and/or stand volume using conventional image analysis approaches, with mixed results (e.g. Anderson *et al.,* 1993; Friedl *et al.,* 1994;

Soares *et al.,* 1995; Trotter *et al.,* 1997; Guerra *et al.,* 1998; Franklin *et al.,* 2000). However, these studies have relied on empirical and/or statistical methods that require extensive field data collection conducted in areas of flat terrain. In this research, a more direct and explicit approach to forest structure and biophysical parameter estimation using a canopy reflectance model was employed and tested in a challenging area of mountainous terrain in western Canada.

Canopy geometric optical reflectance models can estimate a variety of forest structural and biophysical parameters over large regions. Recent advances in model utilization by Peddle *et al.* (1999-2003, described below) have resulted in new ways of using powerful three-dimensional forest models in which little or no *a priori* ground knowledge is required. Information such as land cover, tree height, density and stand volume can be provided over large areas where ground-based measurements are not readily available. As a result, these modeling capabilities are worthy of consideration for large area analyses such as assisting in updates to regional and national scale forest inventories and for monitoring carbon stocks for international policy compliance (e.g. Kyoto Protocol).

The Multiple-Forward-Mode (MFM) approach (Peddle, 1999) to canopy reflectance modeling has been used successfully with different sensors, canopy reflectance models, and in different forest ecosystems in a variety of applications. These include structural change detection of partially harvested mixed forests in New Brunswick (Peddle *et al.*, 2003a), several studies in the BOREAS project involving model-based cluster labeling in unsupervised land cover classification, and independent per-pixel modeling for mapping 25 detailed land cover classes and LAI for a mosaic of 7 Landsat thematic mapper (TM) scenes covering the entire BOREAS region in Saskatchewan and Manitoba (Peddle *et al.*, 2003bc).

This approach has also been used for biomass estimation in western Newfoundland (Pilger *et al.,* 2002; Peddle *et al.*, 2003d), land cover and biophysical parameter estimation in mountainous terrain using compact airborne spectrographic imager (CASI) data (Johnson *et al.*, 2000), and in terrain correction of IKONOS imagery in the Rockies (Soenen *et al.*, 2003). The use of MFM modeling in the national and international landcover mapping forestry contexts was also reviewed by Cihlar *et al.* (2003) and Gamon *et al.* (2003).

In this thesis, the MFM approach was used with the Geometric Optical Mutual Shadowing (GOMS) canopy reflectance model (Li and Strahler, 1992) to estimate forest biophysical parameters and stand volume from high spatial resolution multispectral IKONOS satellite imagery within the Rocky Mountains of southwestern Alberta. These stand volume estimates are relevant to the Alberta Vegetation Inventory (AVI) and for potential inclusion in carbon budget and biomass estimation studies. This study involved fieldwork to provide extensive validation of model results, however, this modeling approach was intended to operate with little or no ground level data collection

Practical benefits of model-driven forest volume assessment queries include:

- Potential for consistent monitoring of Canada's natural forests
- Carbon and biomass estimations
- Vegetative cover distribution for wildlife species monitoring
- Vegetative spectral response for disease and pest monitoring
- Re-growth monitoring and volume estimation of forest cut-blocks
- Use of powerful canopy models with minimal field data inputs required
- Consistency with other MFM modeling applications

1.2 Research Objectives

The central objective of this research was to:

- Derive and evaluate a remote sensing method to estimate forest stand volume from 4-metre multispectral satellite imagery over a mountainous region in southwestern Alberta using a canopy reflectance model in multiple-forward-mode.

Secondary objectives involved the derivation and testing of biophysical variables required for stand volume estimation. These include:

- Derive, test and validate the use of MFM modeling for estimating mean forest stand height; and

- Examine and test a simplified method for stem diameter estimation based on height variables for individual plot basal area estimation

1.3 Organisation of Thesis

This thesis is organized into five chapters. This introductory chapter presents the study and outlined the basis and objectives of the research conducted, as well as the structure of the thesis.

Chapter Two consists of a literature review organized into two key themes, forestry and remote sensing. A brief ecological discussion on key forest vegetation species under investigation in this research is presented along with a description of current forest inventory and survey methods, focusing on the Alberta Vegetation Inventory (AVI). An outline for the extraction of height, basal area, and ultimately stand volume from biophysical forest parameters completes the section. The second theme deals exclusively with remote sensing

practices. Radiometric correction and calibration of multispectral imagery is presented, focusing on atmospheric and terrain correction methodologies. Common environmental remote sensing classification techniques lead into a discussion on vegetative spectral response and the role of vegetation indices and spectral mixture analysis. Background information on canopy reflectance models is presented with reference to model modes, usage, and past studies. Finally, a detailed description of the Geometric Optical Mutual Shadowing canopy reflectance model, and Multiple-forward-mode usage is discussed with a focus pertaining to this research.

In Chapter Three, the research methods and experimental design are presented. The study area, field data collection and equipment, measurement methodologies, and satellite sensor system attributes are discussed. This is followed by pre-classification reflectance processing techniques of the IKONOS satellite data including atmospheric correction, image geo-referencing and alignment. Calibration and calculation of MFM-GOMS model inputs; spectral endmember selection; and model runs are described, followed by query operations of the model output and derivation of stand volume estimation variables and parameters.

Chapter Four presents the outcome of each stage of analysis outlined in Chapter Three, and graphically summarizes the results at each step. This is followed by a discussion and summary of the results presented.

In Chapter Five, a summary and major conclusions of the thesis are presented including perspectives on the applicability of this approach to other areas and operational settings. Finally, contributions to present forest related remote sensing applications and suggestions for future related research are identified.

CHAPTER 2

2.0 Literature Review

2.1 Introduction

This chapter presents a review of literature divided into two key themes, forestry and remote sensing. Serving to provide a context for the following chapters, the forestry section briefly overviews forest ecology, species identification, structure, composition, and distribution. This is followed by a discussion of current inventory methods, structural and biophysical attributes and field-based parameter estimation of forest stand volume. The remote sensing section discusses radiometric correction and calibration methodologies applied to digital image data, including reflectance processing, atmospheric and terrain correction, and image normalization. A description on image classification techniques leads to the principle behind vegetative spectral response and vegetation indices. Spectral mixture analysis (SMA), a key issue in digital image analysis leads into the principal development, and usage of canopy reflectance models.

An outline of some of the modeling techniques employed by remote sensing scientists, as well as the theoretical capabilities and limitations of optical reflectance models are then discussed with descriptions of model inputs and output pertaining to model usage, finishing with a general review of the multiple-forward-mode geometric optical mutual shadowing (MFM-GOMS) model utilized in this research.

2.2 Forest Ecology and Inventory

Forests are the most widely distributed ecosystem on the earth, producing 70 percent of the annual net global terrestrial carbon accumulation resulting in the uptake of atmospheric carbon and the conversion of greenhouse CO_2 to O_2 (Wulder, 1998). Canada contains 10 percent of the global forest cover, with over 50 percent, or 2.4×10^{10} m^3, being commercially viable (Wulder, 1998, Hall *et al.,* 2001).

The role that forests play in maintaining our biosphere, and the extensive variation on species, habitat, and distribution regimes falls well outside the scope of this research. However, a brief discussion pertaining to forest ecology and the primary forest species under investigation in this report merit mention, as site location and distribution play an important role in the validation of MFM-GOMS biophysical modeling.

2.2.1 Forest Ecology and Species Distribution

Ecology is the study of the structure and function of nature where structure includes the distribution and abundance of organisms as influenced by the biotic and abiotic elements of the environment; and function includes all aspects of the growth and interactions of populations, including competition, predation, parasitism, mutualism, and transfers of nutrients and energy among them (Smith, 1996). The branch of ecology related to forest vegetative growth is physiological ecology, or ecophysiology, which is concerned with the responses of individual organisms to temperature, moisture, light, nutrients, and other factors of the local environment (Smith, 1996). Ecophysiology, a tenant of applied ecology, utilizes

the application of ecological principles to major environmental and resource management problems.

Forest type distribution is influenced by a number of environmental conditions that restrict colonization and dispersion. These factors include localized climate, orientation (slope, aspect), soil characteristics, moisture, and access to incident solar radiation, among others. In mountainous zones, such as this research area, microclimate changes on an altitudinal gradient. The change in microclimate going upslope is similar to the broad climatic changes experienced by going to higher latitudes. Approximately every 300m rise in elevation is equivalent to 160km in latitude and a drop in temperature of 1.5 to 3 degrees Celsius, however, in closed canopy forests internal temperatures may be 1-2 degrees higher than outside ambient temperature (Spurr and Barnes, 1973). This temperature gradient in mountainous areas affects the vapour pressure (or humidity) in the region, thus creating a range of microclimates (Smith, 1996).

The greatest microclimate differences in mountainous areas exist between north-facing and south-facing slopes. These differences in slope-aspect orientation have a distinct effect on the moisture and heat budget of different sites affecting the conditions for specific vegetative species growth. High temperatures and associated low vapour pressures induce evapotranspiration of moisture from soil and plants. The evaporation rate often is 50 percent or higher, the average temperature higher, the soil moisture lower, and the extremes of all of these are more variable on south-facing slopes (Smith, 1996). The effect of increased sunlight on south-facing slopes may be accentuated or diminished by prevailing winds and surrounding bodies of water (Spurr and Barnes, 1973). Therefore, localized climatic, geologic and topological factors play a greater role in species distribution than slope

orientation and access to incident solar radiation following a long chain of interactions: solar radiation influences moisture regimes; the moisture regime influences the species of trees and other plants occupying the slopes; the species of trees influence mineral recycling, which is reflected in the nature and chemistry of the surface soil and the nature of herbaceous ground cover (Spurr and Barnes, 1973; Smith, 1996).

The tree layer of montane forests is generally more uniform than that of lowland forests, and often characterized by one dominant species (Grabherr, 2000). In the Kananaskis region, this species is lodgepole pine, whereas trembling aspen and white spruce dominate the lower areas. A discussion of the dominant tree species in the Kananaskis study area follows.

2.2.1.1 Lodgepole Pine

Lodgepole pine (*Pinus contorta* Dougl.) is the most common tree species in the montane forest (Gadd, 1995), covering over 20 million ha in Canada alone (USDA Silvics, 2003). Major growth occurs between elevations of 800 and 2000 m above mean sea level (a.m.s.l.) but often extends up to 2400 m depending on latitude (Archibald *et al.,* 1996).

While lodgepole pine can thrive under a wide variety of climatic conditions in a variety of soil types, including wet depressions (Farrar, 1995), it prefers areas of medium to dry moisture regimes. A highly versatile species, *Pinus contorta* can thrive in a full range of nutrient regimes (USDA Silvics, 2003). Pine forests in the montane region are generally open stands occurring along valley walls of eroding morainal or colluvial materials as well as on exposed rock outcrops (Achuff, 1992). Mature trees range in height between 5 and 20 m with foliage mainly in the upper third due to the low shade tolerance of lodgepole pine needles.

While cones of both sexes are represented on each tree, female seed cones remain may remain closed, usually on the tree, for many years (Farrar, 1995), however, they open rapidly when ambient temperature exceeds 45° C, such as in the presence of fire (Gadd, 1995).

2.2.1.2 Trembling Aspen

Trembling aspen (*Populus tremuloides* Michx.) is the most common deciduous tree in the Rocky Mountains, and one of the most widely distributed species in North America (Farrar, 1995; USDA Silvics, 2003). Major growth for this species occurs between 800 and 1600 m a.m.s.l. Mature trees range in height from 5 to 30 m depending on location and environmental factors as this species can thrive in a full range of nutrient and moisture regimes (Farrar, 1995). However, trembling aspen is most abundant and grows best on sheltered, warm south and southwest aspects with loose sandy and gravelly soils (Farrar, 1995; USDA Silvics, 2003). The occurrence of aspen on south-facing slopes is thus the response to the local-scale drier condition due to aspect.

Trembling aspen is most easily identified through examination of the protective, powder covered photosynthetic bark (Gadd, 1995; USDA Silvics, 2003). The powder is composed of dead cork cells and is a natural defense against ultraviolet radiation. Aspen commonly grow in stands of genetically identical clones and reproduce through propagation along an extensive root system (Gadd, 1995). Seedling reproduction is less common as the tiny seeds lack endosperm, so seedlings must come into immediate contact with moist soils for nutrient and water uptake (Peterson, *et al.,* 1992).

Aspen foliage is sparse and concentrated near the top of the tree with small round pointed leaves. Discrimination between trembling aspen and other poplar species is most

easily performed, aside from differences in bark physiology, by the slender flat stalks that promote rustling of leaves with the slightest breeze (Farrar, 1995).

2.2.1.3 Balsam Poplar

While not as prevalent in the Kananaskis region, balsam poplar (*Populus balsamifera* L.) shares many of the growth characteristics of trembling aspen, such as favouring similar nutrient regimes (Archibald *et al.,* 1996). Balsam poplar can thrive under moister environmental conditions than aspen (Farrar, 1995) preferring low-lying montane and sub-alpine stream courses (Gadd, 1995). Leaves are similar in physiology to those of the aspen, however, they are larger and elongated on round stalks. Unlike aspen, balsam poplar bark is not powdered and is greenish-brown when young, graying with age into flat, scaly ridges separated by narrow black fissures (Farrar, 1995; Peterson, *et al.,* 1992).

2.2.1.4 Spruce

White spruce (*Picea glauca* (Moench) Voss) and Engelmann spruce (*Picea engelmannii* Parry ex Engelm) are the most common spruce species in the Rocky Mountains. These two species interbreed and are often difficult to differentiate (Farrar, 1995). White spruce tends to occur at lower elevations (800-1400 m a.m.s.l.) than Engelmann (1200-1800 m) and both require medium moisture and nutrient regimes (Archibald *et al.,* 1996). While not as common in the Kananaskis study site as lodgepole pine, spruce often intermingles with pine and aspen, especially at lower elevations. Engelmann spruce and/or white/Engelmann hybrids may have (or probably) occurred but since specific identifications of samples spruce

trees were not made, they will be referred to as: 'white spruce'. White spruce has been described as a "plastic" species because of its ability to re-populate areas under highly variable conditions, including extreme climates and soils (USDA Silvics, 2003). However, they generally favor mesic soil sites, especially along stream channels on fluvial terraces (Achuff, 1992), as good growth requires a dependable supply of well-aerated water (USDA Silvics, 2003). White and Englemann spruce has been found to grow on both acid and alkaline soils between a pH range of 4.7 to 7.0 (USDA Silvics, 2003). These species reach a height of 20-30 m at maturity (Gadd, 1995) with foliage often reaching the forest floor. Spruce can be easily identified through examination of their needles that are square in cross section and pointed while pine and fir needles are round, or flat and soft, respectively (Farrar, 1995).

2.2.2 Inventory methods

Forest inventory refers to the assessment of forest resources, including digitized maps and a database describing the location and nature of forest vegetation cover as well as descriptions of other forest properties such as soils, vegetation and wildlife features (http://www.ncfcnfr.net/, 2003). The identification of forest classes additionally allows for conservation planning, sustainable resource usage, wildlife distribution based on suitable habitat, and net biomass estimations (Foody and Hill, 1996). Forest inventory assessment in Canada is done provincially, and then combined at the national level to provide annual updates on the status of national forest resources. For studies involving relatively small areas,

calibration of the data must usually be performed so that aggregation into large areas agrees with corresponding estimates from field measurements (Katila *et al.*, 2000).

One of the greatest challenges facing forest management is the creation of detailed localized inventories using existing estimates generated from larger holdings (Leckie and Gillis, 1995). Generalizations over large regions such as provinces or large regional areas are seldom adequate in describing the high variability present in smaller eco-regions. Aerial photographs are the standard for inventory data acquisition in these smaller regions, however, such data is costly to obtain, and maintain over time. With the advent of high spatial resolution satellite sensors, repetitive data acquisition could be performed without the inherent limitations present in aerial imaging missions such as altitudinal variation, tilt, and yaw.

Techniques offering new and innovative approaches for improving the efficiency and accuracy of forest inventories, especially in geographically remote locations, are in constant demand (Gerling, 1996). By providing essential information extraction from digital imagery, such as stand volume and height, operational, and managerial inventories may be performed in a costly and timely manner. An example of a management based inventory would be complete-coverage stand mapping plus volume estimates derived from field sampling. Maps generated from stratification based on industry maps would then be provided to regional and district forest offices and forest companies for use in forest management planning (Leckie and Gillis, 1995, Robinson *et al.*, 1999).

Each province utilizes an inventory classification system that results in mapped areas represented by polygons within a GIS database (Franklin *et al.,* 2000). Provincial inventories, however, are not standardized. Some, like Alberta, conduct a continuous inventory by

implementing yearly update operations to keep the inventory current while others employ discontinuous inventories in which a percentage of the province is inventoried each year over a 10-20 year period. From such non-uniform practices, it is easy to see how inaccuracies on a national scale can be created.

A forest classification database can be utilized in a variety of ways to determine, among other things, carbon inventory, timber harvest schedules, and biomass estimates (Bragg, 2001). Forest inventories are based on extensive data collection. The next section outlines some of the survey methods employed in obtaining this data.

2.2.2.1 Survey methods

Traditionally, forest classification databases relied on aerial or ground-based survey methods, both of which have proven expensive, time intensive and difficult to maintain (Leckie and Gillis, 1995). In addition, inventories based on aerial photos generally underestimate timber resources relative to ground inventories of the same area (Gerling, 1996). This is primarily due to the airborne camera being unable to view, or photograph, overtopped understory vegetation. While aerial data generally has an advantage of high spatial resolution, and aircraft has the ability to fly below high cloud cover, repetitive observations of the same area are subject to many operational difficulties, such as altitudinal differences, correction for tilt and yaw, and the creation of multi-date image mosaics. Therefore, digital multi-spectral satellite image data for use in forestry analysis is being utilized to overcome such issues and limitations with aerial-based imagery and presently accounts for approximately 22 percent of the annual sales of satellite imagery in this country (Wulder, 1998).

Ground-based methods for the categorization and classification of forest inventories as previously mentioned, are costly in time, money and human resources. Aerial surveys, while more effective for monitoring larger areas compared to field surveys, are impractical for national inventories, especially where repetitive observations are required, such as in change detection analysis.

These inherent restrictions have led to the increased use of satellite imaging sensors for the collection of ground surface data. Standard orbits allow for recurring observations of the same area without the added difficulties in obtaining aircraft, pilots, flight plans, etc., or repetitive calibration of sensor systems prior to and following each flight. Orbital satellite sensors have the advantage of being highly stable throughout their functional lifespan, allowing for consistency in spatial resolution and image geometry. Thus, the formation of image mosaics and comparison of different date imagery is possible without the problems of having to significantly re-size and/or geometrically modify the data.

Another benefit of digital remote sensing over traditional methods is the ability to provide information that is not currently part of existing analog based forest inventories (Franklin *et al.,* 2000) such as spectral stress indicators that may not be visible using standard panchromatic photographs. Such ancillary information may be employed in the evaluation of vegetative health, species dispersal, rates of growth and/or decline, and the generation of ecosystem models over large areas.

2.2.2.2 Alberta Vegetation Inventory

Since 1989, the Alberta Vegetation Inventory (AVI) system has been the standard used to map forests and classify landscapes in the province of Alberta. The AVI is a system

for describing the quantity and quality of vegetation present. It involves the stratification and mapping of the vegetation to create digital data at a 1:20,000 scale according to the AVI Standards Manual and associated volume tables (http://www3.gov.ab.ca). Each map sheet covers 93.24 km^2, or 9,324 ha, with approximately 600 forest stands per sheet. A total of 545 AVI maps are generated to cover the province (Leckie and Gillis 1995). The AVI is used for mapping stands two hectares and larger in terms of several attributes that include species, to 10% composition limits, and height to the closest metre (Nesby, 1997). This level of stand detail, however, is not considered appropriate for most satellite image data (Hall *et al.*, 2000), therefore, the AVI relies heavily upon aerial imaging missions.

Pairs of stereo aerial photographic prints are interpreted utilizing stereographic equipment along with ground survey data in which forest stands are defined and delineated on the basis of species composition, crown closure, stand height, and age characteristics. A site quality parameter is another attribute usually applied to each stand.

Species composition is given by the most prevalent species, each estimated to the nearest 10 percent. Species groupings, such as intolerant hardwood, tolerant hardwood, or spruce-fir, as example, are sometimes used instead of the individual species, where species composition is estimated on the basis of percent crown cover as a percent of the overall stand (Leckie and Gillis 1995). AVI is the basis for a new forest management plan that address both timber and non-timber values, and provides for sustainable development of our forest resources. At the end of 1996, 164,188 km^2 or just over 16.4 million ha of forest has been inventoried using this system (Department of the Environment, 2001).

2.2.3 Stand Volume Assessment

Forest stand volume refers to the total above-ground volume of trees, and is typically expressed in cubic metres per hectare (m^3/ha). This differs somewhat from merchantable timber volume, which is the net volume that may be processed to produce certain wood products based on utilization limits that define the proportion of the tree that may be harvested for a given product (Alberta Environmental Protection, 1994). Individual tree volume is derived as the product of tree height and basal area. Basal area is the cross-sectional area at breast height (1.3 m above ground). Stand volume is determined from the aggregation of individual tree volumes within a stand.

Validation of stand volume assessment based on reflectance characteristics can be inferred only through ground-based field studies, as the spectral characteristics of the forest may be similar in different areas regardless of canopy height, especially where shadowing is negligible. This problem is inherent in remote sensing of any height variable in which viewing from above negates the dimensional qualities of the object of interest. This is not to say that stand volume cannot be assessed through the use of remote sensing, only that ground-based validation was required in at least a few areas common to the image data itself. Therefore, while rudimentary appraisal of height and stand volume can be inferred for a homogeneous forest area, results from one study may not be considered applicable to other forested regions.

While many studies have attempted to map stand volume or biomass through direct estimation (Anderson *et al.,* 1993; Paradella *et al.,* 1994; Friedl *et al.,* 1994; Soares *et al.,* 1995; Trotter *et al.,* 1997; Guerra *et al.,* 1998; Franklin *et al.,* 2000; Banfield *et al.,* 2002,

among others), the vast majority of these studies have dealt with flat terrain using empirical and statistical methods that depended upon extensive field-data collection. Areas of variable relief, such as mountainous zones, contribute a host of factors that affect the spectral response of ground targets. Therefore, a greater understanding of the areas under examination must be known, and additional correction methodologies may be required to normalize the radiance of ground targets.

2.2.3.1 Height Estimation

Individual and stand tree height and diameter are essential for the calculation of forest volume estimates (Peng, 1996). Height is an elusive variable to estimate accurately using remote sensing as the sensor is generally recording areal observations from above. Determination of stand height, however, has been done in a number of ways. The first deals with actual in-field measurements using a laser rangefinder, similar to that in a total survey station, or clinometer, used in this research (Figure 3.4b), and averaging height measurements over a pre-selected area. This method, while providing the most reliable height estimates, is also the most expensive to implement. The second method uses inferences from shadow and/or texture analysis from aerial photographs. This method generally requires high spatial resolution imagery and areas of open stands from which shadow can be easily assessed. A third method infers height through its relationship with other forest structural parameters such as diameter at breast height (Peng, 1996), age (Curtis, 1967), or canopy structure. A fourth method, the one utilized for this research, is the non-empirical modeling method where height is estimated through the use of canopy reflectance models applied to digital imagery. Modeled height computation employs species-specific spectral endmembers

and a range of biophysical inputs to derive reflectance based 'look-up' tables (LUTs). Band specific pixel reflectance values for a specific area are then matched against model generated reflectance values using a query program (e.g. Microsoft® Access), a technique discussed in greater detail later in this chapter.

2.2.3.2 Basal Area Estimation

Basal area is a measure of stand density that is based the cross-sectional area of a tree trunk measured in square inches, or centimeters at breast height, approximately 1.3 meters above ground level. The most commonly used tool for measuring basal area is a dbh-, or diameter tape. The basal area of all trees in a given stand area describes the degree to which an area is occupied by trees and is generally expressed in square meters per hectare (m^2/ha)

Basal area values commonly range from 10 to 60 m^2/ha in both coniferous and deciduous forests of Alberta, however, for high-density stands, values may reach up to 150 m^2/ha. As a means to estimate stand volume from field data, basal area is a computationally simple portion of the stand volume equation, however, it is more difficult to derive from modeled output when dbh values have to be inferred from remote sensing image analysis.

2.3 Remote Sensing

2.3.1 Radiometric Calibration and Corrections

In the application of satellite remote sensing data for quantitative investigations, the first and sometimes most important steps are the calibration of satellite data, atmospheric correction and, when needed, correcting for the topographic effect. Correction and calibration fall under the general term of validation, which is the process of assessing by independent means the quality of the spectral data products derived from the system output (CEOS, 1995, as cited in Teillet *et al.*, 1997).

Spectral response patterns, or spectral signatures, play a central role in detecting, identifying, and analyzing Earth surface materials, however, the Earth's surface is full of complexity and variation. Different material types can be spectrally similar, making identification and classification difficult, as the general understanding of the energy/matter interactions for some earth surface features is still at an elementary level for several materials and virtually nonexistent for others (Lillesand and Kiefer, 1999). Therefore, thoroughly understanding the limitations and constraints of a remote sensing system and its related products is of vital importance in determining the best applications and correction methods to apply for a particular image scene at a given location and time.

Radiometric correction, as with geometric correction, applied to digital data varies significantly among sensors. Radiance measured of any object by a remote sensor is influenced by many factors such as: Bi-directional reflectance distribution, changes in scene illumination, atmospheric attenuation, viewing and topographic geometry, and instrument response characteristics (Teillet, 1986, 1997). Thus, various paths of irradiance and surface

reflectance can alter the apparent at-satellite radiance of a given target. This is referred to as path radiance (Figure 2.1).

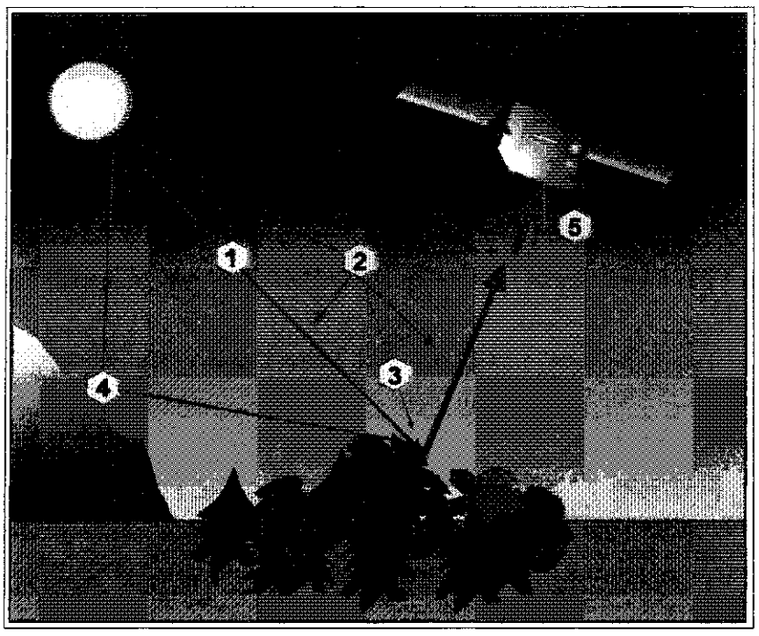

Figure 2.1. Path Radiance - sun to sensor.

Total at-sensor radiance is composed of diffuse, reflected, and emitted radiation. In Figure 2.1, Path 1 provides direct energy from the illumination source (sun), off the target pixel to the satellite sensor. Path 2 consists of diffuse, or scattered irradiance that adds to the apparent 'brightness' of the target pixel without actually being reflected off the pixel of interest. Path 3 also consists of scattered, or diffuse irradiance, however, this path contributes to the apparent reflectance of the target pixel directly through increased illumination. Path 4 indicates path radiance of reflected energy off neighbouring pixels, while Path 5 indicates the total energy reaching the sensor as a result of direct and diffuse path radiance interactions. It is clear from this diagram that the energy reaching the sensor must be calibrated to offset for

such increased illumination effects. The problems associated with such path irradiance can be better understood through the bi-directional reflectance distribution function (BRDF) of a given object at a given time.

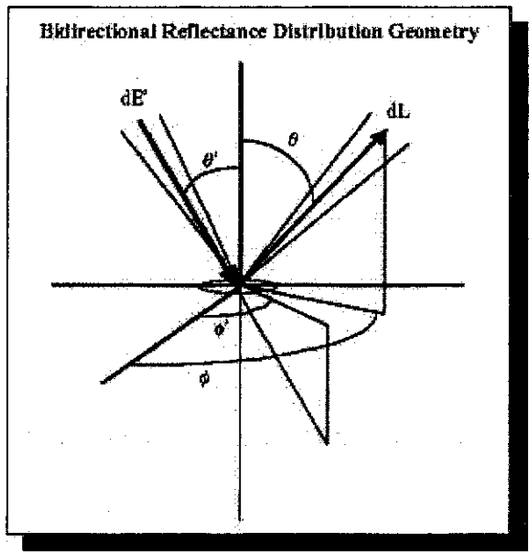

Figure 2.2. Bi-directional Reflectance Distribution Geometry (Wulder, 1998).

The BRDF relates the paths of irradiance from a given directional angle at a surface to the reflected radiance in the viewing, or sensor, direction. More simply, BRDF refers to the reflectance of an object at a multitude of possible view angles at a given time or solar position (Wulder, 1998).

Apparent radiance of an object changes over time and place, as the amount of incoming solar radiation, or irradiance, changes depending on solar / sensor position, atmospheric attenuation, and topographic position of the object(s) of interest. The effects of BRDF can be collected in the field using a spectroradiometer and targets of known

reflectance characteristics. Spectral information collected in a controlled setting allow for 'pure' spectral measurements to be taken of a given object, however, the benefits of collecting BRDF measurements are normally out-weighed by the measurement and calibration difficulties encountered (Wulder, 1998). An understanding of BRDF characteristics is important in relating forest stand structure to biomass, species, and canopy/ surface albedo. Applying correction algorithms to counter the effects of BRDF, especially in areas of variable topography, begins with accurate calibration of the imaging sensor.

2.3.1.1 Sensor Calibration

Generally, the ability of a given sensor to capture quality radiance measurements from ground targets deteriorates over time. Accurate calibration of the onboard detectors must be performed to maintain precise radiance measurements of surface targets. (Robinove, 1982; Markham and Barker, 1987; Teillet *et al.,* 1997). Calibration refers to the relationship between an integer value (digital number) generated for computer processing by the satellite sensor, and the radiation field incident at the satellite instrument, expressed as spectral radiance (Wm^{-2} sr^{-1} μm^{-1}). The International Committee on Earth Observation Satellites (CEOS) defines calibration as the process of quantitatively defining the system response to known, controlled signal inputs (CEOS, 1995, cited in Teillet *et al.,* 1997).

Ground-Look-Calibration of multispectral satellite systems, such as the IKONOS sensor utilized in this research, is performed by acquiring images of specific Earth landmass calibration targets whose biophysical and atmospheric characteristics are especially well known (Jensen, 2000). Repetitive observations of spectrally characterized ground targets

during optimal viewing conditions (clear skies) allows for routine adjustment of calibration coefficients for conversion of the 'raw' signal, to at-sensor radiance values.

2.3.1.2 Atmospheric correction

The atmosphere affects the ability of a given sensor to quantify visible and near-infrared signals in a number of ways. It modifies not only the spectral and spatial distribution of the incident radiation on the surface being detected, but is compounded as the electromagnetic radiation (EMR) passes once again from surface to sensor. Forster (1984), Chavez Jr. (1988), Caselles and Lopez Garcia (1989), and de Hann *et al.* (1991) among others, proposed models which correct for not only atmospheric scattering but atmospheric transmittance and attenuated global irradiance affecting digital imagery as well.

The majority of studies relating to atmospheric correction of imagery obtained by satellite remote sensing systems have been employed under the assumption of Lambertian surfaces (Teillet, 1986). A Lambertian surface is defined as being a perfectly diffuse reflector, appearing equally bright from all viewing angles (Lillesand and Kiefer, 1999).

The purpose of atmospheric corrections in the visible and near-infrared wavelengths for a satellite imaging sensor such as IKONOS is the conversion of image digital numbers (DNs) to surface radiance / reflectance values (Chavez, 1989; Teillet and Fedosejevs, 1995). This is especially important in forestry mapping as the atmosphere modifies the strength and spectral distribution of the electromagnetic energy received by a sensor, restricting 'where we can look' spectrally (Lillesand and Kiefer 1999).

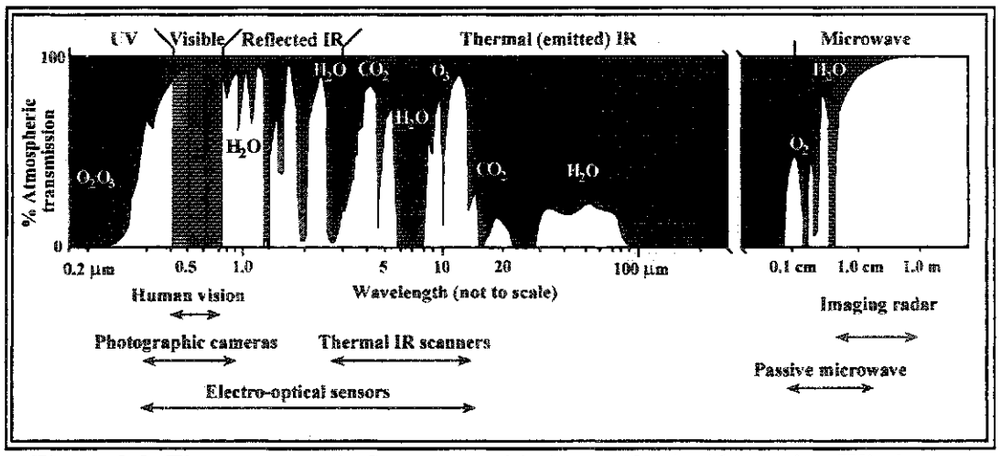

Figure 2.3. Electromagnetic Spectrum with Atmospheric Absorption Windows. Adapted from Avery and Berlin, (1992).

Scattering due to molecules and aerosols in the atmosphere and absorption due to the gaseous constituents of the atmosphere all modify surface reflectance information passing through the atmosphere to the sensor platform (Teillet and Fedosejevs, 1995). Additive atmospheric effects, such as Rayleigh scattering, vary with wavelength from ~0.7µm onwards, however, in the near infrared these effects become slightly negative (Myneni and Asrar, 1994). Multiplicative atmospheric effects are not significantly present in IKONOS satellite multispectral data, as the sensor bands have been selected based upon Landsat Thematic Mapper (TM and ETM+) bands to avoid these absorption effects. Atmospheric transmission is found to be greatest in the imaging portion of the EM spectrum at roughly 0.7µm (Figure 2.3), beyond which atmospheric scattering tends to increase.

Although calculating optical depths due to Rayleigh scattering is computationally straightforward, aerosol scattering poses a more difficult problem because of the significant spatial and temporal variability of tropospheric aerosols (Teillet and Fedosejevs, 1995). Generally, atmospheric aerosol scattering results in an increase in the apparent reflectance of

dark objects and a reduction for bright objects in the image resulting in information loss (Milne, 1988). The goal of atmospheric correction is to reduce the amount of error in estimating the surface reflectance of a target and/or to set a multi-temporal dataset to a common radiometric scale; it is not expected to add new information to the original image (Song *et al.,* 2001).

Atmospheric correction algorithms may be grouped into two different classes, absolute and relative. Each method varies in complexity and utility. Therefore, the employment of atmospheric correction algorithms depends highly on the terms set out by the analyst and the requirements of the end product.

2.3.1.2.1 Absolute Atmospheric Correction

Many atmospheric scattering or haze removal techniques have been developed for use with digital remotely sensed data, several of which can be grouped into a simple dark object subtraction (DOS) method. As a widely used image-based, absolute atmospheric correction (AAC) approach for classification and change detection, DOS assumes the existence of dark objects (zero or small surface reflectance) throughout an image scene and a horizontally homogeneous atmosphere (Song *et al.*, 2001). The tenet behind this technique is based on the minimum DN value for the scene being attributed to the effect of the atmosphere, and this value being subtracted from all pixels in the digital image. DOS assumes a constant haze throughout the image and provides a first-order correction. A different constant DN, however, must be derived and subtracted from each spectral band, with a different set of constraints used from image to image. The DOS technique is somewhat limited by the requirements for very dark pixel values (e.g. deep clear water, or

dark dense forest within the image scene). A problem of using such a uniform correction for an entire image scene is the inclusion of local errors due to non-homogeneity in the atmosphere, and thus should only be employed in studies over relatively small areas (Song *et al.*, 2001).

2.3.1.2.2 Relative Atmospheric Correction

Relative atmospheric correction (RAC) methods differ from absolute techniques in that they do not require estimation of any atmospheric optical properties. Being inherently empirical and based on the assumption of a simple linear relationship among images across time, RAC techniques rely on the ability to identify pseudo-invariant features (PIFs) from the images. Examples of Pseudo-Invariant features would be airport runways, large building rooftops, or parking lots (Figure 2.4), all of which are considered to be spectrally stable over time. One benefit of RAC methods is that they not only correct for the relative difference in atmospheric conditions, but also other unwanted factors such as sensor response and noise (Song *et al.*, 2001).

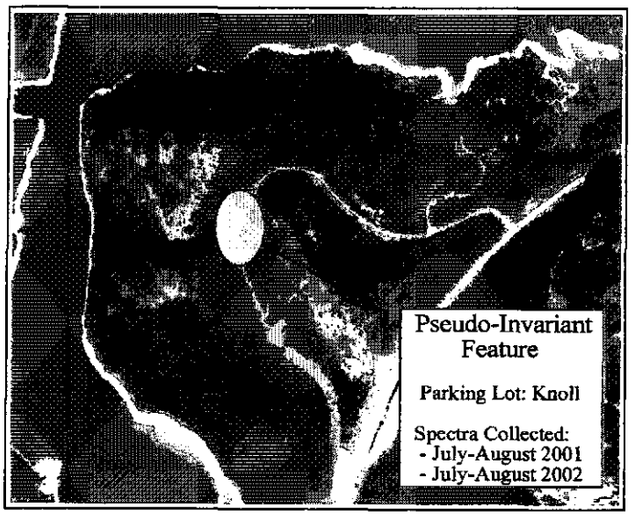

Figure 2.4 Pseudo-Invariant Feature for image RAC.

An optimal atmospheric correction procedure would require no inputs other than that of the digital image. Therefore, no *in-situ* field measurements or ground truthing would be required during the satellite overpass. As a strictly image-based technique, the DOS method is an attempt towards this optimal procedure. The accuracy of the DOS method may not be acceptable for many applications, however, especially those dealing primarily with medium to bright reflectance pixel values due to the requirement for dark image pixels.

Similar to DOS, a dark target (DT) approach to atmospheric correction has been suggested by Teillet and Fedosejevs (1995), with the principle being that the atmosphere contributes most of the signal reaching a sensor from a dark target on the surface of the Earth in the visible and near-infrared wavelengths. Therefore, image pixels from dark targets are indicative of the amount of upwelling path radiance, including atmospheric and surrounding components in each spectral band (Teillet and Fedosejevs, 1995).

As with dark object subtraction (DOS), the DT approach does not take into account atmospheric attenuation, which is a multiplicative effect. Fortunately, IKONOS spectral band ranges have been selected to offset such multiplicative scattering, so attenuation effects are marginal. A key consideration of the DT approach is the assumed value of surface reflectance for the particular dark targets used, in that the histogram lower bound (HLB) for the signal levels in a given spectral band represents dark targets in the visible wavelengths (Teillet and Fedosejevs, 1995).

When repetitive observations of the same area are required, as in forestry mapping, and given that the optical properties of the Earth's atmosphere are not uniform from one location to the next, or over time, compensation for atmospheric effects via some form of

calibration is particularly important (Teillet and Fedosejevs, 1995; Lillesand and Kiefer, 1999). This is due to the fact that atmospheric scattering in the data affects classification results, species identification, forest leaf area index (LAI), temporal analyses, and spectral signature extension (Chavez, 1989).

2.3.1.3 Terrain Correction

It is well known that variations in terrain can significantly affect remotely sensed data. While the accentuation of topographical features has proved useful in many geological applications, and the creation of digital terrain models (DTMs) has enhanced computerized topographic mapping, the effects of topography are generally undesirable for digital image classification and biophysical parameter estimation.

The spectral radiance of an object varies according to position relative to the image sensor. Therefore, the variable image properties extrinsic to the actual terrain reflectance must be removed prior to image analysis, as different slope angles and orientations can result in variable illumination and reflection geometry on the target image pixels (Teillet *et al.,* 1982; Leprieur *et al.,* 1988; Teillet, 1997). Terrain corrections become increasingly important in the quantitative evaluation of multispectral satellite data over rugged terrain to improve accuracies in land-use classification, assessment of erosion hazards, resource management and multi-temporal monitoring (Richter, 1997), as well as biophysical parameter estimation. Such corrections are assisted through the use of Digital terrain models (DTMs) and digital elevation models (DEMs), which are routinely employed to aid in reflectance and radiance corrections in areas of high relief (Leprieur *et al.,* 1988; Richter, 1997).

Several authors have proposed correction algorithms (Teillet *et al.,* 1982; Meyer *et al.,* 1993; Richter, 1997) to compensate for the variability of scene reflectance in mountainous areas. Many are based on the idea that slope and aspect are the most obvious components of the landscape, elevation being negligible (Teillet, 1986; Leprieur *et al.*, 1988). Such effects on scene radiance in alpine regions should be taken into account for reasons as described by Meyer *et al.* (1993) in relation to the BRDF of the object of interest.

1. Atmospheric optical thickness is elevation dependent;
2. Targets may lie in the shadow of surrounding hills or mountains;
3. Slopes can have a reflective brightening effect on adjacent targets; and
4. The irradiance on a pixel is highly dependent on the sun-target geometry through a slope-aspect effect.

An ideal slope-aspect correction would remove all illumination variation as a result of topography in that any two pixels having the same ground reflectance properties would show the same DN regardless of their orientation to the sun's position. In effect, the image scene should lose its relief impression and appear flat (Meyer *et al.*, 1993).

The majority of reflectance models developed for forestry analysis have assumed a Lambertian scattering behaviour. The actual scattering properties of natural surfaces are not easily modeled and differ from the Lambertian assumption to varying extents. It is clear that for analysis in mountainous terrain, any digital image scene will not be Lambertian. However, for simplicity it may be suggested that the majority of surfaces are treated this way, except for areas of extreme topographical relief.

A Lambertian surface reflectance assumption neglects the geometric surface influence and assumes an isotropic reflectance law (Richter, 1997). The reason such an assumption is routinely employed is due primarily to the difficulty in producing an algorithm that takes atmospheric scattering, topographic variation, and geometric properties of different forest species into account. Analyses using a Lambertian assumption are more likely to be valid when analysis is restricted to slopes of less than 25° and effective illumination angles of less than 45° (Teillet *et al.,* 1982).

Three different approaches have been examined in the literature to correct for the varying illumination and reflection geometry caused by topographic variation. The first employs band ratios and statistical transformations like principal component or regression techniques to derive a band specific and scene dependent correction. The second approach employs a radiative transfer code to obtain a deterministic description of the correction of topographic effects (Richter, 1997), which has the advantage of avoiding scene-dependent empirical techniques. The difficulty with this approach is the estimation of radiance, transmittance, and diffuse solar fluxes for each image pixel. General prerequisites to radiometric scene correction are discussed further in Teillet (1986), and Duggin and Robinove, (1990). The third approach utilizes a canopy reflectance model run in multiple-forward-mode (MFM) and is discussed in concert with other reflectance model studies later in this chapter.

Terrain-induced illumination variations often hinder the distinction of forests versus non-forested backgrounds, as well as the ability to separate forest into its major classes. This is especially prevalent when large areas of terrain-induced shadow are present. Four methods to correct the impact of terrain-induced illumination were tested by Meyer *et al.* (1993) in an

attempt to improve the accuracy of forest classifications. These methods tested were the statistical-empirical method, the cosine correction, C-correction and the Minnaert correction.

This general review of terrain corrections serves as a pre-requisite to many remote sensing studies involving mountainous terrain. The research presented in this thesis, however, involved methods for forest biophysical and structural estimation with a minimal set of pre-processing operations. As alluded to earlier, a new method of terrain correction using canopy reflectance modeling will be discussed later. Regardless of the technique employed, topographically induced illumination correction for large-area studies and/or multi-temporal datasets where topographic variation is extreme should result in a reduction of transmittance and backscattering in favor of the intrinsic spectral reflection of the target.

2.3.1.4 Image Normalization

Normalization is a general term that covers several processes designed to equalize multi-date image data such that a direct comparison of corresponding pixel values gives an indication of actual 'true' change (Prakask and Gupta, 1998). Markham and Barker (1986) found that reductions in between-scene variability could be achieved through normalization of solar irradiance by converting spectral ground surface radiance to effective at-satellite reflectance. Other studies (Schott *et al.*, 1988; Hall *et al.*, 1991; Yuan and Elvidge, 1996) achieved varying degrees of success by applying radiometric scene normalization using pseudo-invariant features such as airport runways or industrial areas whose radiative characteristics were not expected to change significantly over time for land cover change analysis. Image normalization is primarily used only when dealing with multiple image sources, or multi-date temporal image analysis, such as for change detection studies.

2.3.2 Classification

In the past, assessment of forest structure through the utilization of orbital remotely sensed spectral data has involved preliminary species classification through appraisal of species-specific spectral signatures and canopy geometry (Katila *et al.,* 2000). Multispectral image classification of calibrated and image corrected data are based on locating patterns of spectral response in relation to land-cover groups known to be present. The process of image classification for the generation of thematic maps involves the grouping of the digital image pixels into classes, or categories based on distinctive patterns of digital numbers (Wulder, 1998). Although MFM-GOMS has been used to perform classification (Peddle *et. al.*, 2003) it is useful to review other, more conventional methods. This section describes the fundamental differences between the most common classification approaches.

2.3.2.1 Supervised Classification

Supervised classification utilizes training sets or regions of interest (ROIs) defined by the analyst through *a-priori* knowledge of the study area. Based on the statistical characteristics of this training data, classification is performed over the entire image scene denoting land cover classes using an algorithm such as maximum likelihood (Hall et al., 2000). Maximum likelihood utilizes a statistical decision rule that examines the probability of a given pixel belonging to a given class based upon its spectral characteristics (Lillesand and Kiefer, 1999). Those pixels having the maximum likelihood of belonging to a specific class or category are then statistically assigned to the class. In effect this produces a thematic

map delimiting the boundaries between each training variable selected (see Appendix 1). Excess noise, un-classified pixels, etc. can then be filtered out to produce a 'clean' map of homogeneous features. The maximum likelihood procedure operates on the assumption of normally distributed data within each class and may be biased by unequally sized training areas (Wulder, 1998). Therefore, care must be taken in respect to the statistical properties of image data, as well as when assigning training regions, or regions of interest (ROIs) to offset such bias.

Ideally, all image pixels will be classified correctly according to their intrinsic spectral characteristics. However, nature is not so precise, and as result of ROI selection error, path radiance effects, and internal algorithm decisions, misclassification of some pixels can occur. An understanding that such errors occur is paramount to the investigation and use of classification maps.

2.3.2.2 Unsupervised Classification

Unsupervised classification does not utilize training classes derived by the analyst. Unlike supervised classification where there must be *a-priori* knowledge of the area being classified, unsupervised classification requires no prior knowledge of the digital image. Classification is derived from statistical algorithms that divide the image into a number of spectral clusters based on statistical groupings present in the data. The analyst then attempts to apply labels to the grouped data to define a final set of land cover classes (Hall *et al.,* 2000). Specification of the number of classes to be applied to the digital image, and statistical range of the pixel values for inclusion to the classes specified is all that is required of the analyst. Statistically-based computer algorithms examine all pixels within the image and

divides the total range of pixel values into the number of classes specified. A further algorithm re-evaluates each pixel and assigns it to whatever class it is most similar from statistical and spectral perspectives. Unsupervised classification is generally applied to imagery where only statistical results are required, or for imagery where there is little to no prior knowledge of the components on the ground (Hall *et al.,* 2000). Of note, however, is that it is often used in large area (regional to national) scale studies where supervised classification is not feasible (e.g. training data requirements). In these and other unsupervised classification studies, the focus becomes that of cluster labeling. There are various ways to achieve this (e.g. Beaubien *et al.,* 1999), with MFM being one approach by which unsupervised cluster labeling can be accomplished.

Improvements in classification accuracy, whether utilizing supervised or unsupervised methods can be attained through the generation of masks that can be 'cut out' or removed from the image prior to classification. A multiple-stage classification technique can additionally be performed to improve accuracy. This method is based on first stratifying or classifying land cover classes of little interest to the researcher and removing them from further analysis. Thus, a reduction in spectral variability occurs and classification is performed in a second run on only the areas under investigation (Hall *et al.,* 2000). Decision-tree algorithms use a related concept based on stratification rules in several classification steps and image passes (Chandra, 2002).

2.3.2.3 Other Classification Approaches

Contextual classifiers allow for classification decisions to be based upon more information than spectral values alone. By utilizing both the spectral and spatial characteristics of a pixel, its contextual information helps drive the classification process. In other words, the nature of the surrounding pixels denotes its classification (Wulder, 1998). Spatial information can be captured explicitly using texture analysis (Peddle and Franklin, 1991), and is important in forestry based remote sensing studies since the spatial patterns of vegetation can provide additional information for classification that is not available using image tone alone.

In mountainous terrain, DTMs have been used to provide elevation, slope, aspect and other morphometric variables that, when used correctly, improve classification accuracy (Johnson *et al.,* 2000). In situations of complex terrain (e.g. mountains) and/or more sophisticated applications (e.g. detailed forest information), where different data variables are required to provide the requisite information, conventional classification algorithms such as Maximum Likelihood do not perform well (Peddle, 1995), primarily since they were never designed for those tasks. Requirements such as differential distribution, statistical assumptions, dimensionality, and data properties are often violated. To address this, alternative approaches such as Neural Networks and Evidential Reasoning classifiers (Peddle, 1995) have been designed to deal with these more complex data sets and environmental applications. In Evidential Reasoning, frequency of occurrence of a given spectral value creates decision rules that enable image classification. This technique has been developed to account for the extreme variability and complexity of environmental data, while Neural Network classification is an attempt to emulate the computational abilities of the

human brain. Peddle *et al.* (1996, 1998) found Evidential Reasoning had higher accuracies, faster run times, and were easier to use than Neural Networks. In a forestry application, Hall *et al.* (2000) used Evidential Reasoning to successfully classify understory spruce in a deciduous dominant forest in northern Alberta using a multisource remote sensing and GIS dataset that could not be analysed using conventional approaches. Additionally, MFM has been used for classification and will be discussed and reviewed later in this chapter. The computational efficiency of classification algorithms, and the choice of classification method ultimately depend on the nature of the data and the analyst's level of knowledge of the image under consideration.

2.3.3 Biophysical Parameter Estimation

2.3.3.1 Vegetation and Spectral Reflectance

Species differentiation using spectral characteristics intrinsic to specific vegetation assemblages is the basis of spectral vegetation classification (http://www-cger.nies.go.jp/, 2003). Estimation of vegetative biophysical parameters, species identification and distribution using remote sensing data is commonly performed using imaging bands calibrated to the red (0.6 - 0.7 μm) and near-infrared (0.7 - 0.9 μm) portion of the electromagnetic spectrum. Variation in the mean spectral response in the red and NIR wavelengths allows for discrimination between species, or respective health of a species to be assessed. Healthy green vegetation can be identified due to its spectral characteristics in the visible and near-infrared wavelengths. Pigments, primarily chlorophyll, absorb electromagnetic energy in the visible wavelengths, while multiple refraction between

intercellular spaces and cell walls results in high net reflectance values in the near-infrared (Sader *et al.*, 1989; Wulder, 1998). As vegetation becomes environmentally stressed, a loss in water content reduces the near-infrared (NIR) reflectance values and an increase in the visible portion of the EM spectrum can be observed.

Wood volume estimation studies have shown that there exists a negative correlation between volume and reflectance in the visible portion of the spectrum, while no clear correlation seems to exist in the infrared. In a study performed by Trotter *et al.* (1997), positive correlation within the NIR tended to occur in closed canopy forests with a high leaf area index (LAI), and negative correlation between volume and wavelength tended to occur in open canopied forests. It is believed that this is due to the higher near-infrared reflectance of sub-canopy vegetation than that which occurs in the canopy itself. Such correlation is attributed to the increased rate of growth and higher water-moisture content in the photo-synthetically active sub-canopy. Reflectance within the NIR can thus be partly attributed to the level of canopy closure and therefore shadow (Trotter *et al.,* 1997).

Whether or not the forest canopy is open or closed, scene elements, or fractions are present within, and contribute to the apparent brightness, of each image pixel. Scene fractions may be sunlit canopy, under-story vegetation, bare wood, shadow, or water, etc. Effects of scene fractions on image pixels increase with a decrease in spatial resolution affecting pixel level classification accuracy. Sub-pixel scene fractions can, however, be extracted from the image, and, as described in the following section, have been found to be useful in biophysical attribute estimation.

2.3.3.2 Spectral Mixture Analysis

Spectral Mixture Analysis (SMA) is a sub-pixel analysis method that is designed to derive the fraction of each component contributing to a given pixel reflectance value (Peddle *et al.,* 2000). It has been shown that SMA is more accurate in estimating biophysical properties of boreal forest biophysical attributes than vegetation indices (Peddle *et al.,* 1999). Biophysical parameters, such as leaf area index (LAI), net primary productivity (NPP), biomass, and structural forest canopy attributes were estimated through the use of SMA and 10 vegetation indices with the result that SMA was the superior predictor at several solar zenith angles (Peddle *et al.,* 2000) because SMA, being a sub-pixel analysis method, extracts information about the forest floor and shadow fractions in addition to the forest canopy while NDVI provides information solely from the mean pixel-level reflectance (Hall *et al.,* 1995).

As the mean reflectance of an image pixel is determined by the spectral components within the pixel image scene, variation in resolution (spatial and spectral) will influence the ability of a given analysis method to reliably extract the individual within-scene components. An increase in spatial resolution of a given pixel often has the effect of an increase in variance so that trees of the same class will often exhibit variable spectral response due to stand position, age, and health (Wulder, 1998). Therefore, spectral mixing resulting from each tree crown represented by a sunlit and shadowed portion, as well as those with visible understory vegetation, will result in variation in the spectral signal return apparent in finer image pixels. Canopy reflectance models incorporate the premise of SMA to derive biophysical parameter estimates from digital imagery.

2.3.3.3 Canopy Reflectance Models

Biophysical modeling in remote sensing entails relating digital image data to biophysical features and phenomena on the ground (Lillesand and Kiefer, 1999). Vegetation canopy reflectance models provide a suite of powerful tools for estimating biophysical information from digital imagery (Abuelgasim and Strahler, 1994) by providing physical descriptions of forest biophysical structure based on the geometry, structure and spectral characteristics of forest stands. These models characterize forest structure and vegetation spectral response with respect to sun-sensor-surface geometry to model the spectral information that would be obtained from a sensor viewing a forest canopy from above (Hall *et al.,* 1995, 1997; Peddle *et al.,* 1997, 1999).

When viewed from above, forest stands comprise several components or endmembers: the canopy, the shadows cast by the canopy, and the background understory vegetation (Peddle *et al.,* 2000). Physical descriptors of forest stands are used as model inputs in terms of characteristic shapes of objects (individual trees), their spatial arrangement and density, and the spectral properties of the forest stand component endmembers of canopy, shadow and background (Li and Strahler, 1985, 1992).

Traditionally, canopy reflectance models have been run in two distinct modes - forward and inverse. Forward mode utilizes physical descriptions of forest stands to compute waveband specific pixel reflectance values as output. Pixel reflectance values are output for each spectral image band along with a set of pixel fractions (sunlit canopy, sunlit background, and shadow) based on structural forest input values (Peddle *et al.,* 2003d) Conversely, inverse mode requires the image reflectance values as input from which the model attempts to solve for the physical descriptors of canopy structure. From a forest inventory standpoint, the output from inversion is sought, however these models do not offer the sophistication present in traditionally forward run

models. Model inversion can also be complex and computationally demanding, with a "no-solution" result not uncommon. Furthermore, many of the more detailed and complex canopy models are not invertible and can only be run in forward-mode, yet this level of model complexity is often required to meet forest information needs (Peddle *et al.,* 2001; Pilger *et al.,* 2002, 2003).

One such non-invertable geometric-optical radiative transfer model is 5-scale. This model represents the merging of two previous models, 4-scale, a radiative transfer model using four scales of forest structure (tree groups, crowns, branches, and shoots), (Chen and Leblanc, 1997) and The Leaf Incorporating Biochemistry Exhibiting Reflectance and Transmittance Yields (LIBERTY) radiative transfer model (Dawson *et al.,* 1998) which simulates the reflectance and transmittance of individual leaves (Peddle *et al.,* 2001b,d). The 5-scale radiative transfer model uses a more realistic treatment of radiative transfer properties providing a superior canopy simulation compared to earlier reflectance models (Peddle *et al.,* 2002) by modeling forest as discrete geometrical objects (cones and cylinders for conifers, and spheroids for deciduous) over a full range of sun-surface-sensor geometry (Peddle *et al.,* 2001b).

As a non-invertable model, 5-Scale required exact model inputs of forest canopy dimension, form, spectral properties and sun-surface-sensor geometry, outputting a pixel reflectance value. Such structural model inputs can be costly to acquire, both in a monetary and temporal sense. In addition, species-specific pixel reflectance values can often be obtained through spectral libraries, or from the image itself. As structural information is the end product sought for forest inventory, such models are limited in their ability to provide biophysical data for forest dimensional analysis.

These problems, among others, were addressed and solved with the development of the Multiple-Forward-Mode (MFM) approach to canopy reflectance modeling (Peddle, 1999).

2.3.3.3.1 Canopy Reflectance Model Studies

While many applications are site and/or sensor specific, the utilization of reflectance models in forestry analysis have proven to assist in classification and characterization of forests with minor discrepancies for national areas (Peddle *et al.,* 2002). Studies performed by Asrar *et al.* (1985), Curran and Williamson (1987), and Friedl *et al.* (1994), among others, have shown that a strong relationship exists between vegetation parameters and canopy reflectance. These relationships, however, have been determined to be time and site dependent and generally require the inclusion of ancillary ground data over large areas to accurately characterize this relationship.

Forests can be difficult to categorize accurately using remotely sensed data alone. The wide array of sizes, shapes, and canopy colours, including seasonal variations of deciduous species and assemblages of a variety of species all impact satellite signal returns (DNs) and thus computed reflectance values. In addition, ground surface, or understory biomass contributes to reflectance distributions used to classify forested terrain (Waring and Running, 1998). Topographic factors such as shadowing and bi-directional reflectance in areas of variable relief, such as mountainous zones, also add to the challenges encountered by reflectance processing of forested terrain (Johnson *et al.,* 2000; Soenen *et al.,* 2003).

Improved methods in the accurate assessment of both spatial distribution and the temporal dynamics of vegetation over large areas are clearly required for large-area inventory studies. Repetitive satellite observations collected over a range of spectral and spatial scales

allow quantitative and qualitative measurement of spatio-temporal dynamics of large vegetative areas for use in studies relating to global change, including, but not limited to, biogeochemical cycles, annual cycles, spatial distribution of plant biomass and respiration, and coupling between the atmosphere and biosphere (Friedl *et al.,* 1994).

Although satellite remote sensing platforms have been used to estimate a number of stand related parameters that have aided in the process of forest inventories, such imagery has primarily been used to augment aerial and ground based data. This is due to the spatial resolution of most orbital sensors being inadequate to fully capture forest stand parameters such as species composition and density with high levels of confidence (Franklin and McDermid, 1993; Wynne *et al.,* 2000). With the advent of high-spatial resolution satellites such as IKONOS, SPOT and Quick Bird, and through the use of canopy reflectance models, forest biophysical parameters which were once limited to aerial or ground-based measurement can now be estimated with moderately high levels of accuracy, albeit at a greater cost than those satellites of 10 years ago.

It is expected that along with the increased spatial and spectral resolution of modern satellite sensor platforms, discrimination and identification of most types of rock, soil and vegetation should be possible, thus reducing the amount of spectral mixing in a given digital image. Problems arise, however, when one includes influences present in real-world measurements, including, but not limited to, viewing angle, atmospheric properties, spectral mixture, vegetative moisture content, and illumination angle (Cochrane, 2000). Additional problems arise through within-species spectral variability and different vegetation assemblages sharing quantitatively similar spectra.

These problems have been addressed and examined through the use of geometric-optical reflectance models. The next section reviews the family of geometric-optical reflectance models in more detail, as this modeling context is a primary focus of this thesis.

2.3.3.3.2 Li-Strahler Geometric Optical Mutual Shadowing Model

Forest canopies in the context of the Geometric Optical Mutual Shadowing model (GOMS) are treated as collections of discrete three-dimensional objects casting shadows on sunlit backgrounds (Figure 2.5).

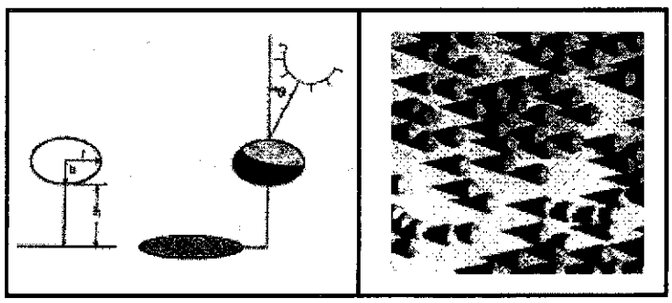

Figure 2.5. Trees as viewed by the GOMS canopy reflectance model.

Specific geometric properties inherent within certain species assemblages, as in the case of conifers, strongly affects stand level reflectance through the inclusion of greater shadow fractions than is in the case with deciduous species (Li and Strahler, 1985). Such geometric properties have led to the progression of optical reflectance models from defining individual trees as cylinders to the use of cones and spheroids in the depiction of coniferous and deciduous species respectively (Li and Strahler, 1985, 1992). The GOMS model was built on previous geometric optical reflectance models allowing for the simulation of pixel-level BRF (Li and

Strahler, 1985). Assuming the image pixels are larger than individual tree crowns, but smaller than physically measured forest stands, the digital image is modeled as a linear combination of reflected energy from tree crowns, shadows, and the forest floor (Johnson, 2000).

Structure input parameters for the GOMS model include: stand density, horizontal crown radius, vertical crown radius, height to crown center, and height distribution. These physical descriptors are coupled with spectral endmember reflectance values for each scene component (sunlit canopy, sunlit background, shadow) for the spectral bands under study. In addition to the aforementioned input/output parameters, GOMS also contains information on slope, aspect, solar azimuth, SZA, and component endmember fractions. In some instances multiple shadow endmembers are used (Li and Strahler 1985, 1992).

2.3.3.3.3 Multiple Forward Mode Reflectance Modeling

Problems associated with invertible and non-invertible models were addressed and solved with the development of the Multiple-Forward-Mode (MFM) approach to canopy reflectance modeling (Peddle, 1999). MFM was introduced as a different way of running canopy reflectance models in which model inversion output was achieved using only forward mode model runs. MFM allows for full advantage of model sophistication and forward-mode speed, with a more robust solution-set that is accessible to any type of canopy model regardless of its level of complexity. Model derived output includes the forest information of interest that is typically provided in a model inversion context. An important aspect of MFM was to provide both this power and simplicity of operation suitable for use at regional and national scales. The multiple forward mode has been applied to 5-Scale and GOMS over a range of Canadian forest types to examine, among other things; partial harvest change in a

New Brunswick forest (Peddle *et al.,* 2003); forest cluster labeling and landcover classification in the Boreal Ecosystem-Atmosphere Study (BOREAS) in Saskatchewan and Manitoba (Peddle *et al.,* 2003bc); biomass and cluster labeling in Newfoundland and Labrador (Pilger *et al.,* 2002; Peddle *et al.,* 2003d); forest height and stand volume estimation (Pilger *et al.,* 2003); and terrain correction (Soenen *et al.,* 2003) in south-western Alberta with successful results.

MFM operates using an algorithm that controls multiple runs of the model in forward mode where the input parameters are systematically varied according to user defined or automatically generated ranges, with all inputs and outputs from each model run stored in a look-up table (LUT) (Peddle *et al.,* 2003ac). The reflectance values output by the model are matched with the remote sensing image reflectance values, with the physical structural model output obtained from the MFM structural input parameters associated with a given match (Figure 2.6).

Another benefit of MFM over forward or inverse mode reflectance modeling is that exact model inputs are not required. Instead, only a model range and increment are used. These are easily obtained or estimated for small or large areas, even if no prior knowledge exists. This approach also enables the spatial variability of forest stands to be more accurately characterized (instead of using one sample mean for a given forward mode input such as crown width, a full range is applied and the best match determined). Consequently, per-pixel analyses are more accurate and representative.

MFM-LUTs also provide a digital library of rich forestry information and serve as a valuable resource of information relating forest spectral response to their corresponding physical attributes. This can be used for direct land cover classification and/or biophysical-

structural estimation, or for a variety of follow-on studies in which selected portions of an MFM-GOMS LUT would be analyzed statistically and/or output in graphical form for further analysis.

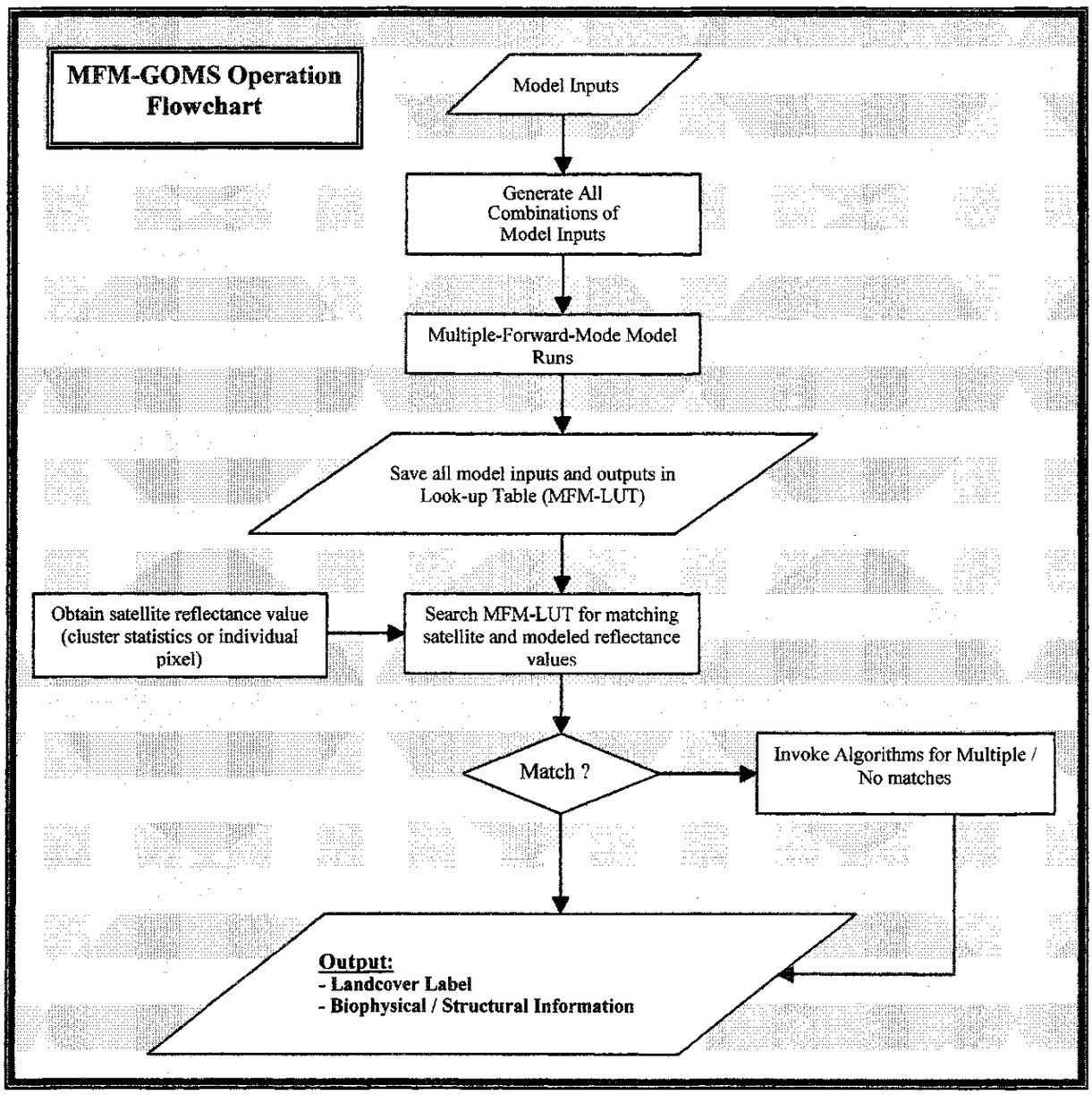

Figure 2.6. MFM-GOMS model operation (adapted from Cihlar *et al.,* 2003).

2.3.3.3.4 Model Evaluation

Model evaluation is based upon inferences that can be made from the model output rather than its correctness (Soares *et al.,* 1995). The validity of modeled biophysical output cannot be separated from the purposes for which it was run, or from the objectives of the analyst.

Several procedures must be followed during model evaluation, including qualitative appraisals of model logic as well as the theoretical and ecological realism of the model. Quantitative examination based upon field measurements and statistical tests for comparison between predictions and observations generated through model usage and sample data independent of those used to fit the model is also necessary to validate and/or appraise the level of agreement of the modeled output to real world measurements (Soares *et al.,* 1995).

Species-specific algorithms must be created to offset for the variability in growth patterns exhibited by different tree species as some, for example, may have smaller canopies but greater heights, variable density within a stand, soil or hydrological differences which affect growth, or topographic conditions affecting access to incident radiation, among others. In an area of dense but varied vegetated growth, the dominant species could be applied to the algorithms with an error matrix incorporated to offset the presence of different species (Herwitz *et al.,* 2000).

It is important to realize that models are mere artifacts whose purpose is to describe, analyse, simplify, or display an ideal system. It is because of these factors that all models will be inadequate or incorrect to some degree. No model, regardless of how complex, can achieve full correspondence with the system it represents (Strahler, 1980).

Vegetation canopy reflectance models, however, allow for the inference of biophysical properties at a much-lessened cost than physical inventory estimates obtained through ground survey. Once a model is proven successful in a variety of applications, the potential exists for adaptation to operate within a wide range of environmental and topographic conditions.

2.4 Chapter Summary

This chapter presented key background reference material associated with the analysis of remote sensing data for biophysical modeling. Although the research presented involves forest volume estimation, background information on forestry was reviewed, albeit minimally, to focus only on the key species present within the scope of this study in the context of remote sensing.

Ecological properties of the forest vegetation used in MFM-GOMS volume analysis presented key differences, not only on structure, but on distribution and site location of the species utilized in this research. Structural differentiation (e.g. canopy dimensions, height) contributes to spectral response variation between species, which allows for digital classification and analysis of variant vegetation assemblages. This spectral information may then be utilized in the update and maintenance of regional forest inventories.

Inventory methods dependent upon aerial and ground-based data collection have been shown to benefit from the use of data from remote sensing satellites due to the addition of spectral information to analog-based inventories. Satellites provide repetitive coverage of large areas with minor geometric variation between temporally different image scenes. This greatly improves upon field-based methodologies of stand volume assessment, including

variable parameterization and computation, when compared to the high cost of ground-survey and independent data extraction through analog means.

Radiometric correction and calibration of satellite data precedes most environmental analysis. This is due to the problematic errors caused by atmospheric and topographic effects and the bi-directional reflectance distribution inherent in digital image pixels. Errors that, if not rectified through radiometric pre-processing, carry through to misclassification and analysis of the digital image scene.

Vegetation is classified through analysis of its spectral response patterns in the red and near-infrared portions of the electromagnetic spectrum. These wavelengths form the basis of vegetation indices and forest classification, and can be utilized to examine, among other things, species distribution, relative health, and canopy structure studies.

Inclusion of a myriad of scene elements within a single image pixel may be analysed through the use of spectral mixture analysis. SMA has been proven to improve both classification accuracy and biophysical structure estimations. The principle of all scene elements contributing to the relative brightness of an image pixel carry through to the development of canopy reflectance models which use the mean spectral response, or endmembers, of image scene components to derive structural and biophysical information from a digital image.

The earliest development of canopy reflectance models and inherent problems in model usage has led to the development of a multiple-forward-mode of canopy reflectance modeling. MFM has consistently been proven to provide reliable results ranging from classification, change detection, cluster labeling, biomass estimation, terrain correction, and in this research will be investigated for forest stand volume estimation.

CHAPTER 3

3.0 METHODS

3.1 Introduction

This chapter outlines the methods and experimental design used in MFM-GOMS modeling of forest stand volume, beginning with a description of the study site and forest dynamics, field methods and equipment. For this study, extensive fieldwork was performed to measure or estimate tree height, canopy closure and dimensions (height and width), diameter at breast height (dbh), and stand age at various elevations, slopes and aspects. These data were used to help guide inputs and validate MFM-GOMS modeling across a variety of topographic conditions. While MFM-GOMS is designed to operate using a minimal set of field data, such validation was required in testing the strength of model output.

Radiometric pre-processing steps of the IKONOS satellite imagery from raw digital counts to reflectance values and calibration and calculation of MFM model inputs from field derived measurements is described in detail, however, the principal methods include the derivation of stand volume equation variables through analysis of MFM-GOMS model output.

3.2 Study Area

The study area was located within Kananaskis Country Provincial Park centered at 51° 1' 13"N - 115° 4' 20"W in the Canadian Rocky Mountains surrounding Barrier Lake, south-western Alberta, Canada (Figure 3.1).

The study area ranges in elevation from just below 1400m at Barrier Lake to 2010m a.m.s.l. at the summit of the 'Prairieview' ridge, covering approximately 75km^2 across a full range of terrain slope and aspects. Average annual precipitation levels for this region vary between 600 and 800 mm with maximum rainfall between May and July. Maximum snowfall occurs between the months of November-December, and March and April. Precipitation during the months of January and February tend to be less, in part as a result of colder temperatures. Temperatures can range between -45° in the winter, to 35°C in summer, and are highly influenced by elevation, slope and aspect. Mean summer temperature is 12°C and mean winter temperature is -7.5°C (Environment Canada, 1997). Climate data collected during the primary field season from the Barrier Lake research station are included in Appendix 2.

In the Kananaskis region, the microclimate ranges from warm and dry (xeric) conditions where trembling aspen (*Populus tremuloides* Michx.) and lodgepole pine (*Pinus contorta* Dougl.) flourish, to cool and moist (mesic) less variable conditions where white spruce (*Picea glauca* (Moench) Voss) prevails. Balsam poplar (*Populus balsamifera* L.) also occurs intermittently within stands dominated by aspen (Achuff, 1992; Kirby, 1973), and in moister sites such as on valley bottoms. Other species present in the study area, to a lesser degree, include Douglas fir (*Pseudotsuga menziesii* Mirb.) and Engelmann spruce (*Picea engelmannii* Parry ex Engelm.).

Kananaskis 2001-2002: Plot and Zone Locations

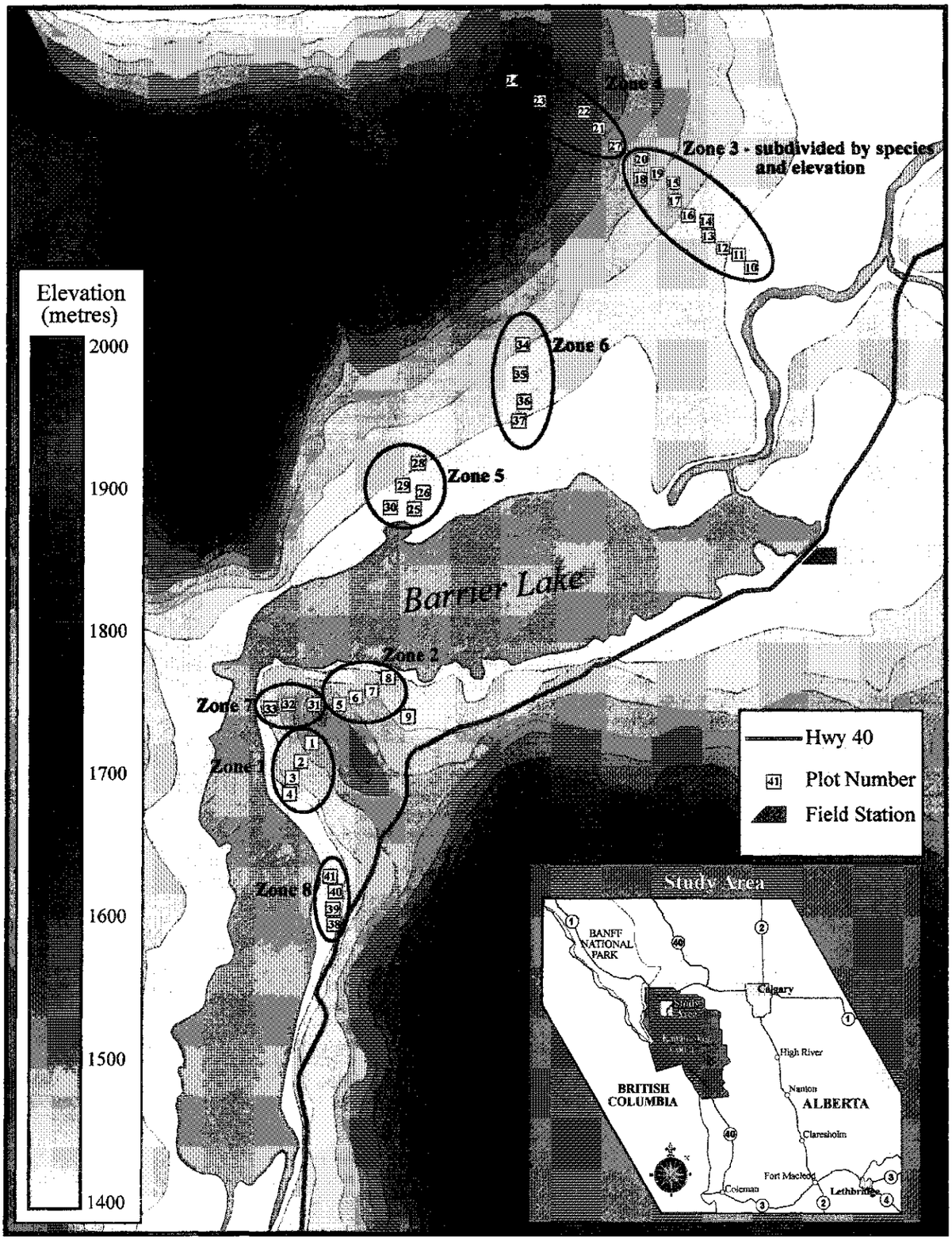

Figure 3.1. Field Plot and Zone Locations (Pilger, 2003).

3.3 Field Data Collection

Field data were collected from early July until late August in 2001 and 2002 at eight distinct areas, or zones, surrounding Barrier Lake (Figure 3.1), with each zone representing a different species/slope/aspect gradient. A total of 41 10m x 10m field plots located in softwood (14), hardwood (21) and mixedwood (6) stands were established throughout the study area. Plot location was based on transects from previously flown (1999) Compact Airborne Spectrographic Imager (CASI) data to facilitate potential future research. Individual plots were aligned according to true north and followed a roughly linear path according to pre-established compass bearings and/or terrain aspect, or circular-clustering within areas of homogeneous stands.

Downslope forest plot aspects (Figure 3.2) indicate the trembling aspen plots under study were situated on southeast facing slopes, while the lodgepole pine plots did not appear to favor specific aspects. This aspect graph can be verified against supervised classification of the area (Appendix 1).

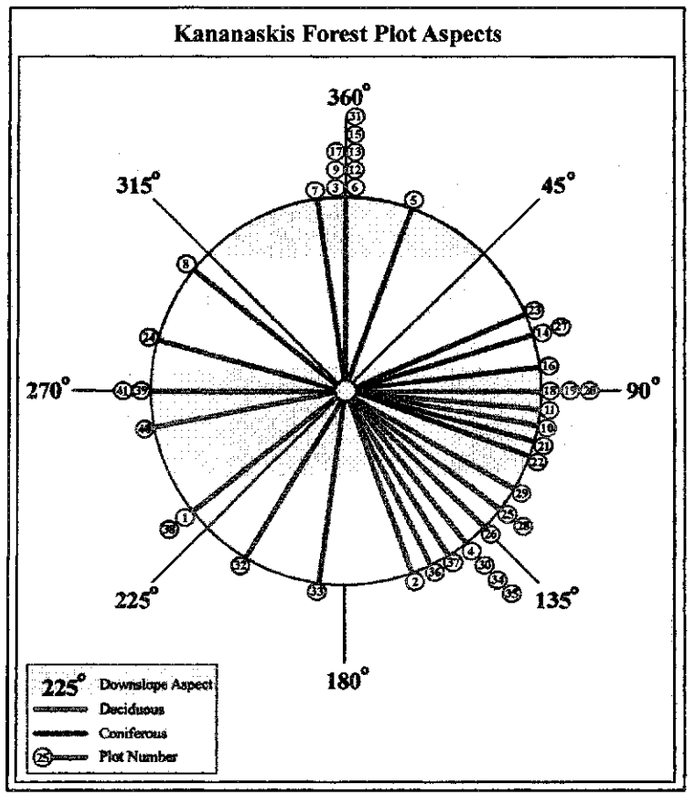

Figure 3.2. Forest Plot Aspects - Kananaskis, Alberta.

Plots were not established at aspects between 300 – 360 degrees primarily due to shadows present on the early morning imagery. Field plot slope and species comparisons were also performed for the knoll area plots of zones 1 and 2 (Figure 3.3).

In examination of the entire study area, elevation was determined to have a greater effect on species distribution than slope, since the majority of aspen plots were situated in lower south/south-east facing areas, while lodgepole pine dominated higher ground regardless of slope or aspect. Although trembling aspen has been known as an early colonizer of sites disturbed by logging, fire, or disease in mountainous areas, no evidence of such disturbance was observed in the field.

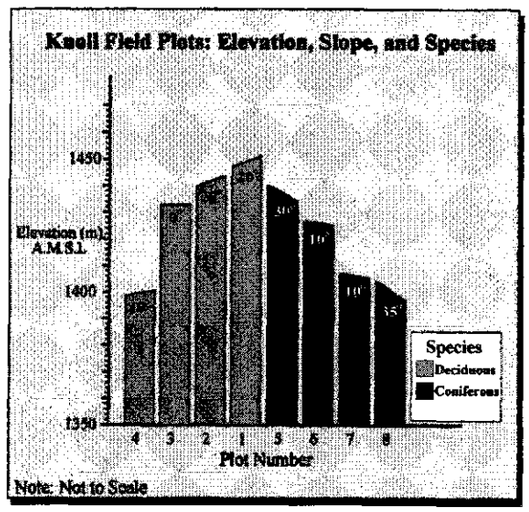

Figure 3.3 Slope/Species/Elevation for Knoll Area Plots.

3.3.1. Manual Measurements

All trees (except overshadowed trees less than 1.5 meters in height, or those directly under larger tree canopies) within each 100 m^2 plot were tape-flagged and relative locations mapped on plot data sheets (Appendix 3) for image-pixel spectral value matching. Individual trunk diameters were measured using a diameter-at-breast-height (dbh) tape (Figure 3.4a), and species noted. Tree height, as well as height to canopy was established using a clinometer (Figure 3.4b) at a geometrically established distance of 15 m from each trunk.

Canopy horizontal width was measured using a tape-rule and prismatic GRS densitometer. Canopy vertical diameter (canopy length) was calculated using the difference between field measured height and height-to-canopy values for each tree within a plot.

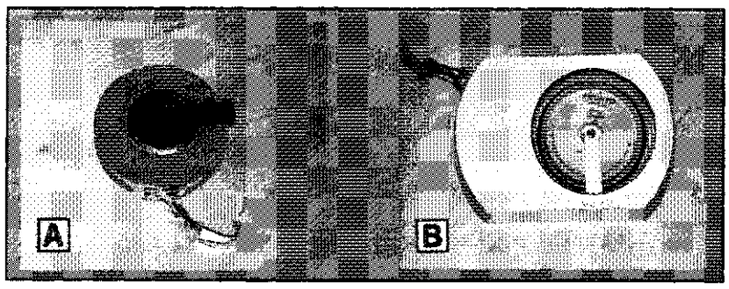

Figure 3.4a - DBH Tape and, 3.4b - Clinometer.

Canopy closure was measured manually in two ways. The first employed spherical densiometer (Figure 3.4c) measurements at the four corners, and center of each plot. Percent canopy closure was calculated through the measurement of 96 points denoting either canopy or sky, multiplying the count by 1.04 to account / adjust for the difference between 96 points and 100 percent coverage value. The second utilized a GRS densitometer (Figure 3.4d) in which three transects running parallel to each other at an equal spacing within each plot were traversed. Measurements taken at one-meter intervals provided a total of 30 measurements per plot in which species, mid-, over-story, or open canopy were charted. The combination of

Figure 3.4c- Spherical Densiometer and, 3.4d - GRS Densitometer.

these two manual canopy measurements provided an estimate, as well as distribution of the vegetative canopy cover for a given area at a given time.

Percent species composition was determined for each species based on tree frequencies within each plot and labeled with the appropriate Alberta Vegetation Inventory (AVI) code. Slope and aspect, determined using clinometer and compass were also measured for each plot.

Handheld Garmin® GPS-12 Global Positioning System measurements were taken at each location to facilitate return navigation to distant plots when climatic conditions were favorable for optical instrumentation. Differentially corrected elevation, plot and trail coordinate information was recorded using the Trimble Pathfinder® Pro-XRS GPS receiver (Figure 3.4e), providing a much higher level of positional accuracy (sub-meter horizontal, 2 meter vertical) than the Garmin® hand-held unit (10 meter horizontal, 50 meter vertical).

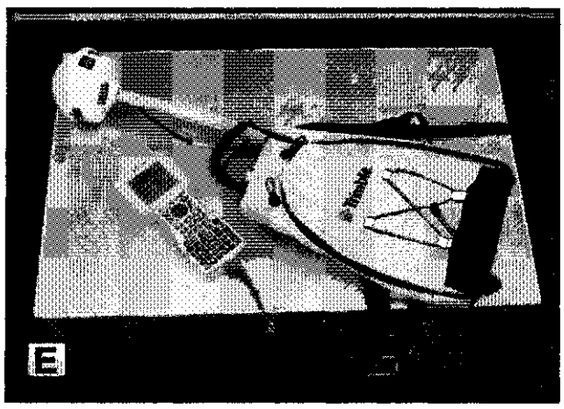

Figure 3.4e. Trimble Pathfinder Pro-XRS GPS receiver and datalogger.

Measurements were taken at the center as well as the four corners of each plot and incorporated into GPS Pathfinder® Office v.2.80 software for placement of forest plots within geometrically corrected digital image scenes. Additional road and trail GPS data were

collected during the 2002 field season for finalizing geometric correction of the IKONOS image data prior to model analysis.

3.3.2 Spectroradiometer Measurements

An Analytical Spectral Devices (ASD) Field-Spec full range spectroradiometer (Figure 3.4f) was used to measure the spectral signatures of dominant forest vegetative species samples from the Kananaskis study area. The basic premise of using spectral signatures is that similar objects or classes of objects will have similar reflective properties of electromagnetic radiation at any given wavelength (http://ltpwww.gsfc.nasa.gov/ , 2002). A spectroradiometer measures the magnitude of reflected energy over a user specified field of view through a lens attached to a pistol grip that may be either hand-held or (preferably) mounted on a tripod. Reflected electromagnetic energy from the target passes through the lens and fiber-optic cable to the main instrument housing where it is split by a holographic diffraction grating into its constituent wavelengths. Three sensors calibrated to specific portions of the EM spectrum (visible, near-infrared and, shortwave-infrared) transfer the percent levels of the incoming radiation to a computer attached to the instrument. Software operating within a Windows-based environment plots the spectra on graphs of reflectance and 'raw DN' energy between 350 and 2500 nanometres. The signature on such a graph can be defined as reflected energy as a function of wavelength.

Prior to capturing spectra, the device must be calibrated against a white reference panel to optimise the light settings for deriving reflectance. For this study, a Spectralon® panel was used since it is a near-perfect Lambertian surface scattering light equally in all directions. The panel is then used to measure irradiance, which is corrected according to

manufacturer provided calibration co-efficients (Labsphere, 2001). Clear cloudless skies are optimal for ground spectra capture as even slight variation in incident radiation can greatly affect the spectral signature of the target of interest. If weather is less than ideal, thin high-cloud conditions can sometimes be acceptable.

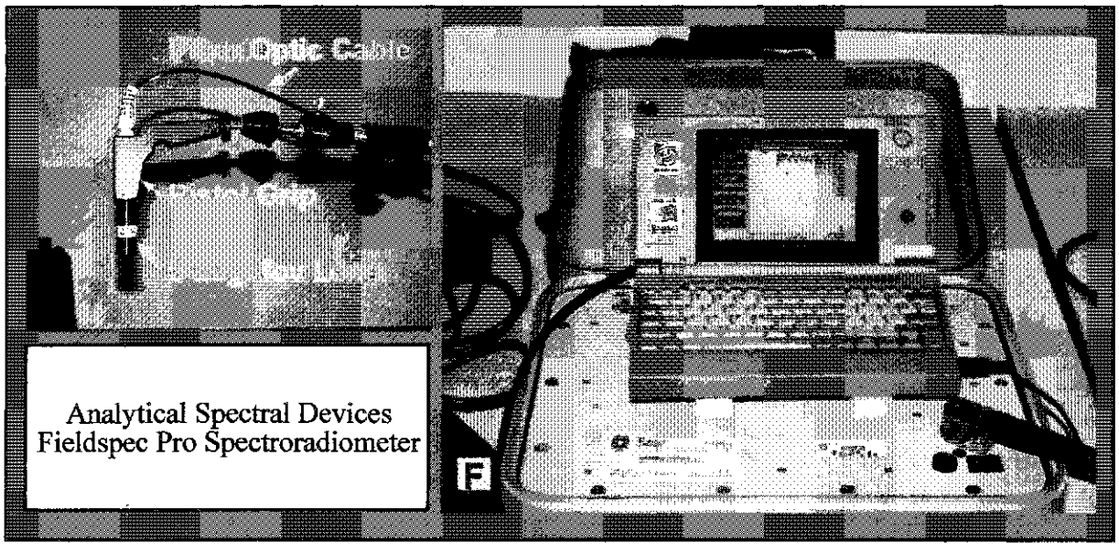

Figure 3.4f. ASD Spectroradiometer

Spectroradiometer data collection was performed under optimal sky conditions on five separate dates over a 4-week period during the 2001 field season at the parking lot calibration site located at the center of the knoll portion of the study area. Since the satellite image acquisition date was unknown at that time, repetitive spectral measurements were required for adequate comparison to the actual image spectral values gathered during satellite overpass. The 'knoll' parking lot served as a pseudo-invariant feature, in that it is considered to be spectrally stable over time, allowing for relative atmospheric correction to be performed. Spectroradiometer readings of forest vegetation types and PIF spectra collected during the summer of 2002 at the same location were compared to spectra available from

previous studies in the Kananaskis region by Johnson (2000) and Davidson (2002) for calculation of species-specific spectral endmembers.

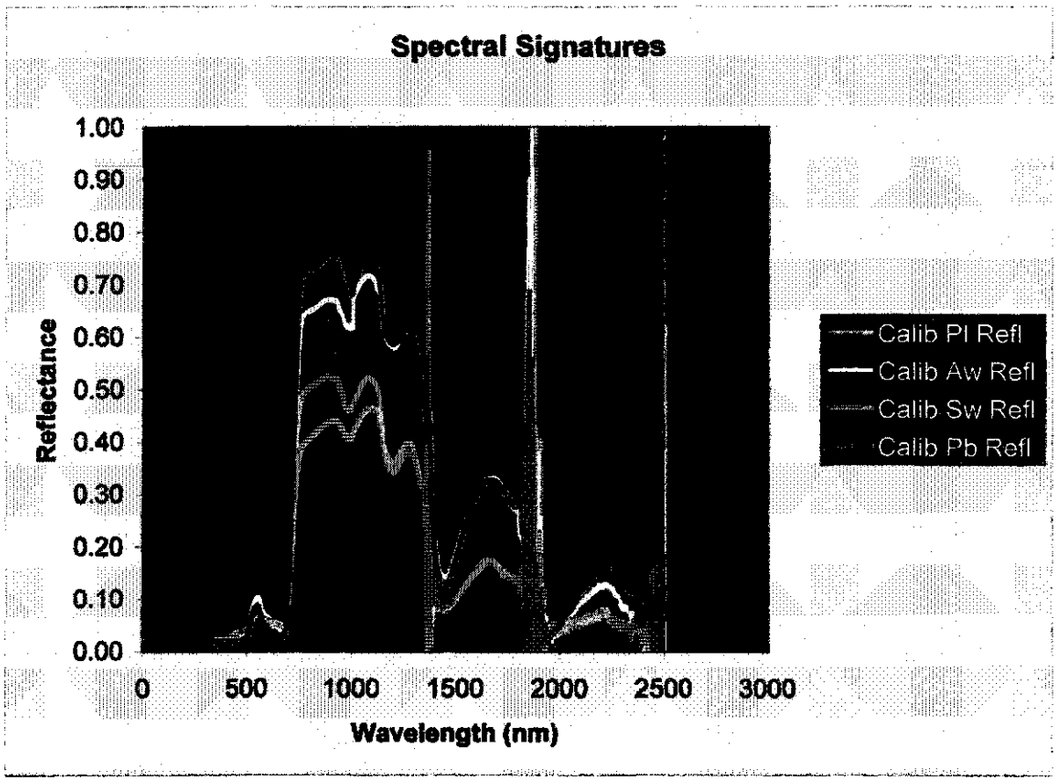

Figure 3.5. Spectral signatures of dominant vegetative species:
Pl (Lodgepole Pine), Aw (Trembling Aspen), Sw (White Spruce), Pb (Balsam Poplar) Note: "spikes" at 1400nm, 1800nm, and 2500nm are due to noise at spectral boundaries between the three sensors.

Each species under investigation had its own distinct spectral signature. As graphed in Figure 3.5, dissemination of specific species may be performed based on the unique spectral response of a forest cover type at a specific wavelength. While all species exhibit similar spectral response in the green portion of the spectrum (500-600 nm), each displayed a distinct variation in the NIR spectral response (750-900nm). Repetitive spectral data collection was performed to account for atmospheric variability between imaging dates in

order to achieve a more representative sample of the spectral characteristics of ground vegetation.

3.4 Remote Sensing data pre-processing

3.4.1 Introduction

Following data collection, several operations were required prior to running the MFM-GOMS model. These included:

- atmospheric and geometric correction;
- reflectance processing;
- cropping the image data;
- calibration of the ASD Spectroradiometer data;
- statistical generation of spectral endmembers from ASD and image scatterplot data and;
- calculation of species specific physical ranges for model input.

In addition to spectral calibration of the image and ASD data, supervised classification (Appendix 1) and NDVI analysis were performed for comparison with the Alberta Vegetation Inventory (AVI) of the study region, field collected data, and eventual model output.

Data extraction and queries of the MFM-LUTs were performed using Microsoft® Excel and Access. Constrained queries against model output reflectance values and image-based reflectance values provided a reasonable range of height estimates from which, with the inclusion of diameter and density functions, plot level stand volume was computed.

Validation was performed by comparing model-derived stand volume variables and field-based measurements to assess the level of agreement and applicability of MFM-GOMS in stand volume estimation for mountainous regions.

3.4.2 IKONOS satellite data

Digital multispectral IKONOS satellite data were acquired on two separate dates, August 16th, and August 27th of 2001. The 16th August data contained atmospheric haze and was therefore discarded from analysis. The August 27th data were collected under clear skies at a solar azimuth of 157.21 and a solar zenith angle of 42.57 degrees. IKONOS captured data in five separate wavelength bands at four metre spatial resolution in the blue, green, red, and near-infrared portion of the EM spectrum, as well as one metre panchromatic data (Table 3.1). At the onset of this research, IKONOS provided the highest spatial resolution of the commercial imaging satellites (Figure 3.6).

Band	Spectral Range (nm)	Bandwidth (nm)	Center (nm)	Spatial Resolution
Panchromatic	525.8 - 928.5	403	727.1	1 m
MS-1 (Blue)	444.7 - 516.0	71.3	480.3	4 m
MS-2 (Green)	506.4 - 595.0	88.6	550.7	4 m
MS-3 (Red)	631.9 - 697.7	65.8	664.8	4 m
MS-4 (VNIR)	757.3 - 852.7	95.4	805.0	4 m

Table 3.1 - IKONOS Spectral Band Characteristics for multispectral (MS) and panchromatic bands (www.spaceimaging.com, 2002).

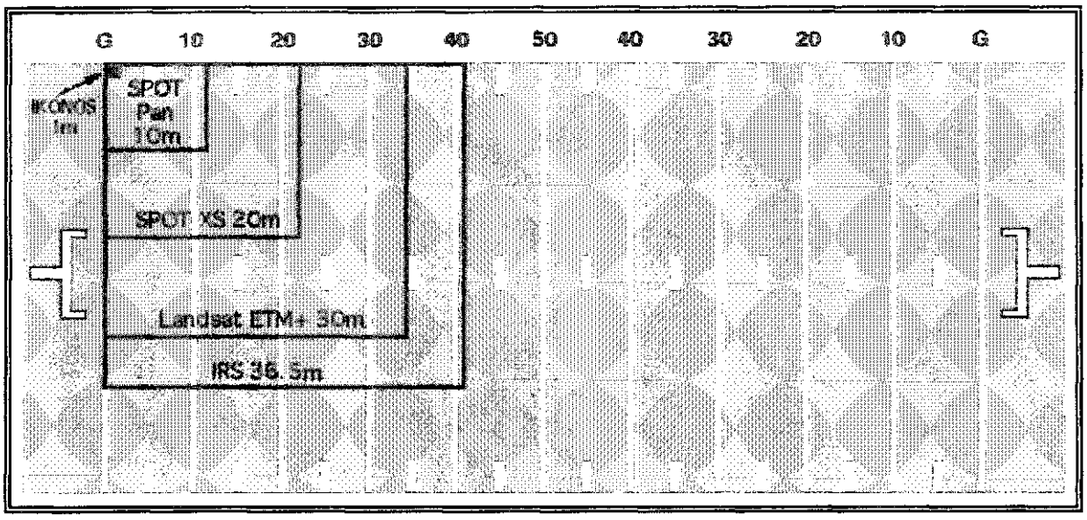

Figure 3.6. IKONOS spatial resolution relative to other sensors

(NFL football field for scale) (http://ltpwww.gsfc.nasa.gov/, 2002).

The IKONOS satellite was launched by SpaceImaging of Boulder Colorado from the Vanderburg Air Force Base in California on September 24th 1999. Orbiting at an altitude of 681 kilometres, with a revisit frequency between 36 and 72 hours, IKONOS' 5 sensors record spectral information between 400 – 900 nanometres. The entire spectral range captured by each sensor cannot be utilized for research as variation, spectral bleeding, and limited reflectance are captured at the periphery of each imaging band. Therefore, reflectance at full width half maximum (FWHM) was utilized for the red and near-infrared image bands in this study. IKONOS captures imagery in 11-kilometer swath widths with a specified ground control based accuracy of 2 meters horizontal, and 3 meters vertical. This accuracy is based upon radiometrically and geometrically corrected data in areas of minimal relief displacement. As the Kananaskis data was acquired within a mountainous area, horizontal accuracy varied between 10 and 60 metres and elevation information had to gathered via in-field GPS.

3.4.3 Radiometric Conversion of IKONOS image data

Conversion of the raw IKONOS satellite data to surface level reflectance was required prior to pixel level image processing. Calibration to reflectance allowed for systematic processing and comparison between the pixel level values at each waveband to the unique spectral characteristics of the reflectance corrected spectroradiometer vegetation species data measured in the field at different dates.

The conversion of the 11-bit image data from raw digital counts to reflectance values for analysis was a two-step process. The first step entailed the conversion from raw digital data to at-aperture sensor radiance. The second step involved conversion from radiance to reflectance.

3.4.3.1 Calibration of IKONOS Imagery to At-Aperture, In-Band Radiance

Image product digital values (DN) of the "raw" IKONOS imagery were converted to physical units of in-band radiance (mW/cm^2-sr) using Equation 3.1 and calibration coefficients (Table 3.2) supplied by SpaceImaging.

$$\mathbf{L_{i,j,k} = DN_{i,j,k} / CalCoef_k} \qquad \text{(Equation 3.1)}$$

Where:

$\mathbf{ijk}$ = IKONOS image pixel ij in spectral band k

$\mathbf{L_{ijk}}$ = in-band radiance at the sensor aperture (mW/cm^2*sr*DN)

$\mathbf{DN_{ijk}}$ = image product digital value

IKONOS Radiometric Calibration Coefficients for 11 bit products values in reflectance: [DN/mW/(cm^2/ster)]				
Production Date	**Blue Channel**	**Green Channel**	**Red Channel**	**NIR Channel**
Pre 2/22/01	633	649	840	746
Post 2/22/01	728	727	949	843

Table 3.2. IKONOS Radiometric Calibration Coefficients. (SpaceImaging.com, 2002).
Note: panchromatic band calibration coefficients not supplied by SpaceImaging.

In-band radiance values calculated from Equation 3.1 required conversion to units of W/m^2*sr*μm, achieved using Equation 3.2 and image bandwidths from (Table 3.1).

The IKONOS spectral radiance in units of W/m^2*sr*μm now becomes:

$$\mathbf{L_\lambda = DN/((CalCoef/10/Bandwidth)} \qquad \text{(Equation 3.2)}$$

Where:

(CalCoef/10)/Bandwidth) {**GRN**} = 72.7 / 88.6 = 0.82

(CalCoef/10)/Bandwidth) {**RED**} = 94.9 / 65.8 = 1.44

(CalCoef/10)/Bandwidth) {**NIR**} = 84.3 / 95.4 = 0.88

All radiometric conversions were performed using ENVI's Band Math interface to the MS-2 (green), MS-3 (red), and MS-4 (NIR) multispectral image bands of the Kananaskis 2001 IKONOS imagery. IKONOS band MS-1 (blue) and the panchromatic band 5 were not utilized in this research, therefore were not converted to reflectance.

3.4.3.2 Radiance to Reflectance

Conversion of IKONOS radiance units from Equation 3.1 and 3.2 to surface reflectance values utilized the formula given in Equation 3.3 (SpaceImaging.com, 2002).

$$\varrho_\varrho = (\pi * L_\lambda * d^2 \ / \ (ESUN_\lambda * \cos(\theta s) \qquad \text{(Equation 3.3)}$$

Where:

ϱ_ϱ = at-sensor reflectance
L_λ = spectral radiance at sensor's aperture
$ESUN_\lambda$ = band dependent mean solar exo-atmospheric irradiance
θs = solar zenith angle
d = earth-sun distance, in astronomical units

$ESUN_\lambda$ values for IKONOS are given in Table 3.3.

Band	$ESUN_\lambda$ values
Blue	1939.429
Green	1847.400
Red	1536.408
NIR	1147.856

Table 3.3 IKONOS band average solar spectral irradiance

The earth-sun distance in astronomical units for the closest date of image capture (Aug 26, 2001) d^2 = 1.02127901047225 (http://sunearth.gsfc.nasa.gov/, 2002), although this level of accuracy is not required for this radiometric correction procedure if it was applied as specified.

The solar zenith angle (SZA) at the time and date of image capture was 47.4334 degrees, therefore: $\cos(\theta s) = 0.6764$, multiplied by the $ESUN_\lambda$ values from Table 3.3 solves for the denominator in Equation 3.3:

$$ESUN_\lambda * \cos(\theta s)\{\mathbf{GRN}\} = 1847.400 * 0.6764$$
$$= 1249.6677$$

$$ESUN_\lambda * \cos(\theta s)\{\mathbf{RED}\} = 1536.408 * 0.6764$$
$$= 1039.2982$$

$$ESUN_\lambda * \cos(\theta s)\{\mathbf{NIR}\} = 1147.856 * 0.6764$$
$$= 776.4635$$

With spectral radiance at the sensor aperture (L_λ) solved using Equation 3.2 and the sun-earth distance supplied, the IKONOS image of August 27, 2001 for the Kananaskis/ Barrier Lake region was converted to at-sensor reflectance. Variations in spectral response due to atmospheric effects were partially corrected for using the reflectance conversion formulae made available from SpaceImaging (2002). However, additional image corrections to surface reflectance to reduce the subtle atmospheric influences were required.

3.4.4 Atmospheric correction of calibrated IKONOS imagery

As the image data utilized for this research encompassed a relatively small area (77 km^2), a simple DOS for atmospheric correction was employed with the assumption of a homogeneous atmosphere across the image scene and validated using PIF spectral data of the

'knoll' parking lot (Figure 2.4). Although terrain variability may result in slight differences in atmospheric optical depth, the extent of the variability was considered minimal for this study. Therefore, DOS was deemed favorable. The pixels employed for the DOS subtraction were selected from dark cast shadows in the south-eastern portion of the image averaged with dark forest pixels from the north-west portion of the study area.

Deep clear water was not represented in the image due in that Barrier Lake is a glacial fed reservoir, with a high concentration of highly reflective suspended particulates. More extensive correction for atmospheric effects would only be required over a much larger area where non-homogeneous atmospheres would be present, or in the case of multi-temporal studies involving change detection (Richter, 1997).

3.4.5 Geometric correction of calibrated IKONOS imagery

SpaceImaging geometrically corrected the IKONOS image scene to latitude/ longitude coordinates prior to data delivery. However, the level of correction was unsuitable for pixel level classification. A field-based Trimble Pathfinder® Pro-XRS GPS measurement at each plot, and along trails, roads and parking areas was utilized to "fine-tune" the image prior to reflectance processing. These measurements were differentially corrected using the Kananaskis field station GPS, combined as a series of data files, and exported into ESRI® ArcView 3.2 GIS software for conversion to integrated shapefile formats and exported to Research Systems Inc. ENVI remote sensing software package for registration. It was found that several discrepancies occurred as a result of GPS noise and scatter that resulted in some irregular paths being recorded in the GPS.

Such GPS signal variation can be attributed to the use of horizon satellites and the effects of interference by surrounding hills and trees within the study area. Spot GPS measurements for plot locations contained a much higher degree of accuracy as multiple signals were clustered and averaged over a 5-10 minute period at each site. Trail and road GPS plots increased in signal error due to signal blocking by dense foliage and extreme terrain variations. Through the combination of several digitized 'paths' for a given trail/road, such discrepancies were reduced. The resultant trails were imported and re-digitized in Arc-View GIS prior to use for geometric correction.

To correct for the lack of GPS ground control points distant from the study area, and to reduce the amount of un-vegetated terrain present in the northern portion of the original image, the image itself was re-sized, centered on Barrier Lake, and registration repeated until the geometrically corrected image fell within 2.5 m, approaching ½ pixel accuracy for all the plots under study.

3.5 Calibration and Calculation of Model Inputs

Model inputs to MFM-GOMS were calculated through the analysis of ground-based field measurements at 8 distinct zones comprising 41 – 100 m^2 forest plots, and spectroradiometer data collected in a controlled setting over two field seasons.

3.5.1 Calibration of ASD Spectroradiometer Data

As previously mentioned, the ASD Spectroradiometer data utilized a Spectralon® panel for in-field calibration. The panel acts as a near perfect Lambertian reflector, reflecting

between 98-99 percent of incident radiation. To correct for the 1-2 percent of scattered radiation which is not taken into account for the generation of spectral libraries, and endmember spectra, calibration must be performed.

Within an Excel spreadsheet, target ASD spectra were corrected using the existing white reference (WR) panel spectra collected in the field and Spectralon® reference calibration coefficients from Labsphere (2001):

$$\textbf{Reflectance} = \textbf{TR} / \textbf{WR} * \textbf{CR} \qquad \text{(Equation 3.4)}$$

Where:

TR = Target Radiance

WR = White Reference (Spectralon® panel) radiance

CR = Spectralon® reference calibration coefficients (Labsphere, 2001)

This equation adjusts for subtle variation in reflectance over the entire recorded wavelength range. To solve for the variant resolution of IKONOS spectral response supplied by SpaceImaging in 5 nm increments with the 1 nm ASD corrected spectra, summary statistics of the 1 nm data in 5 nm increments was performed and the mean reflectance value applied.

3.5.2 Spectral Endmember Selection

Species-specific endmembers were generated in three ways. The reference endmembers utilized spectroradiometer readings of optically thick stacks of new growth vegetation for each species/ ground cover of interest in both direct sun and cast shadow; image endmembers were extracted directly from the image; and the third endmember selection method, also image-based, utilized multi-dimensional scatterplots of pixel regions over known plot regions from the satellite imagery and estimated endmembers based on their location within multi-dimensional spectral space. This last method proved most successful for this research and allowed for model analysis without the direct requirements for field-collected ground spectra. While species-specific assemblages were known at the time of endmember selection, such information could alternatively be collected through the use of supervised classification and vegetation spectral libraries.

The basis of collecting endmembers from multi-dimensional image spectral space can best be explained through the use of an example and diagram. In Figure 3.7, each of the materials has been plotted according to its percent reflectance at two wavelengths for specific spectral bands (in this case, red and NIR). When more than two wavelengths are involved, the plots in multi-dimensional space tend to increase the separability among different materials. This spectral separation forms the basis for multispectral analysis where the goal is to define the bounds of accurately identified data point clusters or spectral endmembers.

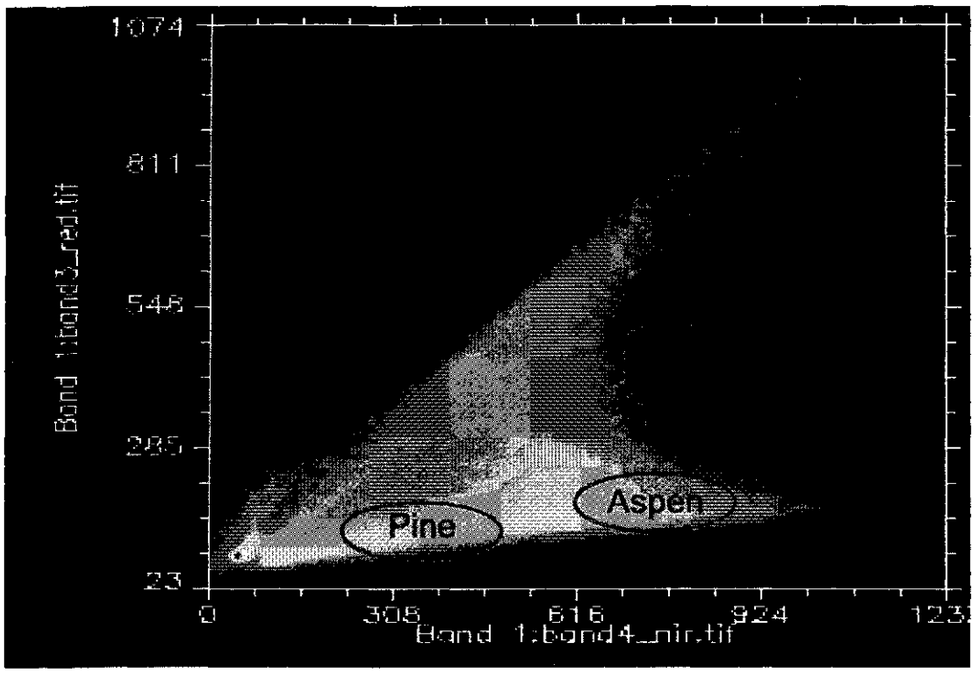

Figure 3.7. Spectral separability of targets using reflectance across two wavebands.

A key benefit of using image-based endmembers is that the spectral characteristics of the component endmembers (sunlit canopy, sunlit background, shadow) are on the same radiometric scale as the image. Therefore, discrepancies in radiometric correction of image spectral properties will not adversely affect the endmember, and subsequent reflectance modeling results.

The presence of "pure" homogeneous pixels of forest canopy within 4 metre IKONOS pixels is rare, however, impurities (shadow, ground fractions, etc.) are acceptable for this research, as the ground vegetation was known at the onset to modeling procedures, and each region to be utilized as either training or validation site consisted of a dominant stand of pure deciduous or conifer species. Therefore, the location of endmembers for this research was determined with respect to prior knowledge of the location of maximum density

stands, and through digital analysis of scatter plots from image spectral space.

Identification of image-based sunlit canopy endmembers consisted of selecting the brightest pixel at the furthest extent of the scatterplot in the red and near-infrared bands for known areas dominated by the forest species under investigation. In terms of the shadow endmembers, close examination of the images revealed a range of shadow pixels whose values were primarily dependent upon their spatial position with respect to tree crowns or mountain slopes. This type of shadow corresponded to the darkest shadows (lowest digital numbers) identified in the original, unmodified IKONOS image bands over forested areas. This is consistent with earlier work involving shadow endmember determination in forest stands by Peddle and Johnson (2000), and was deemed suitable for this research.

3.5.2.1 Multidimensional scatterplot endmember selection

A two-dimensional scatterplot was created with the NIR band along the X-axis and the Red along the Y (Figure 3.7), and using ENVI interactive software fractions, moving a roving window over known homogeneous stands of lodgepole pine and trembling aspen, as well as areas representative of understory vegetation. Polygons digitized from the 2-D scatterplot outer regions highlighted pixels appearing within an image zoom window over known homogeneous species regions. Using an ENVI pixel location/value interface, the pixels highlighted by the region of interest (ROI) were selected and reflectance values for both the NIR and the red band were recorded. This process was repeated over the entire image scene, where known forest stands were located, thus allowing for the highest reflectance values to be selected for sunlit canopy and sunlit background, and the lowest values for shadow.

In comparison with reference endmembers measured in the field with the spectroradiometer, it was found that the 2-D scatterplot-derived values were slightly lower for sunlit canopy in both image bands and higher for shadow reflectance values in the visible (Tables 3.4, 3.5). This method emulates an automated approach inherent within the ENVI remote sensing software environment, but allows for greater operator control in the selection of sites to be utilized for endmember selection.

Reference endmember values		
Trembling Aspen	**IKONOS 3 (%)**	**IKONOS 4 (%)**
Sunlit Canopy	7.22	66.67
Sunlit Background	8.19	46.79
Shadow	0.31	6.92
Lodgepole Pine		
Sunlit Canopy	8.40	52.03
Sunlit Background	12.02	20.91
Shadow	0.32	5.09

Table 3.4. ASD based endmember spectra for dominant species.

Image endmember values		
Trembling Aspen	**IKONOS 3 (%)**	**IKONOS 4 (%)**
Sunlit Canopy	4.17	48.68
Sunlit Background	11.15	38.20
Shadow	1.86	3.88
Lodgepole Pine		
Sunlit Canopy	4.50	37.36
Sunlit Background	10.49	33.29
Shadow	1.09	1.73

Table 3.5. 2-D scatterplot based endmember spectra for dominant species.

3.5.3 Structural Model Inputs

The MFM approach to modeling does not require exact structural parameters for input, but instead only requires ranges of these values. No *a-priori* or field information is required for this, since larger ranges can be specified that would cover any possible stand structure encountered. The disadvantage of utilizing ranged values is that very large model LUTs are produced, however, this can be rectified using a two–stage approach (Peddle *et al.*, 2003b) in which coarse increment steps are first used to define valid structural ranges for more refined modeling. In this study, however, structural information was available from fieldwork, and used to constrain the structural model inputs, thus avoiding unnecessary model runs and excessively large LUTs.

Field data pertaining to physical dimensionality of the trees within each plot were input, by species and area (zone), into an Excel spreadsheet. Each physical input variable per species was generated through analysis of summary statistics. The resultant minimum and maximum, and mean value for each input variable (e.g. height to center of crown) was computed along with an increment value, derived from the standard deviation of the field data physical parameters.

3.6 MFM-GOMS Model Runs

The MFM-GOMS model was run on a UNIX platform linked via telnet to a Dell desktop PC. Three distinct programs contribute to the creation of MFM-LUTs for export.

The first program prompts the user to supply physical and spectral endmember inputs. The structural inputs required by the GOMS model are as follows:

- Density (λ);
- Horizontal crown radius (r);
- Vertical crown radius, or ½ canopy height (b);
- Height to center of crown (h) and;
- Height distribution (dh).

To reduce for error present in outliers, physical ranges (i.e. height to center of crown) were established based on the mean, +/- two standard deviations. This estimate approximates, for example, the height of the taller canopy trees but not unusually tall trees in the stand (Steininger, 2000). Based upon these new minimum and maximum upper and lower bounds and increment specified for each input parameter, the size of the LUT can be determined.

Following the physical parameters, spectral endmember reflectance values for each species and spectral band of interest is required for sunlit canopy, sunlit background, and shadow (Table 3.5). The program then generates all possible combinations of the input parameters and stores each set as a GOMS input file. It also creates a batch file to control all the model runs. The next step in the MFM-GOMS sequence is to run the batch file in which the many (e.g. hundreds or thousands) files generated by the first program are processed. The GOMS model is run one time for each combination of inputs in multiple-forward-mode. The result is a large number of model output files, where each file contains all the model inputs and the modeled reflectance value and component fractions resulting from the forward-mode run. A final program is then run which groups the entire model output into MFM band specific output files, one large file (LUT) per band for each species. Each output file was

then exported into a Microsoft® Excel spreadsheet, where the variable "height" is added through the summation of height to crown center and vertical crown radius for each LUT record, then converted to Access for query.

The model endmember-derived pixel values for each species and spectral band of interest are then matched with image pixel reflectance values using Access queries, resulting in a full range spreadsheet of physical attributes related to the reflectance value of the given pixel. Statistical analysis of the spreadsheet parameters allows for direct estimation of biophysical properties, including species, density and height for the representative vegetative area.

If no matches occur between the image pixel value and the modeled reflectance value, a series of rules is invoked which assigns the nearest matching reflectance value to the LUT range. These rules are constructed as queries in Access using statistically derived reflectance ranges collected from the image data. When multiple matches occurred, a series of specific searches were employed using both image bands and associated LUT variables to reduce the LUT / pixel reflectance value matches. Discussion pertaining to these search limiting constraints are presented later in this chapter.

Initial MFM-GOMS model runs using spectroradiometer reference endmembers (Table 3.4) produced a minimal set of returns (or matches), likely due to the brightness of the endmembers selected, issues with the optically thick stacks of leaves/needle shoots, or with the difference between controlled settings and the natural distribution of standing trees. Therefore, a secondary model operation was performed in which 2-D scatterplot image based endmembers (Table 3.5) were used resulting in entire ranges of produced output in the look-up-tables. Full ranges of output for the LUTs are to be expected, as is the design of the MFM

approach when input variables, specifically endmember spectra is consistent with the digital image pixel values.

3.6.1 Access Queries

Queries performed with the model output LUTs involved user defined searches based on the species assemblages in question. Such searches prompted only the return of records in which all the physical variables (e.g. height, density, crown diameter) ranges between the red band and the NIR band matched. In addition, height returns were limited to those greater than 4 metres, reducing the influence of understory vegetation that would not be visible to the sensor from above. This query resulted in a much more manageable list of possible matches for the species of interest, and justly eliminated understory interference. Example Access search queries for both lodgepole pine and trembling aspen biophysical attributes are detailed in Appendix 4.

3.6.2 Derivation of Height from Reflectance

Statistical analysis of pixels from field plots was performed to obtain mean reflectance values from known forest stand areas. Field plots were located within the digital image through geometrically linked images. The first (NIR, red, green) atmospherically corrected false-colour image with GPS-linked locational plot markers and species composition provided the mean red and NIR reflectance values. The geometrically linked image consisted of a 10-class Maximum-Likelihood supervised classification of the study area (Appendix 1), serving as pre-validation for pixel/ species composition. These pixels were selected based upon field data as well as the reflectance characteristics visible in the

image itself. Summary statistics performed on the image pixels comprising the eight distinct regions or zones (Figure 3.1), were assessed. For each of the eight zones, the mean and standard deviation of reflectance in both the red and NIR bands were extracted and used to confine the search results from the MFM look up tables. By extracting only model reflectance output values which fit within one standard deviation of the pixel based reflectance mean of plot based training areas, then running summary statistics on the returned model height values, comparison between actual field measurements and model output could be performed.

Subsequent analysis entailed Access queries using the mean +/- 1 standard deviation of six pixels at each of the 41 plot locations, thus covering a ground area of 96 m^2 as a reasonable approximation of the area of each plot (100 m^2). These plot specific pixel reflectance values were incorporated into Access for query against the species-specific LUT data for derivation of biophysical attributes during later analyses. Summary statistics of the height variable output from the Access query was performed, and graphically summarized with respect to mean and standard deviation at each plot location.

The reflectance characteristics of a given pixel are dependent upon the scene components at the ground location in question. Certain within-scene objects can greatly affect the spectral characteristics of a pixel, such as the presence of large rocks, fallen trees, bare soil patches, etc. To account for such variance, descriptive statistics were run on the summation of all pixels for the plots (24-36 pixels over 4-6 plots) present within each distinct zonal area for estimation of a more consistent mean reflectance. By increasing the number of image pixels over a homogeneous area, a decrease in the influence of non-vegetated pixel reflectance values which may be present at the plot level occurs, increasing the reliability of

the pixel reflectance(s) being consistent with the forested area in question. In addition, large area (~1 ha) image sampling was examined encompassing the plot locations and surrounding areas as a basis for future research. For these larger areas, descriptive statistics were computed, providing an overall average reflectance value for each imaging band while taking within scene variability into account. It was concluded that the larger image sample significantly reduced the reflectance variability that was present within individual (plot level) samples.

3.6.3 Model operation overview

MFM-GOMS outputs provided the necessary information to derive forest stand volume. The same analysis sequence (Figure 3.8) and set of equations (discussed in following sections), with minor variations, were used for both the field and MFM-based forest stand volume estimates. The key difference with the MFM analysis was that the inputs to these equations were derived using the canopy reflectance model and remote sensing imagery, instead of based upon field measurements. As previously mentioned, the goal of MFM-GOMS for stand volume estimation resides in the ability for structural and biophysical estimation without the requirement for extensive ground data. The field data in this study were used primarily for comparison and validation of MFM results.

For reference and validation purposes the field data set was divided into two sets per major species group (Table 3.6). The less dominant species, balsam poplar (15 samples) and white spruce (92 samples), were dropped from further analysis as they were found to be situated in sparse clusters dominated by trembling aspen and lodgepole pine respectively. Future work may be performed on areas where these two species are more prevalent.

Species	Reference trees	# plots represented	Validation trees	# plots represented
Trembling aspen	130	14	247	15
Lodgepole pine	62	9	189	12

Table 3.6. Reference and validation trees for basal area and volume assessment.

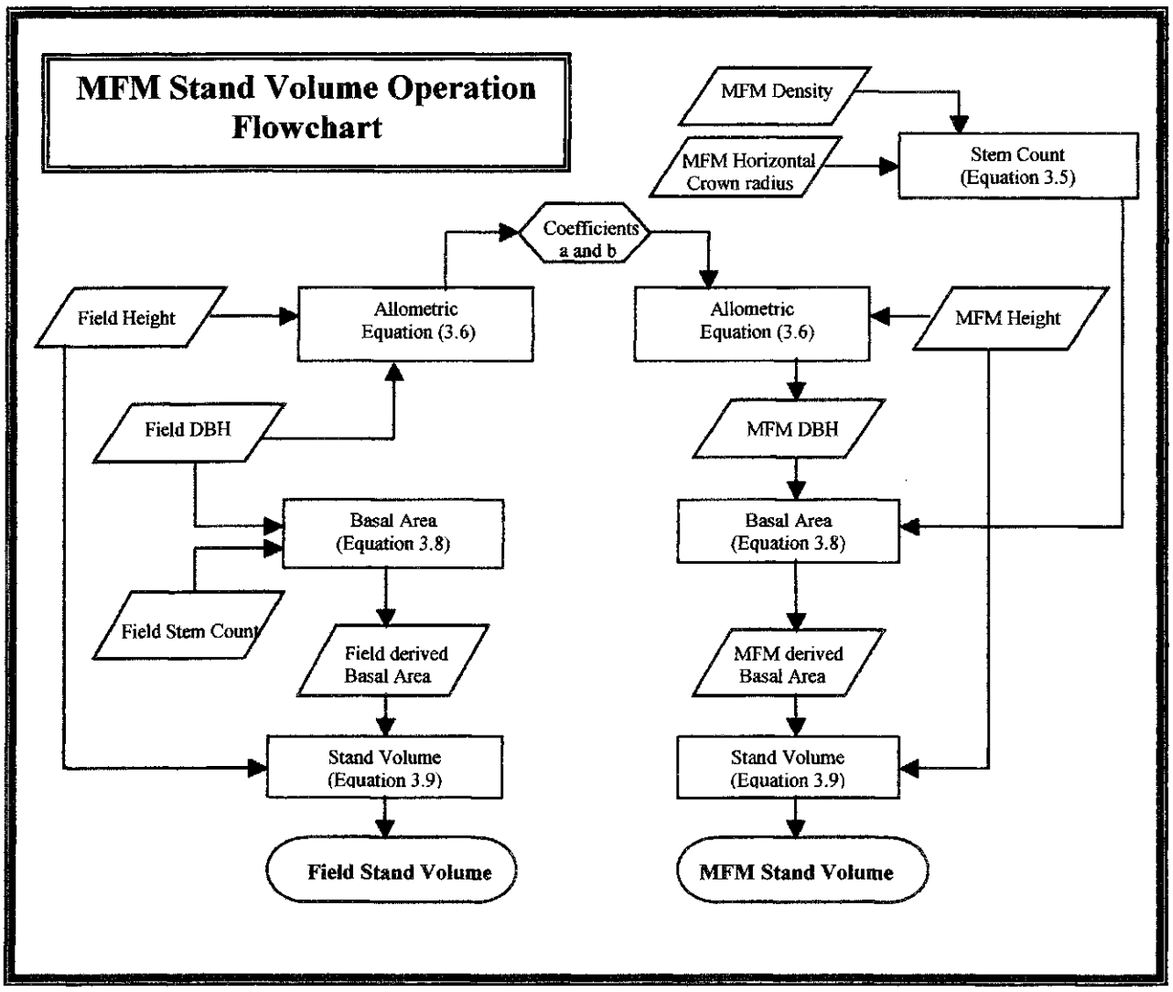

Figure 3.8. Flowchart of model operations for Stand Volume estimation.
(a and b = slope and intercept coefficients derived from scatterplots for Equation 3.6).

3.6.4 Stem count estimation from MFM-GOMS output.

A relationship between physical dimensions of the species of interest was required in order to utilize the MFM-GOMS LUT output to estimate volume. As derivation of height was found to be acceptable using MFM-LUT queries, the second variable in the stand volume equation to be derived was basal area.

Plot, or stand basal area, is defined as the summation of the diameter at breast height (dbh) of all trees within a given area, and is usually expressed in terms of m^2/ha.
The first step in estimating stem diameter, or dbh, was to calculate density and mean canopy radius. Two generalizations were required to be made in this process:

1) the assumption of an even density distribution and
2) non-overlapping tree crowns.

While such assumptions rarely occur in nature, they were made to facilitate the estimation procedure without the requirement of extensive field data.

3.6.4.1 Density and Horizontal Crown Radius Calculation

Using values from plot reflectance tables, mean reflectance +/- 1SD for each of the RED and NIR bands were run through Access query with MFM-LUTs for each species-specific plot. Reflectance values were extracted directly from the digital image and queried against MFM-GOMS look up tables for the dominant species in each location. The query employed for each of the 41 plots matched output that fit within the mean +/- 1SD of the pixel reflectance values for each plot, tabulated during an earlier analysis.

Matching for density and horizontal crown radius was based on the reflectance ranges specified as well as matching between mean heights as output in the MFM-LUT.

Columns containing matching values for the reflectance inputs (density and horizontal crown radius) were analysed using descriptive statistics in Excel, generating the mean values for the variables. The mean values for density (D) and horizontal crown radius (r) were exported to a separate Excel worksheet for tabulation.

3.6.4.2 Estimation of trees per unit area

Estimation of number of trees per $100m^2$ area was performed for each plot, a combination of all plots per zone, and for a larger (> 1 ha) portion of the surrounding forest, including the plots for each particular zone, using the following formula:

$$\mathbf{T = (A * D) / (100\pi r^2)} \qquad \text{(Equation 3.5)}$$

Where:

T = Stem count for plot area

A = Plot area (m^2)

D = MFM density (λ) mean return (%)

r = MFM horizontal crown radius mean return (cm)

This formula derives the maximum number of trees, assuming no crown overlap, that a given area can sustain by multiplying the plot area by the MFM model derived density (λ) mean return, and dividing this product by the mean MFM derived canopy size (πr^2). The

multiplication of the denominator by 100 is used to equate the MFM density (D) from a percentage to decimal value. Output values for the number of trees that were expected to occupy a given plot were validated against actual field-derived measurements and utilized in the derivation of basal area.

3.6.4.3 Height – Stem Diameter Relationships

Diameter at breast height (dbh) is neither an input nor output variable used by MFM-GOMS. As this value is instrumental in the derivation of basal area it must be derived through alternate means.

Relationships between field-measured height and diameter at breast height (dbh) were examined using SPSS and Excel statistical regression models to establish a level of correlation that could be applied to MFM-GOMS model output in the derivation of stem diameter for basal area calculations. Through the analysis of scatterplots and non-linear regression, a range of variable input dbh values were assessed from field validation data and applied to mean MFM-GOMS height ranges.

Allometric equations play an important role in predicting total aboveground biomass, as well as the height of trees if dbh (diameter at breast height) is known. Typically, an increase in dbh will correspond to an increase in height and biomass following a power curve (Peng, 2001). Several non-linear statistical relationships were examined for predictive ability and a logarithmic function (being strongest overall) was applied to obtain intercept and slope coefficients (a and b), which were applied with MFM height values as follows:

$$\mathbf{LN(dbh) = LN\ \beta + \alpha\ LN(height)} \qquad \text{(Equation 3.6)}$$

Where:

dbh = Diameter at breast height (cm)

Height = MFM-GOMS modeled mean height value (m)

β = intercept

α = slope

MFM-GOMS based dbh values were then extracted as centimeter values by inverting the log function as follows:

$$\mathbf{dbh} = e^{(\mathbf{LN(dbh)} + \sigma\text{^}2\ /\ 2)} \qquad \text{(Equation 3.7)}$$

Where:

dbh = Diameter at breast height (cm)

e = base for conversion from logarithmic to arithmetic units

σ^2 = sample variance of the logarithmic equation

Bias introduced as result of utilizing a logarithmic relationship where inversion of LN(dbh) results in an underestimation of dbh by representing the median, not mean value, has been corrected for in this analysis (Equation 3.7) using conversion procedures from the logarithmic to arithmetic units as described by Baskerville (1972) and Parresol (1999).

3.6.5 Basal Area Calculation

Basal area (BA, in m^2/ha) is calculated using the following equation adapted from Brack (1997), in which c is area (in hectares) and the constant (π / 40000) corrects for the difference in units (cm and m) and converts diameter to radius.

$$\mathbf{BA = (\pi / 40000) * (\Sigma\ dbh^2 / a)} \qquad \text{(Equation 3.8)}$$

Where:

BA	= Stand Basal Area (m^2/ha)
dbh	= diameter at breast height
a	= area (hectares)
π / 40000	corrects for the difference in units (cm and m) and diameter to radius

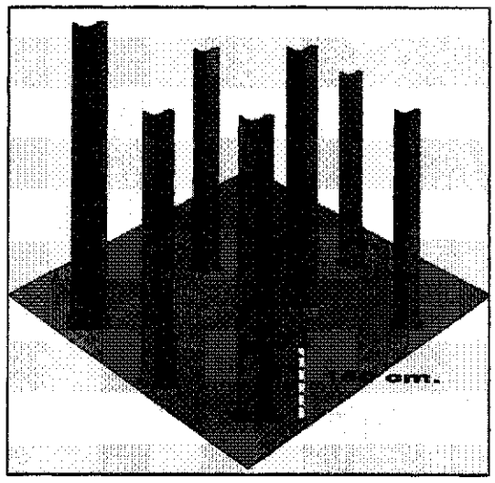

Figure 3.9 Basal Area - dbh calculation. modified from Brack (1997).

As the field plots in this study comprise individual areas of 100 m^2, utilization of a basal area equation based on hectare measures was unfounded. Therefore Equation 3.8 was simply modified to calculate field-based basal area at the plot level by dropping the variable a, providing the total basal area per plot in units of m^2 / 100 m^2.

MFM-based basal area utilized the variable (T), calculated using Equation 3.5 to replace the field-measured sum of all dbh values per plot (Σ). Mean MFM-derived dbh values were estimated by substituting the field height values with MFM-derived height

values in Equation 3.6, inverting the equation and solving for dbh (Equation 3.7), resulting in a new MFM-based basal area formula (Equation 3.9).

$$\mathbf{BA = (\pi / 40000) * (T*dbh^2)} \qquad \text{(Equation 3.9)}$$

Where:

BA = Plot basal area (m^2/100 m^2)

dbh = diameter at breast height (cm)

T = MFM-derived mean stem count per plot

π / 40000 corrects for the difference in units (cm and m) and diameter to radius

Basal area was calculated for homogeneous lodgepole pine and trembling aspen plots using both field and modeled data. Resultant basal area values were employed along with MFM and field-measured height values for plot level stand volume estimation.

3.6.6 MFM-GOMS Stand Volume Estimation

Stand volume can be computed as the product of tree height and basal area (Equation 3.10) and is generally measured in terms of cubic metres per hectare. As the basal area measurements in this research reflect the 100 m^2 plot sizes used for field validation, stand volume measures have been computed in terms of m^3 / 100 m^2.

$$\mathbf{SV = H * BA} \qquad \text{(Equation 3.10)}$$

Where:

SV = stand volume (m^3 / 100 m^2)

H = height (m)

BA = basal area (m^2 / 100m^2)

Stand volume at the plot level computed using Equation 3.10 for MFM-derived variables was validated against field-measured values and graphically tabulated and summarized, along with all other MFM and field derived variables in Chapter 4.

3.6.7 Overview of steps for volume assessment

This section serves to review all steps performed in the estimation of stand volume from multispectral IKONOS imagery using the Geometic Optical Mutual Shadowing canopy reflectance model in Multiple-Forward-Mode.

Image data pre-processing

Step 1) Conversion of image data to reflectance

Step 2) Atmospheric and/or terain correction of image data

Step 3) Geometric correction of image data

Field validation data

Step 4) Ground based physical measurements

Step 5) Ground based optical measurements - for endmember selection

Laboratory analysis -MFM-GOMS

Step 6) Derivation of 2-D image based spectral endmembers

Step 7) Derivation of physical descriptor values for MFM-GOMS (height, height to canopy, horizontal and vertical crown radius, stand density, height distribution)

Step 8) MFM-GOMS model runs with endmember and physical range inputs

Step 9) Conversion of MFM-LUT text files to Excel and Access spreadsheets

Step 10) Pixel level reflectance value collection

Step 11) Access queries to search for matches in the MFM-LUTs against image reflectance values.

Laboratory analysis – MFM-GOMS LUT variable estimation

Step 12) Height derivation from pixel specific matched LUTs.

Step 13) MFM height validation against field data

Step 14) Stand density and mean crown radius extraction from plot specific LUTs

Step 15) Estimation of trees per unit area

Step 16) Height-dbh relationship calculation (logarithmic) for co-efficient derivation

Step 17) dbh estimation from MFM-GOMS height estimates

Step 18) MFM-GOMS basal area estimation from steps 14 through 17

Step 19) MFM-GOMS basal area validation against field derived basal area

Step 20) MFM-GOMS derived stand volume estimation using output from steps 12 and 18

Step 21) Validation of results from step 20 to field derived stand volume.

3.7 Chapter Summary

This chapter presented the operations and procedures employed during all stages of this research. Although the premise of MFM-GOMS for biophysical and structural information extraction is to operate with a minimal amount of field data, such data collection provided both model inputs and measurements for validating the MFM-GOMS biophysical estimates

Reflectance pre-processing, and geometric rectification of the IKONOS remote sensing data corrected for pixel level reflectance at specific plot locations, as well as allowed for the extraction of species-specific image-based spectral endmembers. These image-based spectral endmembers provided superior results when compared to ASD spectroradiometer field-measured spectra of the species under investigation. The utilization of image-based endmember spectra also ensured that the endmembers and image were on the same radiometric scale, thus reducing spectral error propagation.

MFM-GOMS model runs using structural input minimum and maximum values, along with species-specific endmember data, provided a full range of model output representative of a variety of band-specific reflectance values characteristic of field-measured spectra relating to healthy vegetation. By matching between both the red and NIR-based model LUTs, biophysical and structural parameter estimation from the model LUTs was performed.

Mathematical and statistical transformation of MFM-LUT output allowed for the derivation of stem counts, and dbh through statistical relationships between other modeled output. This analysis allowed for the derivation of structural information not part of the model output for plot level basal area estimates. Such estimates, when coupled with MFM derived height values, provided a measure of stand volume at the 100 m^2 level.

MFM-derived structural estimates were compared and validated against field measurements at each 100 m^2 plot location by species. Variation between field and MFM-modeled variable output at the plot level was summarized and mean output values produced. These mean values, along with plot specific biophysical structural parameters are presented in detail in the following chapter.

CHAPTER 4

4.0 RESULTS AND DISCUSSION

4.1 Introduction

This chapter presents all results generated from the methods presented in Chapter 3. Field-derived inputs (Tables 4.1 - 4.2) were combined with spectral endmember data (Table 3.5) and run in multiple-forward-mode using the geometric-optical-mutual-shadowing model. Look-up tables of biophysical and structural information, created by the MFM-GOMS model, were then matched with mean spectral reflectance values obtained from plot locations established on the radiometrically corrected digital IKONOS image.

Several intermediate parameters were derived to enable stand volume to be modeled, including: height, stem count, dbh, and basal area. Tabulation and graphical summaries of each stage of analysis describes the relative level of agreement between MFM and field-measured variables. A final discussion section presents an evaluation of the full modeling capability in relation to the specific forest species under investigation.

4.2 Field Results

Field measurements were statistically summarized based upon species, plot, and zone within the study area. The mean +/- two standard deviations for all species-specific physical measures across the entire study region allowed for minimum and maximum values to be extracted for input to the MFM-GOMS model (Tables 4.1, 4.2). The use of two standard

deviations from the mean allowed for a full range representation of the structural nature of the vegetative species to be represented, while excluding extreme high and low outliers. Increment steps were selected based upon logical divisions of the field data to constrain the MFM-LUTs to a manageable size.

Structural Ranges Trembling Aspen				
Parameter	**Min**	**Max**	**Step**	***n***
Horizontal crown radius (r)	0.5	4	0.5	8
Vertical crown radius (b)	1.5	6.5	0.5	11
Height to center of crown (h)	3.5	18.5	1	13
Height distribution (dh)	16	16	1	1
Density (D)	5	95	10	10
		LUT size (returns)		**11440**

Table 4.1. Physical MFM-GOMS inputs – trembling aspen.

Structural Ranges Lodgepole Pine				
Parameter	**Min**	**Max**	**Step**	***n***
Horizontal crown radius (r)	0.5	4	0.5	8
Vertical crown radius (b)	1.5	9.5	0.5	19
Height to center of crown (h)	5	11	1	9
Height distribution (dh)	16	16	1	1
Density (D)	5	95	10	10
		LUT size (returns)		**13680**

Table 4.2. Physical MFM-GOMS inputs – lodgepole pine.

Although field measured density fell within the range of 25 to 60 percent for all forest plots, a full range was employed in the modeling procedure to account for extremely dense and sparse stands which may be present in a larger context over the study area. The value for

height distribution (dh) was calculated by running simple summary statistics for all field measured heights of all trees per species over the entire study area. The standard deviation of each species' overall height value was multiplied by four, following the specifications for using the GOMS model (Lucht, 1996), resulting in dh values of 16.5 for aspen and 15.5 for the pine samples.

4.3 Height estimates

Mean plot height was estimated using summary statistics of plot-specific MFM-LUTs matched with mean plot reflectance values, and validated against mean field-measured heights (Table 4.3). Mean MFM-derived height estimates statistically derived using all plots were found to slightly underestimate field-measured values by 1.6 m with an absolute mean difference of 2.6 m.

Mean reflectance values from three plot locations (Plot 15, 16, and 27) returned zero matches with either of the lodgepole pine or trembling aspen MFM-GOMS LUTs. As height is a key variable in stand volume estimation, these plots were subsequently dropped from further analysis.

Variation between MFM and field-measured mean height variables are clearly defined when examined graphically (Figure 4.1). An underestimation by MFM-GOMS for height occurs for most plots, with the greatest discrepancy occurring for plots composed of mixed-species assemblages (plots 11, 14, 30, and 33). Conversely, overestimations by MFM derived height were found to occur at plots with south-facing aspects (Figures 3.1, 3.2). Potential for discrepancy between modeled and measured height estimates, as well as for all other computed variables are presented in the discussion section at the end of this chapter.

Plot #	MFM Ht (m)	MFM StdDev (m)	Field Ht (m)	Field StdDev (m)	MFM-Fld Height Diff (m)	Absolute Height Diff (m)	Species Code
1	12.8	4.7	10.5	4.2	2.4	2.4	Aw
2	13.7	4.8	11.9	2.6	1.8	1.8	Aw
3	12.8	4.8	17.5	0.8	-4.7	4.7	Aw
4	13.7	4.8	13.7	4.1	0.0	0.0	Aw
5	14.6	3.1	16.4	7.1	-1.8	1.8	Pl
6	14.7	3.0	16.8	5.1	-2.1	2.1	Sw
7	14.7	2.9	16.7	3.7	-2.0	2.0	Pl
8	14.6	2.9	17.0	2.0	-2.4	2.4	AwSw
9	13.1	4.8	11.2	1.9	1.8	1.8	Aw
10	13.4	4.8	13.1	4.7	0.3	0.3	Aw
11	13.1	4.4	20.1	4.1	-7.0	7.0	AwSw
12	14.7	2.8	14.0	3.5	0.6	0.6	Pl
13	14.7	3.1	15.6	3.7	-0.9	0.9	Pl
14	14.1	3.1	19.0	1.4	-4.9	4.9	PlAw
17	12.8	4.7	15.4	2.6	-2.6	2.6	Aw
18	12.8	4.8	17.5	1.5	-4.7	4.7	Aw
19	13.4	4.9	16.1	2.1	-2.7	2.7	Aw
20	12.9	4.8	16.3	1.6	-3.5	3.5	Aw
21	14.7	3.0	17.1	2.3	-2.4	2.4	Pl
22	14.6	3.0	16.3	4.3	-1.7	1.7	Pl
23	14.7	3.0	18.8	3.4	-4.0	4.0	Pl
24	14.6	3.0	15.9	4.3	-1.3	1.3	Pl
25	13.5	4.8	18.8	1.3	-5.3	5.3	Aw
26	13.6	4.8	17.3	1.0	-3.7	3.7	Aw
28	13.8	4.1	17.6	2.1	-3.9	3.9	Aw
29	12.9	4.8	17.8	2.9	-4.9	4.9	Aw
30	12.9	4.8	18.3	1.1	-5.4	5.4	AwPb
31	15.0	2.9	9.9	2.4	5.1	5.1	Pl
32	14.9	3.3	14.0	3.1	0.9	0.9	PlSw
33	14.4	2.9	8.0	2.9	6.4	6.4	PlSw
34	13.4	4.8	14.4	3.2	-0.9	0.9	Aw
35	13.0	4.7	12.3	2.1	0.7	0.7	Aw
36	13.0	4.7	13.6	1.4	-0.6	0.6	Aw
37	13.2	4.8	16.5	2.4	-3.3	3.3	Aw
38	13.5	2.2	14.4	4.2	-0.9	0.9	Pl
39	13.4	1.4	14.4	4.1	-1.1	1.1	Pl
40	12.5	4.7	13.8	1.3	-1.3	1.3	Aw
41	15.0	3.0	14.3	3.8	0.6	0.6	Pl
			Mean Difference		**-1.6 m**	**2.6 m**	
			Standard Deviation		**2.9**	**1.9**	

Table 4.3. MFM vs. field-derived height estimates for all plots.

SPECIES CODE: Aw: trembling aspen, Pl: lodgepole pine, Sw: white spruce, Pb: balsam poplar

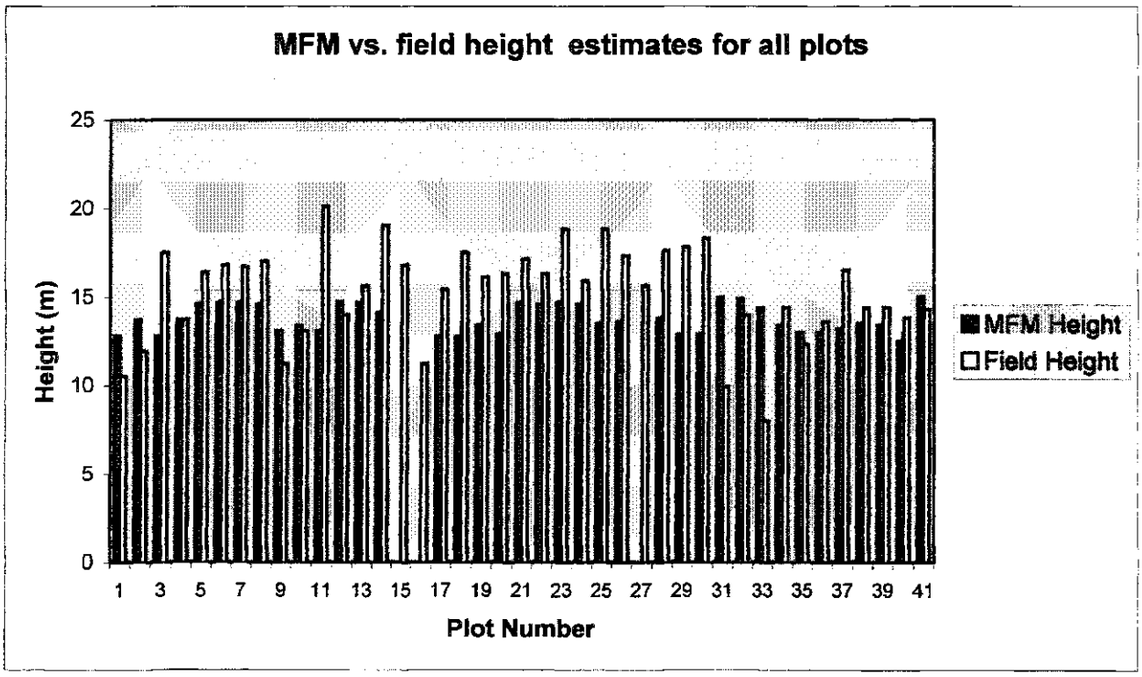

Figure 4.1. Mean MFM vs. field-derived height estimates for all plots.

Note: Plots 15, 16, and 27 did not return MFM reflectance matches; therefore no height variable was calculated.

Plots were separated by species with analysis run independently to determine whether species type had an influence on the relative level of agreement between MFM and field-measured variables. For height estimation, Tables 4.4 and 4.5 indicate a higher level of agreement between lodgepole pine dominated plots than for trembling aspen. A graphical summarization of these results (Figures 4.2, 4.3) clearly identifies the variation between species-level height agreements.

Trembling Aspen						
Plot #	MFM Ht (m)	MFM StdDev (m)	Field Ht (m)	Field StdDev (m)	MFM-Fld Ht Diff (m)	Absolute Ht Diff (m)
1	12.9	4.7	10.5	4.2	2.4	2.4
2	13.7	4.8	11.9	2.6	1.8	1.8
3	12.8	4.8	17.5	0.8	-4.7	4.7
4	13.7	4.8	13.7	4.1	0.0	0.0
9	13.1	4.8	11.2	1.9	1.9	1.9
10	13.4	4.8	13.1	4.7	0.3	0.3
17	12.8	4.7	15.4	2.6	-2.6	2.6
18	12.8	4.8	17.5	1.5	-4.7	4.7
19	13.4	4.9	16.1	2.1	-2.7	2.7
20	12.9	4.8	16.3	1.6	-3.4	3.4
25	13.5	4.8	18.8	1.3	-5.3	5.3
26	13.6	4.8	17.3	1.0	-3.7	3.7
28	13.8	4.1	17.6	2.1	-3.8	3.8
29	12.9	4.8	17.8	2.9	-4.9	4.9
30	12.9	4.8	18.3	1.1	-5.4	5.4
34	13.4	4.8	14.4	3.2	-1.0	1.0
35	13.0	4.7	12.3	2.1	0.7	0.7
36	13.0	4.7	13.6	1.4	-0.6	0.6
37	13.2	4.8	16.5	2.4	-3.3	3.3
40	12.5	4.7	13.8	1.3	-1.3	1.3
				Mean	**-2.0 m**	**2.7 m**
				Std Dev	**2.6**	**1.7**

Table 4.4. Mean MFM vs. field-derived height estimates for trembling aspen plots.

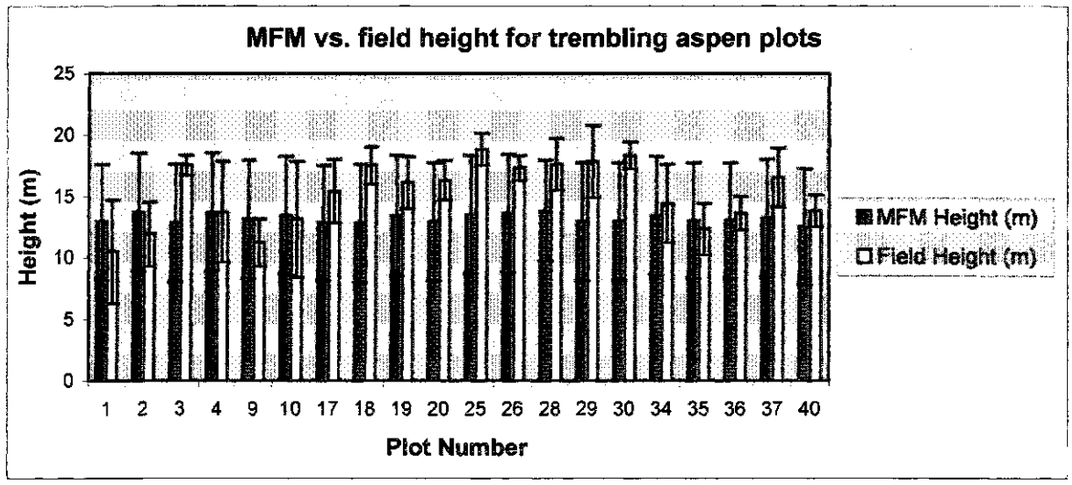

Figure 4.2. Mean MFM vs. field-derived height estimates for trembling aspen plots with standard deviation bar.

Lodgepole Pine						
Plot #	MFM Ht (m)	MFM StdDev (m)	Field Ht (m)	Field StdDev (m)	MFM-Fld Ht Diff (m)	Absolute Ht Diff (m)
5	14.6	3.1	16.4	7.1	-1.8	1.8
7	14.7	2.9	16.7	3.7	-2.0	2.0
8	14.6	2.9	16.7	3.7	-2.0	2.0
12	14.7	2.8	14.0	3.5	0.7	0.7
13	14.7	3.1	15.6	3.7	-0.9	0.9
21	14.7	3.0	17.1	2.3	-2.4	2.4
22	14.6	3.0	16.3	4.3	-1.7	1.7
23	14.7	3.0	18.8	3.4	-4.1	4.1
24	14.6	3.0	15.9	4.3	-1.3	1.3
31	15.0	2.9	9.9	2.4	5.1	5.1
32	14.9	3.3	14.0	3.1	0.9	0.9
38	13.5	2.2	14.4	4.2	-0.9	0.9
39	13.4	1.4	14.4	4.1	-1.0	1.0
41	15.0	3.0	14.3	3.8	0.7	0.7
				Mean	**-0.8 m**	**1.8 m**
				Std Dev.	**2.2**	**1.3**

Table 4.5. Mean MFM vs. field-derived height estimates for lodgepole pine plots.

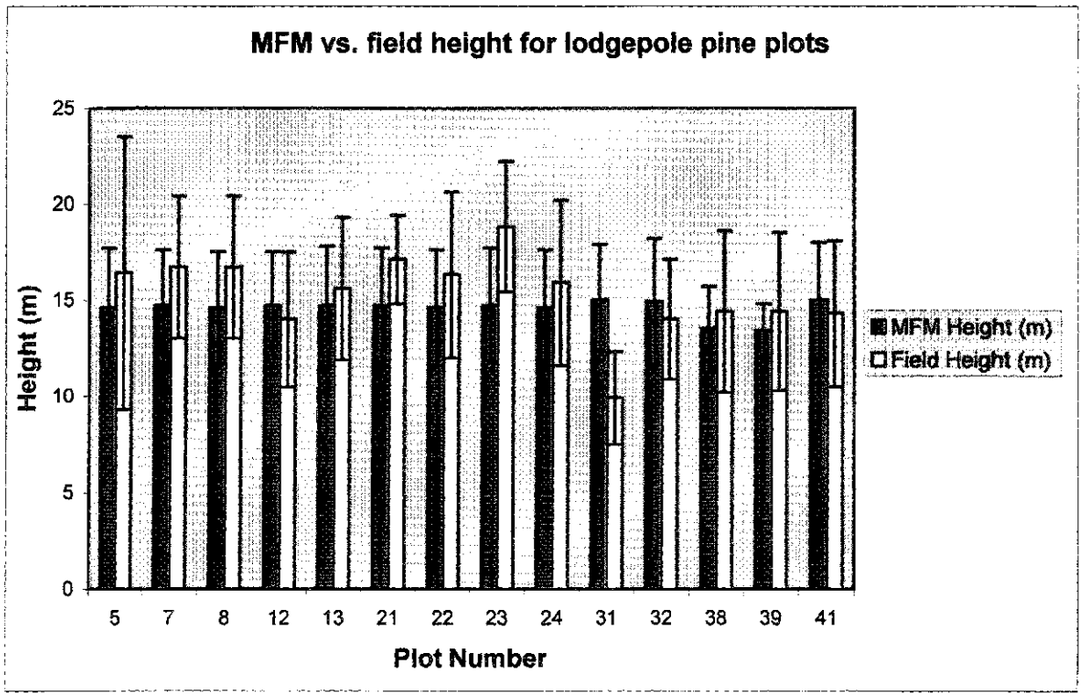

Figure 4.3. Mean MFM vs. field-derived height estimates for lodgepole pine plots with standard deviation bar.

increased spectral variation between trembling aspen plots compared to lodgepole pine locations as result of only six image pixels being utilized in the MFM-LUT matching process. However, further investigation utilizing a greater number of species and samples across variable topography would be required to substantiate these claims.

4.4 Basal area stem count variable estimates

Basal area is a required variable to calculate stand volume. As basal area is not a variable output using the MFM-GOMS model it must be calculated independently for each forest plot. Basal area Equations (3.8, 3.9) were applied to field and MFM data. Irrespective of the generalized assumptions made in MFM-derived stand volume calculation, a high mean level of agreement between measured and MFM-derived stem counts exists for both species types (Tables 4.6, 4.7) with an average absolute mean difference of 5 trees per 100 m^2 plot.

While MFM generally overestimated stem counts for the trembling aspen plots (Figure 4.4), a slight underestimation occurred for the lodgepole pine (Figure 4.5) and as with mean stand height, investigation of stem count estimate standard deviations share a higher degree of overlap with the lodgepole pine plots than for the trembling aspen. Two representative plots for each species type (Plots 17 and 36 for trembling aspen; Plots 13 and 21 for lodgepole pine) returned nil stem count values according to a pre-established constraint to discard values below 5, or above 50 trees per 100 m^2 area, therefore, these plots were discarded from further analysis.

plot	MFM Density (%)	MFM horizontal crown radius (r)	pi*r^2	MFM trees / 100m^2	field stem counts / 100m^2 plot	MFM-Fld difference	Absolute difference
3	16.8	0.5	0.8	21.3	30	-8.7	8.7
4	19.2	0.5	0.8	24.3	21	3.3	3.3
9	21.3	0.5	0.8	27.0	22	5.0	5.0
10	17.5	0.5	0.8	22.3	15	7.3	7.3
18	17.2	0.5	0.8	21.8	23	-1.2	1.2
19	18.2	0.5	0.8	23.0	19	4.0	4.0
20	20.9	0.5	0.8	26.5	23	3.5	3.5
25	13.1	0.5	0.8	16.6	11	5.6	5.6
26	12.2	0.5	0.8	15.4	19	-3.6	3.6
28	11.9	0.5	0.8	15.1	17	-1.9	1.9
29	21.3	0.5	0.8	27.0	18	9.0	9.0
30	21.3	0.6	1.1	19.4	14	5.4	5.4
34	14.0	0.5	0.8	17.7	13	4.7	4.7
35	21.7	0.6	1.2	18.1	17	1.1	1.1
37	16.9	0.5	0.8	21.4	15	6.4	6.4
40	53.5	0.7	1.5	35.7	30	5.7	5.7
			Mean	**22**	**19**	**2.9**	**4.8**
			Std Dev.	**5.3**	**5.5**	**4.6**	**2.4**

Table 4.6. MFM vs. field-derived stem count estimates for trembling aspen plots.
Note: Plots 17 and 36 returned no matches when model constrained to return stem counts between 5 and 50 so were dropped from further analysis.

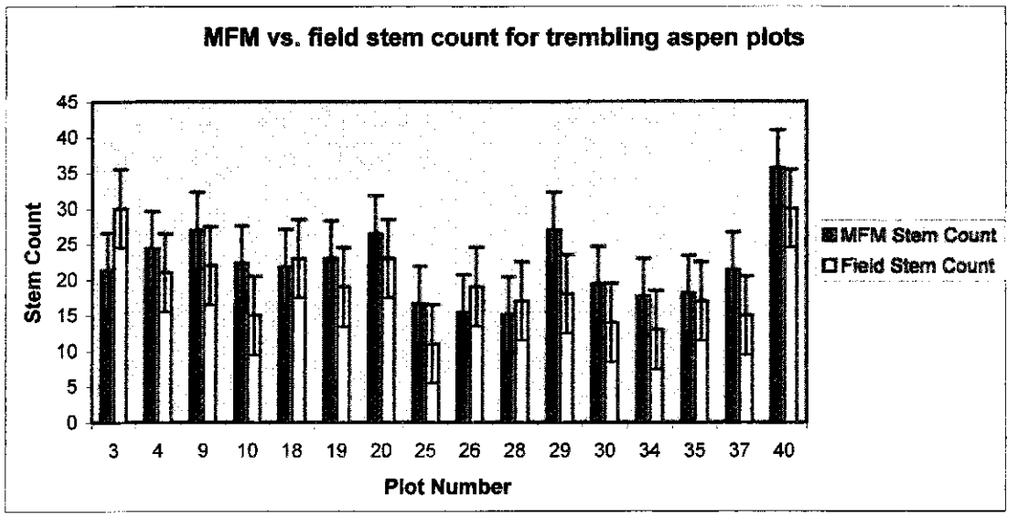

Figure 4.4. MFM vs. field-derived stem count estimates for trembling aspen plots.

Plot	MFM Density	MFM Horizontal crown radius (r)	pi*r^2	MFM trees / 100m^2	field stem counts / 100m^2 plot	MFM-Fld difference	Absolute difference
5	22.6	0.5	0.9	26.0	18	8.0	8.0
7	20.1	0.6	1.1	18.6	18	0.6	0.6
8	22.4	0.6	1.1	20.9	18	2.9	2.9
12	30.7	0.7	1.6	19.2	23	-3.8	3.8
22	26.5	0.6	1.1	25.0	22	3.0	3.0
23	23.3	0.6	1.1	21.5	20	1.5	1.5
24	25.0	0.6	1.1	22.5	30	-7.5	7.5
31	23.4	0.6	1.2	19.0	26	-7.0	7.0
32	24.5	0.6	1.2	20.4	34	-13.6	13.6
38	37.1	0.6	1.3	28.1	31	-2.9	2.9
39	38.9	0.6	1.2	31.9	26	5.9	5.9
41	24.2	0.6	1.0	23.5	30	-6.5	6.5
			Mean	**23**	**25**	**-1.6**	**5.3**
			Std Dev.	**4.1**	**5.7**	**6.3**	**3.6**

Table 4.7. MFM vs. field-derived stem count estimates for lodgepole pine plots.

Note: Plots 13 and 21 returned no matches when model constrained to return stem counts between 5 and 50 so were dropped from further analysis

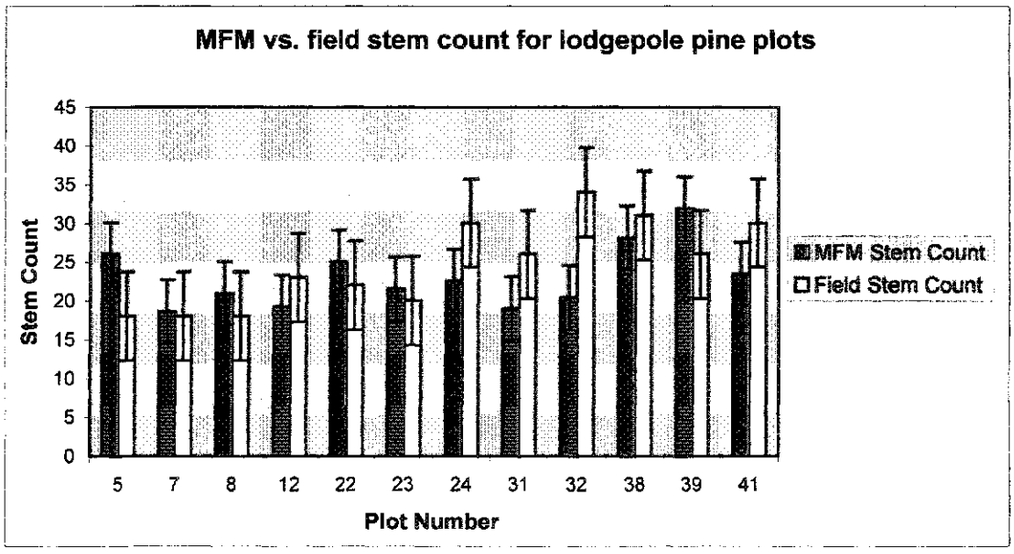

Figure 4.5. MFM vs. field-derived stem count estimates for lodgepole pine plots.

4.5 Basal area stem diameter (dbh) estimates

As diameter at breast height (dbh) is not a variable output by the MFM-GOMS modeling procedure, this parameter was estimated for both trembling aspen and lodgepole pine across the entire study area based upon the relationship exhibited between height and dbh values from field data. Preliminary regression analysis indicated a strong linear relationship (r^2 = 0.88) between field-measured dbh and height values for white spruce, however, a significantly weaker linear correlation existed for trembling aspen (r^2 = 0.53) and lodgepole pine (r^2 = 0.49), making apparent the non-linear relationship between height and dbh of the species under investigation. Scatterplot analysis of field height and dbh values for all species-specific trees (Figures 4.6, 4.7) indicates a logarithmic relationship between the two variables with r^2 values of 0.62 and 0.64 for trembling aspen and lodgepole pine respectively.

Slope and intercept values for each species was obtained through regression analysis of the height and dbh variables, and input to Equations 3.7 and 3.9. Substituting MFM-derived mean plot height variables and inverting the equation computed model-derived dbh estimates. Minimum, maximum and mean field measured dbh and height values for log equation formulation are presented over the following two pages.

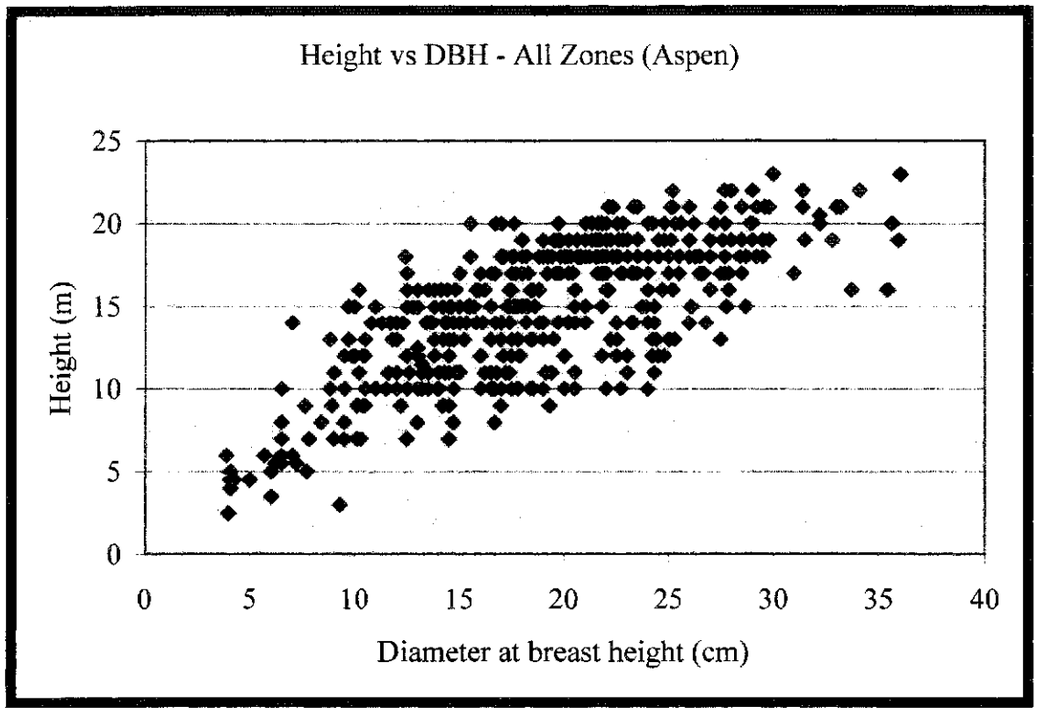

Figure 4.6 Field height vs. dbh scatterplot for all trembling aspen samples.

n= 427	min	max	mean	Standard Deviation
Height (m)	2.5	23	14.8	4.22
DBH (cm)	3.9	36	19.0	6.63
LN(dbh) = LN(1.5506) + 0.9201*LN(Height)				
$dbh = e^{(LN(dbh) + \sigma^2 / 2)}$ $r^2 = 0.62$				

Table 4.8 Height / dbh scatterplot values and log equation for trembling aspen plots.

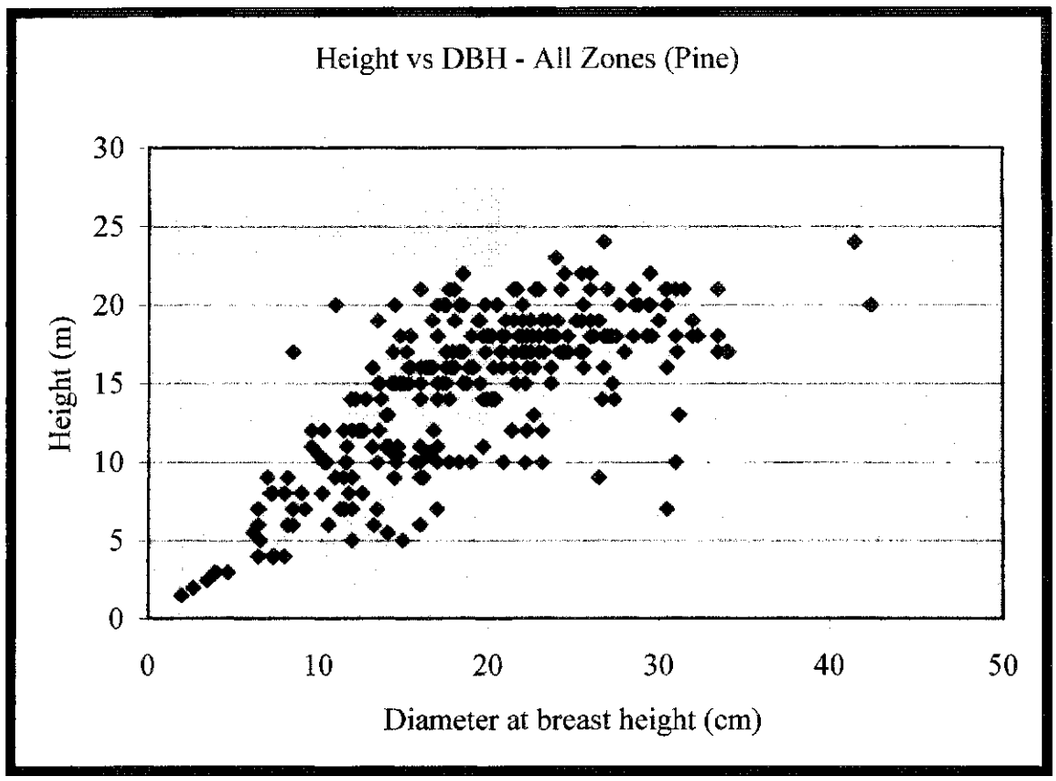

Figure 4.7 Field height vs. dbh scatterplot for all lodgepole pine samples.

n= 294	min	max	mean	Standard Deviation
Height (m)	1.5	24	14.8	4.84
DBH (cm)	2.0	42.4	19.2	7.05
LN(dbh) = LN(2.2135) + 0.7941*LN(Height)				
dbh = $e^{(LN(dbh) + \sigma^2 / 2)}$				**r^2 = 0.64**

Table 4.9 Height / dbh scatterplot values and log equation for lodgepole pine plots.

Logarithmically derived and bias corrected dbh values from MFM-based height estimates share a closer level of agreement for lodgepole pine plots than for trembling aspen on a plot by plot basis (Tables 4.10, 4.11; Figures 4.8, 4.9), however, both exhibit high levels of agreement to the field based mean measurements allowing for this method of dbh extraction to be accepted for further investigation.

Plot #	MFM DBH (cm)	field DBH (cm)	MFM-Fld Difference (cm)	Absolute Difference (cm)
3	16.9	17.2	-0.3	0.3
4	18.0	19.4	-1.4	1.4
9	17.2	14.1	3.1	3.1
10	17.7	13.6	4.1	4.1
18	16.9	20.8	-3.9	3.9
19	17.7	22.3	-4.6	4.6
20	16.9	17.9	-1.0	1.0
26	17.9	22.1	-4.2	4.2
28	18.1	25.4	-7.3	7.3
29	17.0	22.1	-5.1	5.1
30	17.0	24.5	-7.5	7.5
34	17.7	23.2	-5.5	5.5
35	17.1	16.6	0.5	0.5
37	17.4	22.1	-4.7	4.7
40	16.5	13.3	3.2	3.2
Mean	**17.3**	**19.6**	**-2.3 cm**	**3.8 cm**
Std Dev	**0.5**	**4.0**	**3.4**	**2.2**

Table 4.10. MFM vs. field-derived dbh values for trembling aspen plots.

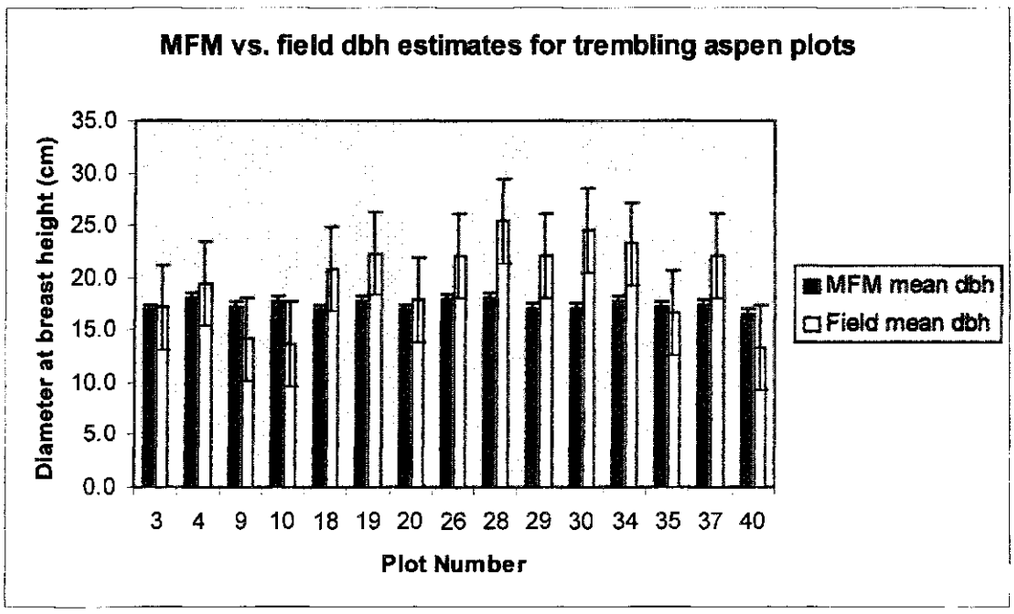

Figure 4.8. MFM vs. field-derived dbh values for trembling aspen plots.

Plot #	MFM DBH (cm)	field DBH (cm)	MFM-Fld Difference (cm)	Absolute Difference (cm)
5	19.1	20.6	-1.5	1.5
7	19.2	19.2	0.0	0.0
8	19.1	18.8	0.3	0.3
12	19.2	16.4	2.8	2.8
22	19.1	22.9	-3.8	3.8
23	19.2	20.9	-1.7	1.7
24	19.1	18.8	0.3	0.3
31	19.5	15.2	4.3	4.3
32	19.4	18.9	0.5	0.5
38	18.0	17.5	0.5	0.5
39	17.7	19.8	-2.1	2.1
41	19.5	21.1	-1.6	1.6
Mean	**19.0**	**19.2**	**-0.2 cm**	**1.6 cm**
Std Dev	**0.6**	**2.1**	**2.2**	**1.4**

Table 4.11. MFM vs. field-derived dbh values for lodgepole pine plots.

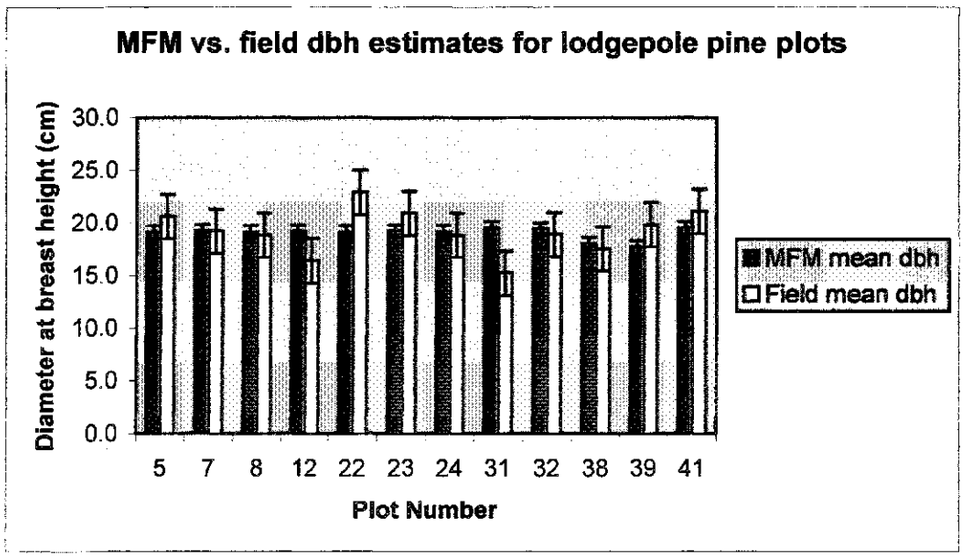

Figure 4.9. MFM vs. field-derived dbh values for lodgepole pine plots.

4.6 Basal Area Estimates

Basal area was computed at each plot location using dbh (Tables 4.10, 4.11), stem count estimates (Tables 4.6, 4.7), and Equations 3.8 and 3.9. Although traditionally expressed in terms of m^2/ha, extrapolation to this scale was deemed unfounded, therefore, results are presented at the plot level in terms of m^2/100 m^2.

While a high variability exists between individual plot locations, agreement between mean field-derived and MFM modeled basal area output (Tables 4.12, 4.13) is apparent in the results. Basal area estimates for lodgepole pine plots are more consistent than those of trembling aspen as apparent in examination of the standard deviation (Figures 4.10, 4.11), which shares a greater degree of overlap for the pine plots.

As basal area is a key input variable to the stand volume equation, a high level of agreement is required for model assessment. While the estimates presented in the following tables and figures represent a small sample, the mean MFM derived values correspond highly with field measured estimates of basal area.

Plot # ($100m^2$)	MFM BA ($m^2/100m^2$)	Field BA ($m^2/100m^2$)	MFM-Fld diff ($m^2/100m^2$)	Absolute diff ($m^2/100m^2$)
3	0.10	0.21	-0.11	0.11
4	0.15	0.12	0.03	0.03
9	0.17	0.08	0.09	0.09
10	0.12	0.08	0.04	0.04
18	0.11	0.16	-0.05	0.05
19	0.13	0.14	-0.01	0.01
20	0.16	0.13	0.03	0.03
26	0.06	0.11	-0.05	0.05
28	0.06	0.15	-0.09	0.09
29	0.17	0.12	0.05	0.05
30	0.09	0.09	0.00	0.00
34	0.08	0.05	0.03	0.03
35	0.08	0.06	0.02	0.02
37	0.11	0.07	0.04	0.04
40	0.27	0.12	0.15	0.15
Mean	**0.12**	**0.11**	**0.01**	**0.05**
StdDev	**0.06**	**0.04**	**0.07**	**0.04**

Table 4.12. MFM vs. field-derived basal area estimates for trembling aspen plots.

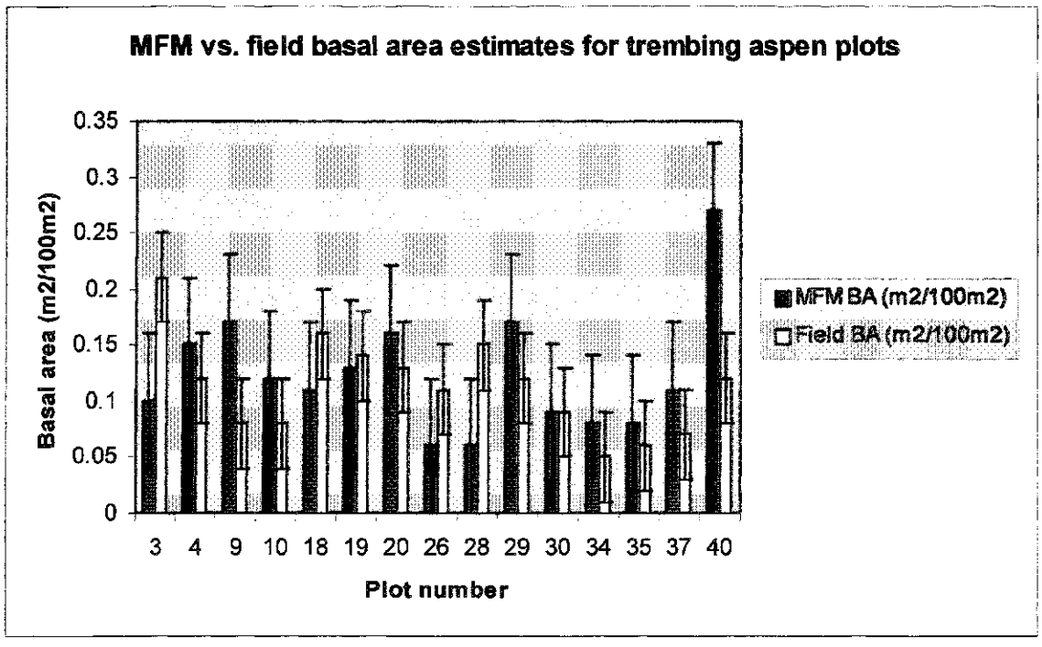

Figure 4.10. MFM vs. field-derived basal area estimates for trembling aspen plots.

Plot # ($100m^2$)	MFM BA ($m^2/100m^2$)	Field BA ($m^2/100m^2$)	MFM-Fld diff ($m^2/100m^2$)	Absolute diff ($m^2/100m^2$)
5	0.19	0.10	0.09	0.09
7	0.10	0.08	0.02	0.02
8	0.13	0.09	0.04	0.04
12	0.11	0.11	0.00	0.00
22	0.18	0.18	0.00	0.00
23	0.13	0.13	0.00	0.00
24	0.14	0.17	-0.03	0.03
31	0.11	0.12	-0.01	0.01
32	0.12	0.24	-0.12	0.12
38	0.20	0.20	0.00	0.00
39	0.25	0.14	0.11	0.11
41	0.16	0.21	-0.05	0.05
Mean	**0.15**	**0.15**	**0.01**	**0.04**
StdDev	**0.05**	**0.05**	**0.06**	**0.04**

Table 4.13. MFM vs. field-derived basal area estimates for lodgepole pine plots.

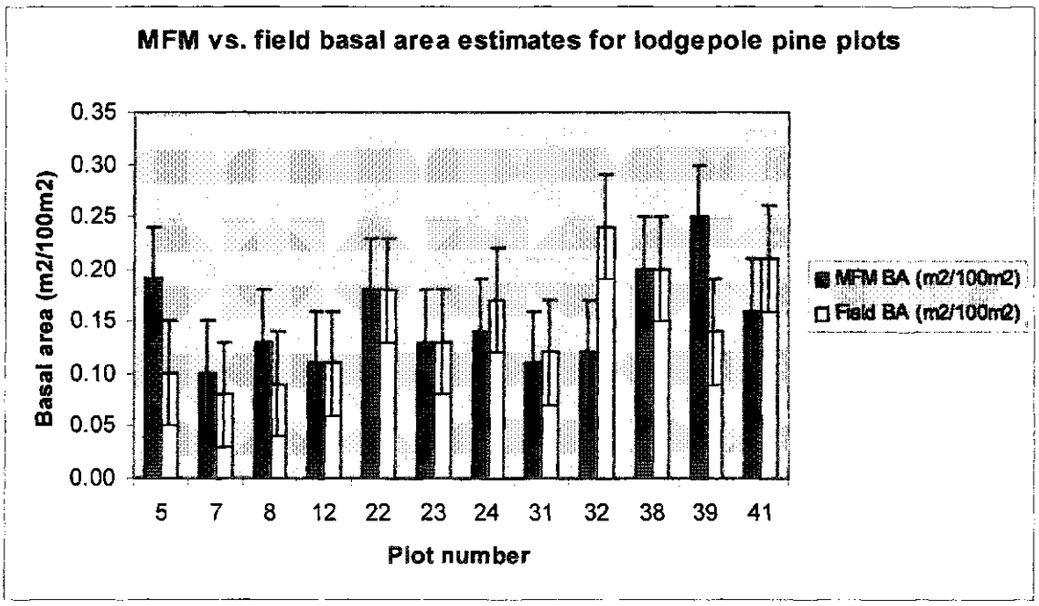

Figure 4.11. MFM vs. field-derived basal area estimates for lodgepole pine plots.

4.7 Stand Volume Results

Although stand volume is usually expressed as m^3/ha, it has been presented here as $m^3/100m^2$ to represent the actual plot size used in this research for the same reasons as described previously for the basal area estimates.

Stand volume results for trembling aspen (Table 4.14) and lodgepole pine (Table 4.15) indicate variation in MFM versus field-derived stand volume values at a greater degree for trembling aspen plots than for the lodgepole pine, yet at a level suitable for further investigation. As with basal area estimates, there is a greater degree of overlap present in examination of the plot level standard deviations between each stand volume estimate for the lodgepole pine plots.

Within plot variation is noticeable for both species under investigation, however, mean and absolute mean values indicate a great potential for the continuation of this research in a larger setting. A discussion pertaining to potential solutions in the reduction of such variation is presented in the discussion following these results.

100m^2 Plot #	MFM Stand Volume ($m^3/100m^2$)	Field Stand Volume ($m^3/100m^2$)	MFM-Fld Difference ($m^3/100m^2$)	Absolute Difference ($m^3/100m^2$)
3	1.28	3.68	-2.40	2.40
4	2.06	1.64	0.42	0.42
9	2.23	0.90	1.33	1.33
10	1.61	1.05	0.56	0.56
18	1.41	2.80	-1.39	1.39
19	1.74	2.25	-0.51	0.51
20	2.06	2.12	-0.06	0.06
26	0.82	1.90	-1.08	1.08
28	0.83	2.64	-1.81	1.81
29	2.19	2.14	0.05	0.05
30	1.16	1.65	-0.49	0.49
34	1.07	0.72	0.35	0.35
35	1.04	0.74	0.30	0.30
37	1.45	1.16	0.29	0.29
40	3.38	1.66	1.72	1.72
Mean	**1.62**	**1.80**	**-0.18**	**0.85**
StdDev	**0.68**	**0.84**	**1.12**	**0.72**

Table 4.14. MFM vs. field-derived stand volume estimates for trembling aspen plots.

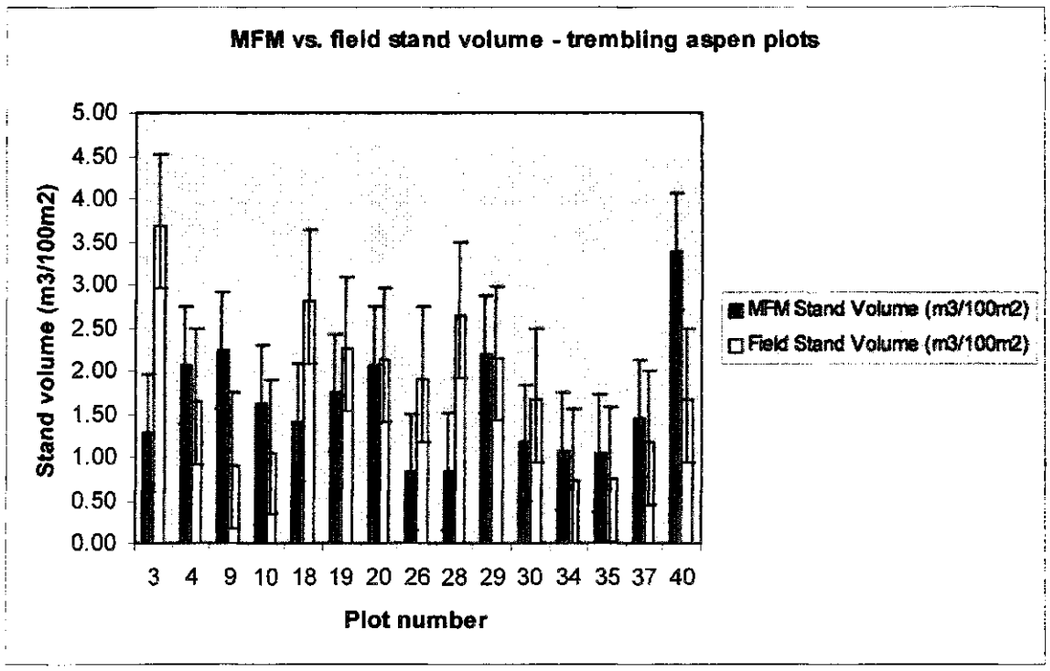

Figure 4.12. MFM vs. field-derived stand volume estimates for trembling aspen plots.

100m² Plot #	MFM Stand Volume ($m^3/100m^2$)	Field Stand Volume ($m^3/100m^2$)	MFM-Fld Difference ($m^3/100m^2$)	Absolute Difference ($m^3/100m^2$)
5	2.77	1.64	1.13	1.13
7	1.47	1.34	0.13	0.13
8	1.90	1.50	0.40	0.40
12	1.62	1.54	0.08	0.08
22	2.63	2.93	-0.30	0.30
23	1.91	2.44	-0.53	0.53
24	2.04	2.70	-0.66	0.66
31	1.65	1.19	0.46	0.46
32	1.79	3.36	-1.57	1.57
38	2.70	2.88	-0.18	0.18
39	3.35	2.02	1.33	1.33
41	2.40	3.00	-0.60	0.60
Mean	**2.19**	**2.21**	**-0.03**	**0.61**
StdDev	**0.58**	**0.76**	**0.80**	**0.48**

Table 4.15. MFM vs. field-derived stand volume estimates for lodgepole pine plots.

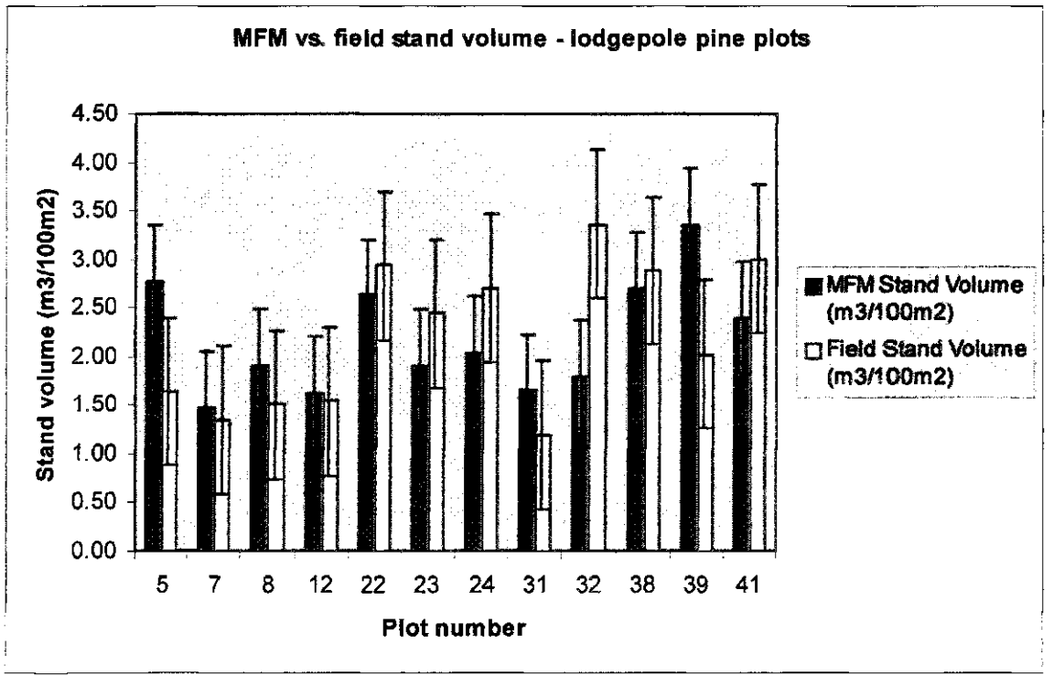

Figure 4.13. MFM vs. field-derived stand volume estimates for lodgepole pine plots.

4.8 Discussion

This research has presented an additional means for forest structural parameter estimation. While for the most part the height variable, a key component in stand volume analysis, is difficult to directly estimate from a nadir-viewing sensor, canopy reflectance models allow for height to be estimated as a function of reflectance, much as it was formerly estimated through regression analysis of density and crown closure (Hall *et al.,* 1998).

Previous research in structural parameter estimation utilized statistical/ empirical techniques for biophysical information extraction in mapping stand volume or biomass (Anderson *et al.,* 1993; Paradella *et al.,* 1994; Friedl *et al.,* 1994; Soares *et al.,* 1995; Trotter *et al.,* 1997; Guerra *et al.,* 1998; Hall *et al.,* 1998; Franklin *et al.,* 2000; Banfield *et al.,* 2002, among others). These studies, however, were dependent upon extensive field-data collection and were performed in low relief areas. Areas of variable relief, such as mountainous zones, contribute a host of BRDF factors that affect the spectral response of ground targets resulting in spectral matching variation between reflectance and the structural biophysical parameters.

Through the use of a geometric-optical-reflectance-models running in a multiple-forward-mode framework, physical parameters relating to height and basal area have been estimated which combined form the basis for stand volume estimation. Structural field measurements, coupled with spectral endmember data were employed in the generation of minimum, maximum and increment structural inputs for the MFM-GOMS model. Additionally, this information was utilized for validation of analysis throughout the stand volume estimation process.

MFM-GOMS is designed to run with minimal field inputs. As structural information may be input as a range of values, which can be derived either from existing inventory data,

or full ranges based on mensuration tables, all that is required, aside from sun-surface-sensor geometry is the image endmembers for the species under study. These endmembers may be obtained from spectral libraries, or, if the study area is known, from the image itself. The quality of endmember spectra is important to the identification and quantification of the species under study, therefore the higher quality of the endmembers with respect to the image, the better. If endmembers are to be derived from the image, the advantage is the common radiometric scale for which they are set, however, the disadvantage is that the spectral endmembers may not be 'pure' in that the isolation of species-specific sunlit canopy fractions will be limited based on spectral variability within a given pixel. This condition increases with the spatial resolution of the image sensor utilized.

It was expected that MFM-GOMS would overestimate the forest structural attributes as it models trees as discrete three-dimensional spheroids and cones (Li and Strahler, 1985, 1992), however, in most instances, MFM consistently estimated the structural parameters within an acceptable range of field measurements for both species types examined.

Several variations between modeled parameters and real-world measurements can be explained through the ecological intricacies of forest vegetation types. One source of variation difficult to control is differences among individual trees at different sites, or microenvironments (Smith, 1996). Because such factors are impossible to control, the response of a number of individuals in various locations have been examined, rather than relying on single location observations. Through the replication of standardized statistical models for each species of interest, correlation or regression between field and modeled volume parameters can be derived.

By examining the research in a broader context, the ability to detect and characterize forest biophysical structure without the requirements for field-measured inputs creates a myriad of possible courses for this research to take. Additional studies involving coarser imaging sensors, larger plot areas, and a variety of terrain and vegetation types are required, however, prior to making any non-substantiated claims. This research has shown that forest structural data can be extracted with a reasonable level of agreement to small forest plots in south-western Alberta using MFM-GOMS and radiometrically corrected IKONOS digital imagery.

While there exists an alternate means for deriving stand volume from field data (Huang, 1994), this would involve a multiple step analysis in the modification of MFM-LUT data that was considered beyond the scope of this research. The alternative means, using statistical analysis software (SAS) (Huang, 1994) computes individual tree volume by dividing it into discrete units of cones and cylinders, rather than estimating tree volume by height and dbh alone. Current work has focused on an improved field validation data set with stand volume derived from these taper functions that more closely incorporates tree form into volume computation (Hall *et al.,* 2001) for which improvements in the correspondence of these new field values with the MFM-GOMS stand volume output presented here has been found. This process may be examined as a more refined method for using MFM modeling of stand volume in future research.

4.9 Chapter Summary

Although the sample size was limited in this study, mean results presented in this chapter share an acceptable level of agreement with field-derived measurements (Tables 4.16, 4.17) demonstrating potential for further evaluation.

Parameter	MFM results			Field Results			Absolute Difference		
	Mean	Min	Max	Mean	Min	Max	Mean	Min	Max
Height (m)	13.2	12.5	13.8	15.1	10.5	18.8	2.7	0.0	5.4
Stem Count	22	15	36	19	11	30	5	1	9
dbh (cm)	17.3	16.5	18.1	19.6	13.3	25.4	3.8	0.3	7.5
Basal area ($m^2/100m^2$)	0.12	0.06	0.27	0.11	0.05	0.21	0.05	0.00	0.15
Stand volume ($m^3/100m^2$)	1.62	0.82	3.38	1.80	0.72	3.68	0.85	0.06	2.40

Table 4.16. MFM vs. field results for trembling aspen.

Parameter	MFM results			Field Results			Absolute Difference		
	Mean	Min	Max	Mean	Min	Max	Mean	Min	Max
Height (m)	14.6	13.4	15.0	15.3	9.9	18.8	1.8	0.7	5.1
Stem Count	23	19	32	25	18	34	5	1	14
dbh (cm)	19.0	17.7	19.5	19.2	15.2	22.9	1.6	0.0	4.3
Basal area ($m^2/100m^2$)	0.15	0.10	0.25	0.15	0.08	0.24	0.04	0.00	0.12
Stand volume ($m^3/100m^2$)	2.19	1.47	3.35	2.21	1.19	3.36	0.61	0.08	1.57

Table 4.17. MFM vs. field results for lodgepole pine.

Initial results indicate that MFM-GOMS is suitable for the estimation of height at relatively small plot locations. While stem count calculations were inflated to a small degree for both species under investigation, remaining structural parameters were estimated with a high level of agreement to field derived measurements. Logarithmic bias corrected mean dbh fell within 3.8 cm for trembling aspen, and 1.6 cm for lodgepole pine plots allowing for absolute mean basal area calculation within 0.05 $m^2/100m^2$ for trembling aspen, and 0.04

$m^2/100m^2$ for lodgepole pine plots. Coupled with initial height estimates, MFM derived stand volume was within 0.85 m^3 / $100m^2$ and 0.61 m^3 / $100m^2$ absolute mean difference for trembling aspen and lodgepole pine plots respectively.

While MFM-GOMS has been shown to provide promise in the derivation of stand volume from high-resolution digital imagery, further testing is required utilizing different species assemblages and mixed forest samples over a range of spatial scales prior to operational use.

CHAPTER 5

5.0 CONCLUSIONS

5.1 Summary of Results

A new structural data extraction of biophysical information from digital satellite imagery was required that was not dependent upon extensive field data collection. MFM-GOMS was shown to provide good correspondence between spectral reflectance and biophysical information, specifically in classification, cluster labeling, and biomass estimation.

This study was undertaken to evaluate the capability of the geometric-optical-mutual-shadowing canopy reflectance model, run in multiple-forward-mode to estimate forest stand volume and respective physical variables from high spatial resolution multispectral IKONOS satellite imagery.

A new method of digital image height extraction was presented, and considering the limited pixel sample size per plot, results provided a respectable level of agreement to actual field-measured values. MFM was found to generally underestimate height, resulting in lower than expected basal area and stand volume estimates.

Excluding the height variable, no general over-, or underestimation was apparent on behalf of the MFM-GOMS output compared to field measurements with some plots exhibiting higher or lower MFM derived values. Mean values, however, for all structural parameters share a high level of agreement between MFM and field measurements.

Structural variable estimates between modeled and field-measured lodgepole pine plots were more closely matched than for trembling aspen at all stages through to stand volume calculation.

MFM-GOMS was found to provide a repeatable, and reliable method of structural data extraction without the requirement for extensive ground data consistent with other MFM approaches. Field and MFM model results shared a respectable level of agreement in height, stem count, dbh, basal area and stand volume.

A limitation of this study was the relatively small sample size employed. Larger plot sizes would be better suited in the reduction of BRDF effects. A larger sample size would also result in a greater range of pixel reflectance values, providing a more robust sample for image reflectance / MFM-LUT structural parameter matching.

As stand volume is dependent upon accurate height estimation for which more variability is expected on a per-pixel basis, it is recommended that the scale of the analysis correspond to that of forest stands or plots. By running MFM-GOMS using a larger sample of pixel reflectance values, rather than simply using the mean and standard deviation from six pixels per plot, localized variance would be reduced in favour of more reliable height estimates. Therefore, for an operational study, several model access queries utilizing a range of red and near-infrared reflectance means and standard deviations should be employed at the stand level.

The results generated from access queries stem from a single look-up table generated per-species, therefore, MFM-GOMS physical values should maintain a high level of agreement (e.g. with field validation data), and although variation exists in relation to actual

field-plot measurements, mean un-weighted averages appear to be consistent between field-measured and MFM modeled output at the scale of forest stands.

5.2 Conclusions

The Multiple-Forward-Mode Geometric Optical Mutual Shadowing modeling approach has provided a capability for estimating forest stand volume at the plot level from satellite image data in a complex area of mountainous terrain in western Canada. To achieve this, a variety of forest structural parameters such as tree height, stem counts, dbh and basal area were derived using MFM canopy reflectance modeling. Stand level height estimates were similar to field height measurements, providing a key basis from which stand volume was derived. This model-based approach provides a different means of forest information extraction without the requirements for expensive fieldwork.

MFM-GOMS model results provide an abstract representation of a real system. They let us predict the response of a dependent variable(s), based on an explicit assumption or set of assumptions. In this case, the assumption is a forest ecosystem with spectral and structural properties that are modeled. While the GOMS model used in this work is highly sophisticated, no model can capture the full level of complexity or site-specific variability that occurs in nature. Therefore, differences between real world and modeled results are inevitable. Although this modeling approach was applied and validated against small plot areas, successful extrapolation to hectare size areas would allow for an independent capability without the requirement for extensive ground based field measurements or, it may be integrated with existing air photo or satellite based forest inventories with distinct advantages over current methods. The goal of the scientific process is to understand the

patterns of variation in nature, and the MFM-GOMS model allows for these patterns to be established.

A number of major conclusions regarding MFM-GOMS modeling of forest height and stand volume in the Kananaskis region have been made.

- By removing the requirement for exact model inputs, the multiple-forward-mode approach allows for a range of input structural variables to be utilized. This allows for greater accessibility and use of the model over a range of geographical and topographical conditions providing explicit linkages between pixel reflectance, terrain, and forest structure.

- MFM-GOMS was found to estimate mean forest structural parameters with minor variation to field measurements demonstrating potential for further evaluation.

- Diameter at breast height exhibits a curvilinear logarithmic relationship to height, and may be derived through bias-corrected allometric relationships using MFM height estimates.

- MFM-GOMS stand volume estimates share a higher level of agreement when modeling lodgepole stands compared to trembling aspen at each stage of structural data computation. This can be attributed to variation in stand structures that are exhibited to a greater degree for the aspen plots.

- The modeling context has its greatest potential to be applied over larger areas (i.e. huge regions) where fieldwork to establish ground measurements of height, basal area, and stand volume become impractical.

5.3 Contribution to Research

The research presented in this thesis allows for an alternative means for generalized height and volume estimation of forests in areas of variable relief. The analyses performed here can also be implemented in flat terrain analysis, with projected higher degrees of accuracy, as the influence of BRDF would be minimized from multispectral image reflectance analysis. As a complement to existing forest inventories, such as the Alberta Vegetation Inventory (AVI), mean volume estimates allow for inferences to be made about the quantity, and quality of forest resources on which management decisions can be based.

This research can additionally be employed in applied ecology; primarily restoration ecology, landscape ecology, and conservation biology related to forests. While forestry was once only concerned with the raising of trees for harvest, it now emphasizes biomass accumulation, nutrient cycling, and the effects of timber harvesting on nutrient budgets.

As an alternate method to stand volume estimation using semi-automated approaches to digital satellite imagery with minimal ground-based data requirements, the techniques presented in this research complement other MFM canopy reflectance modeling studies, and may be used as a component in a wide-spread forest inventory study, involving classification, cluster labeling, biomass estimation, and terrain correction.

5.4 Future Research

Suggestions for future research include:

- Application and comparison of MFM-GOMS height and stand volume estimates using Landsat ETM+ and IKONOS imagery scaling for larger area application with a greater range of species;

- Application of MFM-GOMS IKONOS and/or Landsat ETM+ stand volume estimation over non-mountainous areas for comparison of improved agreement to mountainous analysis;

- Studying the effect of spectral mixing on image pixels for variation of species-specific physical parameters as result of mixed forest inclusions and understory vegetation; and

- Specific height/slope and age/diameter relationships and their influence on pixel reflectance and spectral mixture analysis utilizing the forest species investigated in this thesis for a smaller subset of the study region.

REFERENCES CITED

Abuelgasim, A.A, and A.H. Strahler. 1994. Modeling Bidirectional Radiance Measurements Collected by the Advanced Solid-State Array Spectroradiometer (ASAS) over Oregon Transect Conifer Forests. *Remote Sensing of Environment.* 47:261-275

Achuff, P.L. 1992, Natural Regions, Subregions and Natural History Themes of Alberta: A classification for protected areas management. Parks Service, Alberta Environmental Protection, Edmonton, Alberta.

Alberta Environmental Protection. 1994. Alberta Timber Harvest Planning and Operating Ground Rules. Alberta Environmental Protection, Edmonton, Alberta. Publication number 71.

Anderson, G.L., J.D. Hanson, and R.H. Haas. 1993. Evaluating Landsat Thematic Mapper Derived Vegetation Indices for Estimating Above-Ground Biomass on Semiarid Rangelands. *Remote Sensing of Environment.* 45:165-175.

Archibald, J.H., G.D. Klappstein, and I.G.W. Corns. 1996. Field Guide to Ecosites of Southwestern Alberta. Special Report 8 – Canadian Forest Service, Northwest Region, Northern Forestry Centre, Canada. UBC Press, Vancouver, British Columbia, Canada.

ASD, 1998. Analytical Spectral Devices Inc. FieldSpec FR User's Guide. Boulder, Colorado. Variously paged.

Avery, T.E. and G.L. Berlin. 1992. Fundamentals of Remote Sensing and Airphoto Interpretation. 5th ed. Prentice Hall, New Jersey.

Banfield, G.E., J.S. Bhatti, H. Jiang, and M.J. Apps. 2002. Variability in regional scale estimates of carbon stocks in boreal forest ecosystems: results from West-Central Alberta. *Forest Ecology and Management.* 169: 15-27.

Barker Schaaf, C., and A.H. Strahler. 1993. Solar Zenith Angle Effects on Forest Canopy Hemispherical Reflectances Calculated with a Geometric-Optical Bidirectional Reflectance Model. *IEEE Transactions on Geoscience and Remote Sensing.* Vol.31, No.4, 921-927

Baskerville, G.L. 1972. Use of Logarithmic Regression in the Estimation of Plant Biomass. *Canadian Journal of Forestry.* Vol.2:49

Beaubien, J., J. Cihlar, G. Simard, and R. Latifovic. 1999. Land cover from multiple Thematic Mapper scenes using a new enhancement-classification methodology. *Journal of Geophysical Research*, Vol. 104(D22), pp. 27909-27920

Blackburn, G.A., and C.M. Steele. 1999. Towards the Remote Sensing of Matorral Vegetation Physiology: Relationships between Spectral Reflectance, Pigment, and Biophysical Characteristics of Semiarid Bushland Canopies. *Remote Sensing of Environment.* 70:278-292.

Brack, C. 1997. Stand Basal Area. http://online.anu.edu.au/Forestry/mensuration/S_BA.HTM Accessed January 13, 2003.

Bragg, D.C. 2001. A Local Basal Area Adjustment for Crown Width Prediction. *Northern Journal of Applied Forestry* 18(1):22-28.

Caselles, V. and M. J. Lopez-Garcia. 1989. An alternative simple approach to estimate atmospheric correction in multi temporal studies. *International Journal of Remote Sensing* 10:1127-1134

Chandra, B., 2002. Elegant Decision Tree Algorithm for Classification in Data Mining. In, *Proceedings, Third International Conference on Web Information Systems Engineering (Workshops) – (WISEw'02)*. December 11-11, 2002. Singapore. Institute for Electrical and Electronic Engineers.

Chavez, P. S. 1996. Image-based atmospheric corrections – revisited and improved. *Photogrammetric Engineering and Remote Sensing* 62:1025-1036

Chavez, P. S. 1989. Radiometric calibration of Landsat Thematic Mapper spectral images. *Photogrammetric Engineering and Remote Sensing* 55:1285-1294

Chavez, P. S. 1988. An improved dark-object subtraction technique for atmospheric scattering correction of Multi spectral data. *Remote Sensing of Environment* 24:459-479

Chen J.M. and S. G. Leblanc, 1997. A Four-Scale Bidirectional Reflectance Model Based on Canopy Architecture. *IEEE Transactions on Geoscience & Remote Sensing* 35, pp. 1316-1337.

Cihlar, J., B. Guindon, J. Beaubien, R. Latifovic, D. Peddle, M. Wulder, R. Fernandes, and J. Kerr. 2003. From need to product: a methodology for completing a land cover map of Canada with Landsat data. *Canadian Journal of Remote Sensing*, Vol. 29, No. 2, pp. 171-186.

Cochrane, M.A. 2000. Using vegetation reflectance variability for species level classification of hyperspectral data. *International Journal of Remote Sensing.* Vol.21, No.10, 2075-2087.

Crist, E. P. and R. J. Kauth. 1986. The tasseled cap de-mystified. *Photogrammetric Engineering and Remote Sensing* 52:81-86

Curran, P., and H. Williamson, 1987. GLAI estimation using measurements of red, near infrared and middle infrared radiance. *Photogrammetric Engineering and Remote Sensing*. Vol.53, 493-507.

Danson, F.M. 1998. Teaching the Physical Principals of Vegetation Canopy Reflectance Using the SAIL Model. *Photogrammetric Engineering and Remote Sensing*. Vol.64, No.8: 809-812.

Davidson, D. 2002. Sensitivity of NPP Models to Remotely Sensed LAI. *Masters Thesis; Department of Geography, University of Lethbridge.*

Department of the Environment. 2001. *State of the Environment Report, Terrestrial Ecosystems.* Edmonton: n.p.

de Haan, J. F., J. W. Hovenier, J. M. Kokke and H. T. van Stokkom 1991. Removal of atmospheric influences on satellite-borne imagery: a radiative transfer approach. *Remote Sensing of Environment* 37:1-21

Duggin, M. J. and C. J. Robinove 1990. Assumptions implicit in remote sensing data acquisition and analysis. *International Journal of Remote Sensing* 11:1669-1694

Ekstrand, S. 1994. Assessment of Forest Damage with Landsat TM: Correction for Varying Forest Stand Characteristics. *Remote Sensing of Environment.* 47:291-302.

Farrar, J.L. 1995. Trees in Canada. Fitzhenrey & Whiteside Ltd., and the Canadian Forest Service, Natural Resources Canada.

Foody, G.M., and R.A. Hill. 1996. Classification of tropical forest classes from Landsat TM data. *International Journal of Remote Sensing.* Vol.17, No.12, 2353-2367.

Forester, B. C. 1984. Derivation of atmospheric correction procedures for LANDSAT MSS with particular reference to urban data. *International Journal of Remote Sensing* 5:799-817

Franklin, S.E., M.A. Wulder, and G.R. Gerylo. 2001. Texture analysis of IKONOS panchromatic data for Douglas-fir forest age class separability in British Columbia. *International Journal of Remote Sensing.* Vol.22, No.13, 2627-2632.

Franklin, S.E., R.J. Hall, L.M. Moskal, A.J. Maudie, and M.B. Lavigne. 2000. Incorporating texture into classification of forest species composition from airborne multispectral images. *International Journal of Remote Sensing*. Vol.21, No. 1 ,61-79.

Franklin, S.E., and G.J. McDermid. 1993. Empirical relations between digital SPOT HRV and CASI spectral response and lodgepole pine (*Pinus contorta*) forest stand parameters. *International Journal of Remote Sensing*. Vol.14, No.12, 2331-2348.

Franklin, S.E., and D.R. Peddle, 1989. Spectral texture for improved class discrimination in complex terrain. *International Journal of Remote Sensing.* Vol.10, No.8, 1437-1443.

Friedl, M.A., J. Michaelsen, F.W. Davis, H. Walker, and D.S. Schimel. 1994. Estimating grassland biomass and leaf area index using ground and satellite data. *International Journal of Remote Sensing.* Vol.15, No.7, 1401-1420.

Gadd, B. 1995. Handbook of the Canadian Rockies – 2nd edition. Corax Press, Jasper, Alberta, Canada.

Ganapol, B.D., L.F. Johnson, C.A. Hlavka, D.L. Peterson, and B. Bond. 1999. LCM2: A Coupled Leaf/Canopy Radiative Transfer Model. *Remote Sensing of Environment.* 70:153-166.

Gerling, L.R. 1996. Point-Sampling of Tree Crowns using Aerial Photographs for Forest Inventory. *Southern Journal of Applied Forestry.* Vol.21, No.4, 28-36.

Gilabert, M.A., F.J. Garcia-Haro, and J. Melia. 2000. A Mixture Modeling Approach to Estimate Vegetation Parameters for Heterogeneous Canopies in Remote Sensing. *Remote Sensing of Environment.* 72:328-345.

Gopal, S., and C. Woodcock. 1996. Remote Sensing of Forest Change Using Artificial Neural Networks. *IEEE Transactions on Geoscience and Remote Sensing.* 34:398-403.

Government of Alberta. 1996. Forests and Timber Management: Kananaskis Country. The Kananaskis Country Environmental Library. pp. 3-9, 33-35.

Grabherr, G., 2000. Biodiversity of mountain forests. *Forests in Sustainable Mountain Development: a State of Knowledge Report for 2000,* Task Force on Forests in Sustainable Mountain Development, IUFRO Research Series 5, CABI Publishing, Wallingford, UK.

Guerra, F., H. Puig, and R. Chaume. 1998. The forest-savanna dynamics from multi-date Landsat-TM data in Sierra Parima, Venezuela. *International Journal of Remote Sensing.* Vol.19, No.11, 2061-2075.

Hall, F.G., D.R. Peddle, and E.F. LeDrew. 1997. Remote sensing of biophysical variables in boreal forest stands of *Picea mariana*. *International Journal of Remote Sensing*. Vol.17, No.15, 3077-3081.

Hall, F.G., Y.E. Shimabukuro, and K.F. Huemmrich. 1995. Remote Sensing of Forest Biophysical Structure using Mixture Decomposition and Geometric Reflectance Models. *Ecological Applications 5(4): 993-1013.*

Hall, F. G., D. E. Strebel, J.E. Nickeson, and S. J. Goetz. 1990. Radiometric rectification: toward a common radiometric response among multi-date, muti-sensor images. *Remote Sensing of Environment* 35:11-27

Hall, R.J., D.P. Davidson, and D.R. Peddle, 2003. Ground and remote estimation of leaf area index in Rocky Mountain forest stands, Kananaskis, Alberta. *Canadian Journal of Remote Sensing*. Vol.29, No.3, 411-427

Hall, R.J., Y. Wang, and D.J. Morgan. 2001. Estimating Tree Diameter and Volume with a Taper Model and Large-Scale Photo Measurements. *Northern Journal of Applied Forestry.* 18(4): 110-118.

Hall, R.J., D.R. Peddle, and D.L. Klita. 2000. Mapping conifer understory within boreal mixedwoods from Landsat TM satellite imagery and forest inventory information. *The Forestry Chronicle.* 6:887-902

Hall, R.J., D.R. Peddle, and D.L. Klita. 1999. Application of Maximum Likelihood and Evidential Reasoning Classifiers for Mapping Conifer Understory. *Presented at the 4th International Airborne Remote Sensing Conference and Exhibition/ 21st Canadian Symposium on Remote Sensing, Ottawa, Ontario, Canada, 21-24 June 1999.*

Hall, R.J., P.H. Crown, and D.J. Titus. 1984. Change Detection Methodology for Aspen Defoliation with Landsat MSS Digital Data. *Canadian Journal of Remote Sensing.* Vol.10, No.2, 135-142.

Herwitz, S.R., B. Sandler, and R.E. Slye. 2000. Twenty-one years of crown change in the Jasper Ridge Bilogical Preserve based on georeferenced multitemporal aerial photographs. *International Journal of Remote Sensing.* 21: 45-60

Huang, S. 1994. Ecologically based individual tree volume estimation for major Alberta tree species. Alberta Environmental Protection, Land and Forest Services, Edmonton, Alta. Publication no. T/288.

Jensen, J.R. 2000. Remote Sensing of the Environment: An Earth Resource Perspective. New Jersey, Prentice-Hall, Inc.

Jensen, J.R. 1996. Introductory Digital Image Processing: A Remote Sensing Perspective. 2nd Ed. New Jersey, Prentice-Hall, Inc.

Johnson, R.L., 2000. Airborne Remote Sensing of Forest Leaf Area Index in Mountainous Terrain. *Masters Thesis; Department of Geography, University of Lethbridge.*

Johnson, R.L., D.R. Peddle and R.J. Hall, 2000. A modeled-based sub-pixel scale mountain terrain normalization algorithm for improved LAI estimation from airborne casi imagery. In, *Proceedings, 22nd Canadian Symposium on Remote Sensing,* Victoria, BC., Canada. Canadian Aeronautics and Space Institute, Ottawa: 415-424.

Kirby, C.L. 1973. The Kananaskis Forest Experiment Station, Alberta (History, Physical Features, and Forest Inventory). Northern Forest Research Centre Information Report NOR-X-51.

Leblanc, S.G., J.M. Chen, and J. Cihlar. 1997. NDVI Directionality in Boreal Forests: A Model Interpretation of Measurements. *Canadian Journal of Remote Sensing*, 23: 293-379.

Leckie, D.G., and M.D. Gillis. 1995, Forest Inventory in Canada with emphasis on map production. *The Forestry Chronicle*. Vol.71, No.1, 74-88.

Leprieur, C. E., J. M. Durand and J. L. Peyron. 1988. Influence of Topography on forest reflectance using Landsat thematic mapper and digital terrain data. *Photogrammetric Engineering and Remote Sensing* 54:491-496

LI-COR Inc. 1992. LAI-2000 Plant Canopy Analyzer: Operating Manual. Lincoln, Nebraska, USA.

Li, X. and A.H. Strahler, 1992. Geometric-Optical Bi-directional Reflectance Modeling of the Discrete Crown Vegetation Canopy: Effect of Crown Shape and Mutual Shadowing. *IEEE Transactions on Geoscience and Remote Sensing*, Vol. 30: 276-296.

Li, X. and A.H. Strahler, 1988. Modeling the Gap Probability of a Discontinuous Vegetation Canopy. *IEEE Transactions on Geoscience and Remote Sensing*, Vol. 26, No.2: 161-170

Li, X. and A.H. Strahler, 1985. Geometric-optical modeling of a conifer forest canopy. *IEEE Transactions on Geoscience and Remote Sensing*, Vol. GE-23 no. 5:705-720.

Lillesand, T.M., and R.W. Kiefer 1999. Remote Sensing and Image Interpretation. 4th Ed. New York, John Wiley & Sons, Inc.

Lucht, W., 1996. GOMS User Manual. Boston University, Boston, USA.

Markham, B. L. and J. L. Barker. 1987. Radiometric Properties of U.S. Processed Landsat MSS data. *Remote Sensing of Environment* 22:39-71

Markham, B. L. and J. L. Barker. 1986. Landsat MSS and TM post calibration dynamic ranges, exoatmospheric reflectances and at satelite temperature. In *EOSAT Landsat Technical Notes* 1:3-7

Meyer, P., K. L. Itten, T. Kellenberger, S. Sandmeier and R. Sandmeier. 1993. Radiometric corrections of topographically induced effects on Landsat TM data in an alpine environment. *ISPRS Journal of Photogrammetry and Remote Sensing* 48:17-28

Milne, A. K. 1988. Change detection analysis using Landsat imagery: a review of methodology. In Proceedings of IGRARSS'88 Symposium, Edinburgh, UK:541-544

Myneni, R.B., and G. Asrar. 1994. Atmospheric Effects and Spectral Vegetation Indices. *Remote Sensing of Environment.* 47:390-402

Paradella, W.R., M.F.F. Da Silva, N. De A. Rosa, and C.A. Kushigbor. 1994. A geobotanical approach to the tropical rain forest environment of the Carajás Mineral Province (Amazon Region, Brazil), based on digital TM-Landsat and DEM data. *International Journal of Remote Sensing.* Vol.15, No.8, 1633-1648.

Parresol, B.R. 1999. Assessing Tree and Stand Biomass: A Review with Examples and Critical Comparisons. *Forest Science.* 45(4).

Peddle, D.R. 1999. Integration of a Geometric Optical Reflectance Model with an Evidential Reasoning Image Classifier for Improved Forest Information Extraction. *Canadian Journal of Remote Sensing.* Special Issue on Remote Sensing Models and Image Processing. 25(2): 189-196.

Peddle, D.R. 1995, Knowledge Formulation for Supervised Evidential Classification. *Photogrammetric Engineering and Remote Sensing*. Vol.61, No.4, 409-417.

Peddle, D.R., S.E. Franklin, R.L. Johnson, M.A. Lavigne and M.A. Wulder, 2003(a). Structural change detection in a disturbed conifer forest using a geometric optical reflectance model in Multiple-Forward Mode. *IEEE Transactions on Geoscience and Remote Sensing*. 41(1): 163-166.

Peddle, D.R., R.L. Johnson, J. Cihlar and R. Latifovic, 2003(b). Large area forest classification and biophysical parameter estimation using the 5-Scale canopy reflectance model in Multiple-Forward Mode. *Remote Sensing of Environment.* BOREAS Special Issue. (in press).

Peddle, D.R., R.L. Johnson, J. Cihlar, S.G. Leblanc and J.M. Chen, 2003(c) . MFM-5-Scale: A physically-based inversion modeling approach for unsupervised cluster labeling and independent forest landcover classification. *Canadian Journal of Remote Sensing* (accepted).

Peddle, D.R., J.E. Luther, N. Pilger and D. Piercey, 2003(d). Forest biomass estimation using a physically based 3-D structural modeling approach for Landsat TM cluster labeling. In, *Proceedings, 25th Canadian Symposium on Remote Sensing*, Montreal, PQ., Canada. Oct. 14-17, 2003. Canadian Aeronautics and Space Institute, Ottawa.

Peddle, D.R., S.E. Franklin, R.L. Johnson, M.B. Lavigne, and M.A. Wulder, 2001(a). Physically-Based Multiple-Forward-Mode Reflectance Modeling of Forest Partial Harvest Change, Fundy Model Forest, New Brunswick. Proceedings, *23rd Canadian Symposium on Remote Sensing/ 10e AQT*: Quebec City, Canada.

Peddle, D.R., H.P. White, R.J. Soffer, J.R. Miller, and E.F. LeDrew. 2001(b) Reflectance Processing of Remote Sensing Spectroradiometer Data. *Computers & Geoscience.* 27:203-213.

Peddle, D.R., S.P. Brunke, and F.G. Hall, 2001(c). A Comparison of Spectral Mixture Analysis and Ten Vegetation Indices for Estimating Boreal Forest Biophysical Information from Airborne Data. *Canadian Journal of Remote Sensing*. 27(6): 627-635

Peddle, D.R., and R.L. Johnson. 2000. Spectral Mixture Analysis of Airborne Remote Sensing Imagery for Improved Prediction of Leaf Area Index in Mountainous Terrain, Kananaskis Alberta. *Canadian Journal of Remote Sensing*. Vol.26, No.6, 176-187.

Peddle, D.R., F.G. Hall, and E.F. LeDrew. 1999. Spectral Mixture Analysis and Geometric-Optical Reflectance Modeling of Boreal Forest Biophysical Structure. *Remote Sensing of Environment.* 67: 288-297.

Peddle, D.R., and C.R. Duguay. 1998. Mountain Terrain Analysis using a Knowledge-Based Interface to a GIS. *Geomatica.* Vol.52, No.3, 265-272.

Peddle, D.R., F.G. Hall, E.F. LeDrew, and D.E. Knapp. 1997. Classification of Forest Land Cover in BOREAS. II: Comparison of Results from a Sub-pixel Scale Physical Modeling Approach and a Training Based Method. *Canadian Journal of Remote Sensing.* Vol.23, No.2, 131-142.

Peng, C., 2001. Developing and Validating Nonlinear Height-Diameter Models for Major Tree Species of Ontario's Boreal Forests. *Northern Journal of Applied Forestry.* 18(3).

Peterson, D.W. and D.L. Peterson. 1994. Effects of climate on radial growth of subalpine conifers in the North Cascade Mountains. Canadian Journal of Forest Research 24:1921-1932.

Pilger, N., D.R. Peddle and R.J. Hall, 2003. Forest Volume Estimation using a Canopy Reflectance Model in Multiple-Forward-Mode. In, *Proceedings, 25th Canadian Symposium on Remote Sensing*, Montreal, PQ., Canada.

Pilger, N., D.R. Peddle and J.E. Luther, 2002. Estimation of Forest Cover Type and Structure from Landsat TM Imagery using a Canopy Reflectance Model for Biomass Mapping in Western Newfoundland. In, *Proceedings, IEEE International Geoscience and Remote Sensing Symposium (IGARSS '02) / 24th Canadian Symposium on Remote Sensing*, Toronto, ON., Canada. June 24-28, 2002. Institute for Electrical and Electronic Engineers, USA / Canadian Aeronautics and Space Institute, Ottawa. (CD-ROM).

Prakesh, A. and R. P. Gupta. 1998. Land use mapping and change detection in a coal mining area: a case study in the Jharia coalfield, India. *International Journal of Remote Sensing* 19:391-410

Richter, R. 1997. Correction of atmospheric and topographic effects for high spatial resolution satellite imagery. *International Journal of Remote Sensing*. 5:1099-1111

Robinove, C. J. 1982. Computation with physical values from Landsat data. *Photogrammetric Engineering and Remote Sensing* 48:781-784

Robinson, A.P., D.C. Hamlin, and S.E. Fairweather. 1999. Improving Forest Inventories. *Journal of Forestry*. Vol.97, No.12, 38-42.

Rowe, J.S. 1972. Forest Regions of Canada. *Canadian Forest Service.* Ottawa, ON. Publication No. 1300, 172 pp.

Sader, S. A. 1995. Spatial characteristics of forest clearing and vegetation regrowth as detected by Landsat thematic mapper imagery. *Photogrammetric Engineering and Remote Sensing* 61:1145-1151

Sader, S.A., R.B. Waide, W.T. Lawrence, and A.T. Joyce. 1989. Tropical Forest Biomass and Successional Age Class Relationships to a Vegetation Index Derived from Landsat TM Data. *Remote Sensing of Environment*. 28:143-156.

Schott, J. R., C. Salvaggio and W. J. Volchok. 1988. Radiometric scene normalization using psuedoinvariant features. *Remote Sensing of Environment* 26:1-16

Smith, R.L. 1996. Ecology and Field Biology, 5th edition. New York. Harper Collins College Publishers.

Soares, P., M. Tomé, J.P. Skovsgaard, and J.K. Vanclay. 1995. Evaluating a growth model for forest management using continuous forest inventory data. *Forest Ecology and Management.* 71: 251-265.

Soenen, S.A., D.R. Peddle and C. Coburn, 2003. Topographic correction of remote sensing imagery using a canopy reflectance model. In, *Proceedings, 25th Canadian Symposium on Remote Sensing*, Montreal, PQ., Canada. Oct. 14-17, 2003. Canadian Aeronautics and Space Institute, Ottawa. (CD-ROM)

Song, C., C.E. Woodcock, K.C. Seto, M.P. Lenney, and S.A. Macomber. 2001. Classification and Change Detection Using Landsat TM Data: When and How to Correct Atmospheric Effects? *Remote Sensing of Environment.* 75:230-244.

Spurr, S.H., and B.V. Barnes. 1973. Forest Ecology – 2nd edition. The Ronald Press Company, New York, NY. pp 571.

Steininger, M.K. 2000. Satellite estimation of tropical secondary forest above-ground biomass: data from Brazil and Bolivia. *International Journal of Remote Sensing*. Vol.21, No.6&7, 1139-1157.

Strahler, A.N. 1980. Systems Theory in Physical Geography. *Physical Geography.* Vol 1, No.1, 1-27.

Strahler, A.H., C.E. Woodcock, and J.A. Smith. 1986. On the Nature of Models in Remote Sensing. *Remote Sensing of Environment.* 20:121-139

Teillet, P.M. 1997. A Status Overview of Earth Observation Calibration/Validation for Terrestrial Applications: Review Paper, *Canadian Journal of Remote Sensing,* 4:291-298

Teillet , P. M. 1986. Image correction for radiometric effects. *International Journal of Remote Sensing* 12:1637-1651

Teillet, P.M., D.N.H. Horler, and N.T. O'Neill. 1997. Calibration, Validation, and Quality Assurance in Remote Sensing: A New Paradigm: Technical Note, *Canadian Journal of Remote Sensing,* 4:401-414

Teillet, P.M., and G. Fedosejevs 1995. On the Dark Target Approach to Atmospheric correction of Remotely Sensed Data. *Canadian Journal of Remote Sensing.* 4:374-387

Teillet, P. M., B. Guindon and D. G. Goodenough. 1982. On the slope aspect correction of multi spectral scanner data. *Canadian Journal of Remote Sensing* 8:84-106.

Tompkins, S., J.F. Mustard, C.M. Pieters, and D.W. Forsyth. 1997. Optimization of Endmembers for Spectral Mixture Analysis. *Remote Sensing of Environment.* 59:472-489.

Trotter, C.M., J.R. Dymond, and C.J. Goulding. 1997. Estimation of timber volume in a coniferous plantation forest using Landsat TM. *International Journal of Remote Sensing.* Vol.18, No.10, 2209-2223.

USDA. 2003. Forest Service Agriculture Handbook 654. Available online: http://www.na.fs.fed.us/spfo/pubs/silvics_manual/table_of_contents.htm Accessed Dec. 5, 2003.

Waring, R.W., and S.W. Running. 1998. Forest Ecosystems: Analysis at Multiple Scales, 2nd ed. Academic Press, London.

Woodcock, C.E. and Strahler, A.H. 1987. The Factor of Scale in Remote Sensing. *Remote Sensing of Environment.* 21:311-332

Wulder, Mike. 1998. Optical remote-sensing techniques for the assessment of forest inventory and biophysical parameters. *Progress in Physical Geography.* 22,4:449-476

Wynne, R.H., R.G. Oderwald, G.A. Reams, and J.A. Scrivani. 2000. Optical Remote Sensing for Forest Area Estimation. *Journal of Forestry.* Vol.98, No.5, 31-36.

Yuan, D. and C. D. Elvidge 1996. Comparison of relative radiometric normalization techniques. *ISPRS Journal of Photogrammetry and Remote Sensing* 51:117-126

World Wide Web References

www – online. http://www.ccrs.nrcan.gc.ca/ccrs/tekrd/rd/ana/calval/calhome.html accessed March 1, 2001

www – online. http://www.geog.uvic.ca/geog322/htmls/radiometric_calib.html accessed February 25, 2001

www – online. http://terra.nasa.gov/FactSheets/Aerosols/ accessed February 25, 2001

www – online. http://www.spaceimaging.com/aboutus/satellites/IKONOS/spectral.htm accessed August 22, 2001.

www – online. http://ltpwww.gsfc.nasa.gov/IAS/handbook/handbook/htmls/chapter6/chapter6.html accessed March 19, 2002

www – online. http://sunearth.gsfc.nasa.gov
accessed August 27, 2002

www – online. http://online.anu.edu.au/Forestry/mensuration/S_BA.HTM
accessed January 19, 2003

www – online. http://www3.gov.ab.ca/srd/forests/fmd/directives/glossary.html
accessed October 21, 2003

www – online. http://www.cfl.scf.rncan.gc.ca/ecosys/classif/intro_regions_e.asp
accessed December 8, 2003

www – online. http://www-cger.nies.go.jp/wetland/kushiro/Classify_TM/index-e.html
accessed December 8, 2003

www – online. http://www.na.fs.fed.us/spfo/pubs/silvics_manual/table_of_contents.htm
accessed December 8, 2003

www – online. http://www.ncfcnfr.net/glossary.html
accessed December 8, 2003

Appendix 1: Maximum Likelihood Classification and Output Rule

A 10-class Maximum-Likelihood supervised classification was performed on the Kananaskis study area IKONOS imagery. The training data, or regions of interest, were selected based upon ground truth data collected during field-work in the area. These regions are visible in the classified image (figure A1-1).

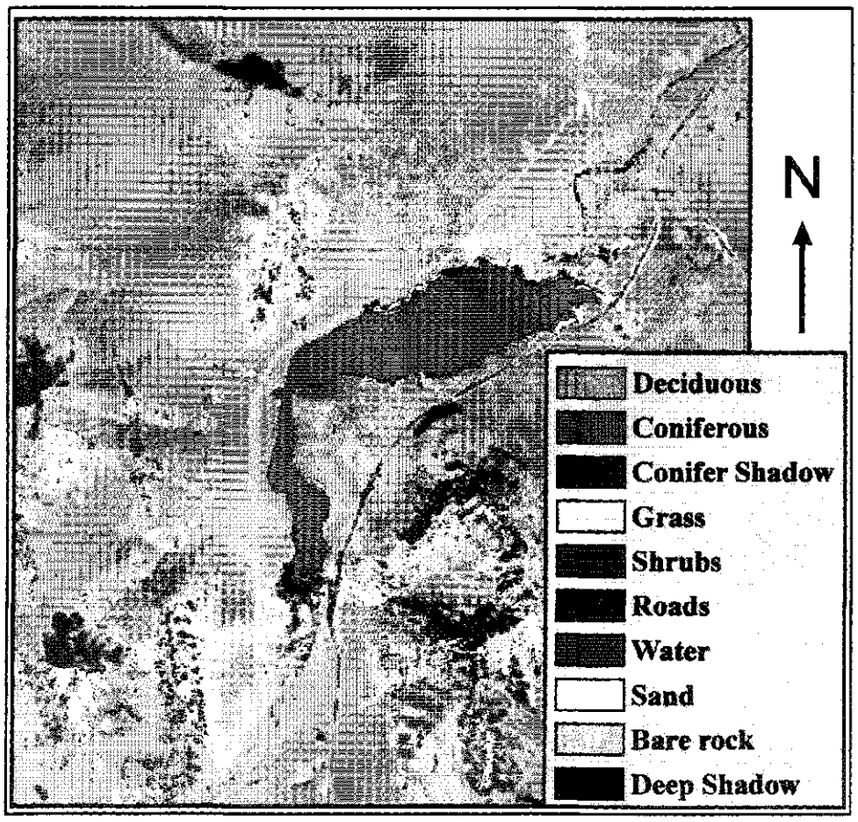

Figure A1-1. 10-class maximum likelihood supervised classification.

Areas which may be distinctly different, yet spectrally similar are commonly misclassified. Therefore, output rules are created for visual inspection of classified pixels and a secondary classification may be run on these misclassified pixels. Through the investigation of one to three classes at a time, one can determine where misclassification is occurring. While it may be difficult to discern misclassification within the non-vegetation components, such misclassification is clearly identifiable when examining output rules of vegetated areas. Figure A1-2 indicates forest vegetation classes with all other spectral classes being un-classified.

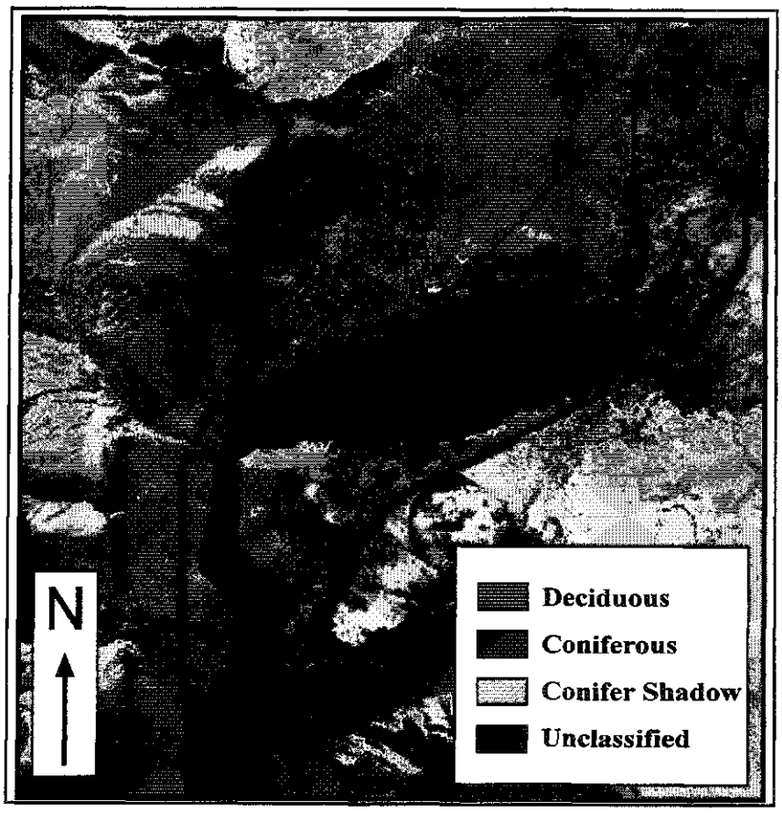

Figure A1-2. Supervised Classification Output Rule - forest vegetation

Appendix 2: Kananaskis Field Season 2001 Climate Data

Date	Minimum Temperature (deg.C)	Maximum Temperature (deg.C)	Minimum Relative Humidity (%)	Maximum Relative Humidity (%)	Minimum Wind Speed 2 minute average (km/hr)	Maximum Wind Speed 2 minute average (km/hr)
1-Jul-01	7.2	26.5	18.34	100.8	1.1	20.4
2-Jul-01	12	24.3	41.4	92.5	0	21.5
3-Jul-01	5.5	27.7	37.2	99.8	0	24.8
4-Jul-01	7.2	31.7	12.6	99	0	29.9
5-Jul-01	7	25.9	14.8	89.9	3.5	31.5
6-Jul-01	1.9	25.2	18	93.4	0.2	26.3
7-Jul-01	12.4	26.6	22.2	53.7	0	28.5
8-Jul-01	8.8	28.3	19.7	78.3	1.3	23.4
9-Jul-01	8	28.3	56.5	158.5	0.8	29.7
10-Jul-01	7.1	32.5	34.4	159.4	0.2	26.4
11-Jul-01	8.8	27.8	24.5	158.8	0.8	25.9
12-Jul-01	12.6	25.7	154.3	159.3	1.1	19.7
13-Jul-01	8.5	25	41.6	160.3	0.4	57.3
14-Jul-01	6	24.8	33.2	160.6	0.9	29.4
15-Jul-01	6.1	25.6	39.8	160.4	0.2	18.8
16-Jul-01	10.8	23.3	154.9	159.7	0	15.5
17-Jul-01	8.6	17.1	156.5	160.2	2.8	40.7
18-Jul-01	10	16.8	157.9	160.2	9.7	40.1
19-Jul-01	5	19.5	155.6	160.9	2.5	29.8
20-Jul-01	4.8	23.3	154.9	160.9	1.3	24.4
21-Jul-01	5.8	23.3	154.6	160.7	0.2	24.5
22-Jul-01	7.2	20	155.9	160.5	0	21.2
23-Jul-01	6	25.9	154.4	160.8	0.2	18.9
24-Jul-01	6	20.4	156.1	160.6	1.3	49.5
25-Jul-01	3.3	19.2	157	161.3	1	22.7
26-Jul-01	3.2	22.8	155.3	161.4	0	15.4
27-Jul-01	3.7	25.4	154.4	161.3	0.1	31.5
28-Jul-01	5.9	22.2	155.1	160.9	0.1	39.6
29-Jul-01	11	19.1	156.9	160	7.4	36.4
30-Jul-01	6.6	19.8	155.5	160.7	1.7	28.9
31-Jul-01	4.2	21.9	155.1	161.2	0.4	15.8

Appendix 2(a). July 2001 Field Season Climate Data. source: Kananaskis Meteorological Station.

Date	Minimum Temperature (deg.C)	Maximum Temperature (deg.C)	Minimum Relative Humidity (%)	Maximum Relative Humidity (%)	Minimum Wind Speed 2 minute average (km/hr)	Maximum Wind Speed 2 minute average (km/hr)
1-Aug-01	8.5	21.5	114.5	160.4	2.2	25.9
2-Aug-01	8.1	25.8	155.1	160.3	0.1	34.9
3-Aug-01	6.3	31.2	46.4	159.9	1.8	31.4
4-Aug-01	9.8	22.8	155.6	160	1.8	32.7
5-Aug-01	9.5	23	155.2	159.8	3.2	38.6
6-Aug-01	10.8	27	154.9	159.7	2.9	36.3
7-Aug-01	7.8	25.9	53.3	160.4	0.1	18.2
8-Aug-01	7.4	22	64.3	159.9	0.1	20.2
9-Aug-01	5.4	25	30.6	159.5	0	20.4
10-Aug-01	3.7	26.9	33.9	160.9	0.1	21.6
11-Aug-01	4	28.4	40.7	160.7	0	20.6
12-Aug-01	5.1	31.9	33.6	160.1	0.7	15.3
13-Aug-01	6.5	30.3	72.7	160.2	0.2	32.2
14-Aug-01	6.6	30.3	64.1	160.1	0.8	25
15-Aug-01	5.7	31.4	39.6	160.3	0.1	19.9
16-Aug-01	6	31.4	31.2	160	1.8	21.3
17-Aug-01	5.7	33.6	42.5	160.1	0	26.6
18-Aug-01	8.5	29.2	40.7	160	0.4	42.4
19-Aug-01	9.6	22.4	111.1	159.9	1.4	29.2

Appendix 2(b). August 2001 Field Season Climate Data. source: Kananaskis Meteorological Station.

Appendix 3: Field data sheet

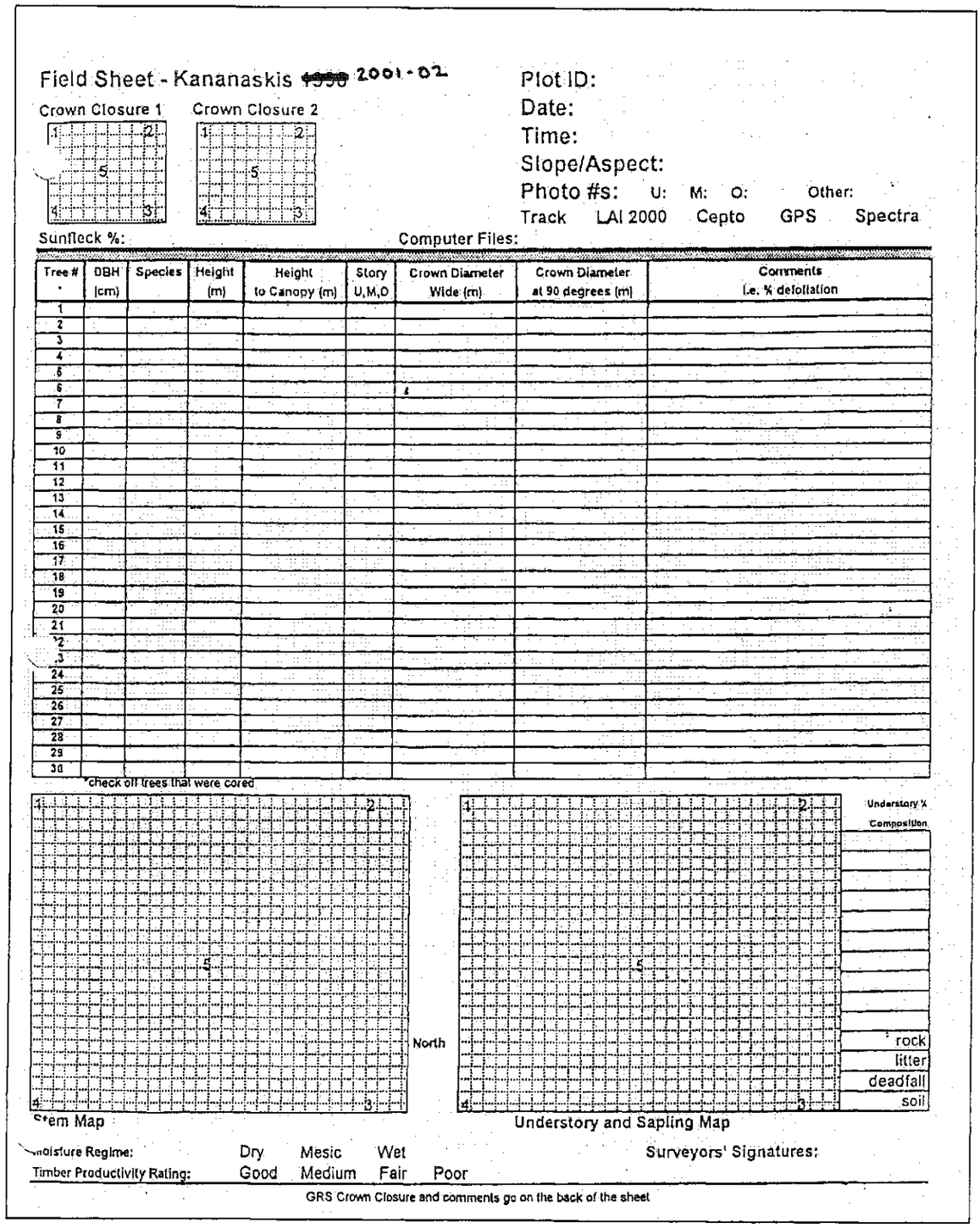

Field Sheet - Kananaskis ~~1998~~ 2001-02

Plot ID:
Date:
Time:
Slope/Aspect:
Photo #s: U: M: O: Other:
Track LAI 2000 Cepto GPS Spectra

Crown Closure 1 Crown Closure 2

Sunfleck %: Computer Files:

Tree #	DBH (cm)	Species	Height (m)	Height to Canopy (m)	Story U,M,O	Crown Diameter Wide (m)	Crown Diameter at 90 degrees (m)	Comments i.e. % defoliation
1								
2								
3								
4								
5								
6								
7								
8								
9								
10								
11								
12								
13								
14								
15								
16								
17								
18								
19								
20								
21								
22								
23								
24								
25								
26								
27								
28								
29								
30								

*check off trees that were cored

North

Understory % Composition
rock
litter
deadfall
soil

Stem Map

Understory and Sapling Map

Moisture Regime: Dry Mesic Wet

Timber Productivity Rating: Good Medium Fair Poor

Surveyors' Signatures:

GRS Crown Closure and comments go on the back of the sheet

Appendix 3 (a). Kananaskis field data sheet – front

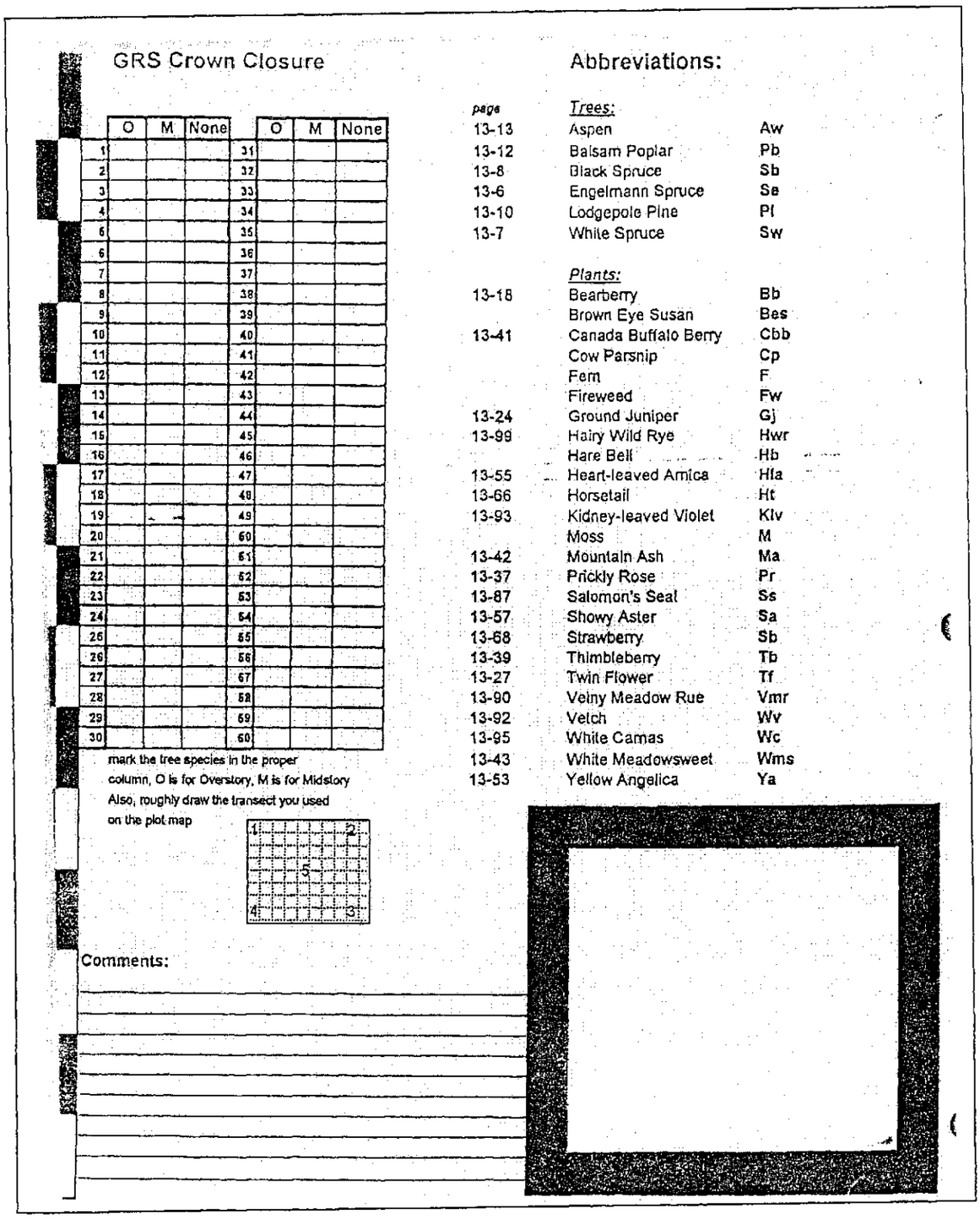

GRS Crown Closure

	O	M	None		O	M	None
1				31			
2				32			
3				33			
4				34			
5				35			
6				36			
7				37			
8				38			
9				39			
10				40			
11				41			
12				42			
13				43			
14				44			
15				45			
16				46			
17				47			
18				48			
19				49			
20				50			
21				51			
22				52			
23				53			
24				54			
25				55			
26				56			
27				57			
28				58			
29				59			
30				60			

mark the tree species in the proper column, O is for Overstory, M is for Midstory
Also, roughly draw the transect you used on the plot map

Comments:

Abbreviations:

page	Trees:	
13-13	Aspen	Aw
13-12	Balsam Poplar	Pb
13-8	Black Spruce	Sb
13-6	Engelmann Spruce	Se
13-10	Lodgepole Pine	Pl
13-7	White Spruce	Sw
	Plants:	
13-18	Bearberry	Bb
	Brown Eye Susan	Bes
13-41	Canada Buffalo Berry	Cbb
	Cow Parsnip	Cp
	Fern	F
	Fireweed	Fw
13-24	Ground Juniper	Gj
13-99	Hairy Wild Rye	Hwr
	Hare Bell	Hb
13-55	Heart-leaved Arnica	Hla
13-66	Horsetail	Ht
13-93	Kidney-leaved Violet	Klv
	Moss	M
13-42	Mountain Ash	Ma
13-37	Prickly Rose	Pr
13-87	Salomon's Seal	Ss
13-57	Showy Aster	Sa
13-68	Strawberry	Sb
13-39	Thimbleberry	Tb
13-27	Twin Flower	Tf
13-90	Veiny Meadow Rue	Vmr
13-92	Vetch	Wv
13-95	White Camas	Wc
13-43	White Meadowsweet	Wms
13-53	Yellow Angelica	Ya

Appendix 3 (b). Kananaskis field data sheet – back

Appendix 4: Access Queries

Sample Microsoft Access queries are presented below. In these queries, matching between mean pixel reflectance values for each of the image bands was performed. The terms Aw3, Aw4, Pl3, and Pl4 refer to the species and band being used in the query.

Sample Trembling Aspen (Aw) model run: (plot 1 reflectance values used as example)

SELECT Aw3.pixellevel, Aw4.pixellevel, Aw3.templam, Aw4.templam, Aw3.tempr, Aw4.tempr, Aw3.tempb, Aw4.tempb, Aw3.temph, Aw4.temph, Aw3.tempdh, Aw4.tempdh, Aw3.Height, Aw4.Height

FROM Aw3, Aw4

Where Aw3.pixellevel > (3.8565 - 0.4123) And Aw3.pixellevel < (3.8565 + 0.4123) And Aw4.pixellevel > (37.6279 - 4.0605) And Aw4.pixellevel < (37.6279 + 4.0605)

And Aw3.templam = Aw4.templam
And Aw3.Height = Aw4.Height
And Aw3.tempb = Aw4.tempb
And Aw3.tempr = Aw4.tempr

Lower values in MFM output could be attributed to the presence of understory vegetation and smaller trees contributing to increased reflectance, or increased shadow in the canopy.

Sample Lodgepole Pine (Pl) model run: (plot 41 reflectance values used as example)

SELECT Pl3.pixellevel, Pl4.pixellevel, Pl3.templam, Pl4.templam, Pl3.tempr, Pl4.tempr, Pl3.tempb, Pl4.tempb, Pl3.temph, Pl4.temph, Pl3.tempdh, Pl4.tempdh, Pl3.Height, Pl4.Height

FROM Pl3, Pl4

Where pl3.pixellevel > (3.0324 - 0.279) And pl3.pixellevel < (3.0324 + 0.279)
And pl4.pixellevel > (17.4579 - 2.7588) And pl4.pixellevel < (17.4579 + 2.7588)

And Pl3.templam = Pl4.templam
And Pl3.Height = Pl4.Height
And Pl3.tempb = Pl4.tempb
And Pl3.tempr = Pl4.tempr